Chapter 6
Calorimetry at the Solid–Liquid Interface

Jerzy Jozef Zajac

Abstract Broad principles of Solid-Liquid calorimetry together with some illustrative examples of its use in the field of catalysis are presented here. The first use is related to the determination of surface properties of catalysts, adsorbents and solid materials in contact with liquids. In particular, it is shown how to evaluate the capacity of a given solid to establish different types of interaction with its liquid environment or to calculate its specific surface area accessible to liquids. The second use includes the measurement of the heat effects accompanying catalytic reactions and the related interfacial phenomena at Solid-Liquid and Liquid-Liquid interfaces. Examples of competitive ion adsorption from dilute aqueous solutions, as well as the formation of surfactant aggregates either in aqueous solution or at the Solid-Liquid interface are considered in view of potential applications in Environmental Remediation and Micellar Catalysis.

6.1 Introduction

*Micro*calorimetry, also *nano*calorimetry to follow the recent trends in thermal instrumentation and analysis, is a measuring technique that can be used to study interfacial phenomena occurring at the Solid-Liquid interface. Immersion of a solid in a pure liquid or a solution, wetting of a solid initially in contact with a gas or vapour by a liquid, adhesion between two condensed phases upon their "molecular" contact are examples of exothermic phenomena which are accompanied by significant heat evolvement. Competitive adsorption from solution is an important exception to the exothermicity of interfacial phenomena. This is because certain components of the

J. J. Zajac (✉)
Institut Charles Gerhardt Montpellier, UMR-5253 CNRS-UM2 Equipe Agrégats, Interface, et Matériaux pour l'Energie (AIME), Université Montpellier 2, C.C. 1502 Place Eugène Bataillon, 34095 Montpellier Cedex 5, France
e-mail: jerzy.zajac@univ-montp2.fr

A. Auroux (ed.), *Calorimetry and Thermal Methods in Catalysis*,
Springer Series in Materials Science 154, DOI: 10.1007/978-3-642-11954-5_6,

solution may compete against each other to adsorb at the interface. Adsorption from solution is thus considered as an exchange process and formally split into several adsorption and desorption steps. If one of the components is to be preferentially accumulated at the interface, the transfer of its molecules to the interface must be accompanied by the transfer of an equivalent amount of molecules of another component in the reverse direction, i.e., from the interface to the interior of the solution. The "displacement" is a frequent term for this process. The overall effect of such a displacement may be endothermic in numerous systems, thereby giving rise to an entropy-driven phenomenon. The complexity of displacement process is the main reason why the van't Hoff procedure for heat determination based on the measurement of the temperature dependence of adsorption isotherms frequently leads to unreliable values. In consequence, direct measurement of the thermal effect in these systems by calorimetry is strongly recommended.

Frequently the heat values for the displacement are relatively small, and thereby difficult to be detected. With the recent progress in ultra-sensitive heat flow measurements and the use of a wide variety of accessories to control the experimental conditions, new commercially available calorimeters offer maximum sensitivity, flexibility, and productivity. Nowadays it becomes possible to study the competitive adsorption phenomena with increased sensitivity and lower detection limits than previously possible.

In the field of catalysis, calorimetry may be used in two manners. The first use is related to the determination of surface properties of catalysts, adsorbents and solid materials in contact with liquids. In particular, it is possible to evaluate the capacity of a given solid to establish different types of interaction with its liquid environment or to calculate its specific surface area accessible to liquids. The second use of calorimetry includes the measurement of the heat effects accompanying catalytic reactions and the related interfacial phenomena at Solid-Liquid and Liquid-Liquid interfaces. In the present chapter, this group of calorimetry applications will be illustrated by following the examples of competitive ion adsorption from dilute aqueous solutions and the formation of surfactant aggregates either in aqueous solution or at the Solid-Liquid interface.

The present chapter does not pretend to be an exhaustive record of Solid-Liquid calorimetry applications in Surface Science and Technology. It should be rather regarded as an introductory course with some illustrative examples. It is important to realise that the individual author's experience in the field has been the principal criterion for selection of specific instruments and their uses, without any intention of neglecting other contributions. The presentation of calorimetry methods will be restricted only to interfacial systems composed of a pure liquid or a dilute binary, at the most, solution in contact with a solid which does not dissolve in the liquid phase. This formalism may be still employed in the case of solutions which are not strictly binary but may be viewed as such (e.g., solutions containing ionizable solutes, background electrolytes or other additives that may be lumped together as constituting a mean solvent or a mean solute).

6.2 Thermodynamic Treatment of the Solid–Liquid Interface and the Related Interfacial Phenomena

This opening paragraph reviews some basic ideas and methods relating to interfacial phenomena at the Solid-Liquid interface. Usually, the subject is characterised by two main approaches: the presentation of these phenomena in terms of thermodynamics and their molecular interpretation. The detailed treatment of such general concepts and relationships can be found in numerous standard texts [1–5] and the interested reader should consult these texts. Here only a very brief review is provided on which to base the entire text, in particular the language that will be widely used in further discussion.

6.2.1 Surface Excess Functions and Surface Phase Model

Contrary to the bulk liquid phase which is homogeneous in three directions in space, has a characteristic composition, and is also autonomous (i.e., its extensive properties depend only on the intensive variables characterising this phase such as the temperature T, the pressure P, and the chemical potentials of the solvent μ_1 and the solute μ_2), the formal thermodynamic description of a Solid-Liquid interface presents a serious difficulty. In the interfacial region, the density ω of any extensive quantity Ω changes continuously throughout the thickness (Fig. 6.1a).

For real solids, even the two-dimensional homogeneity of the interface is very difficult to attain, because the solid boundary is heterogeneous both in a physical and in a chemical sense (surface heterogeneity and roughness) [6, 7]. In order to overcome this difficulty, the only possible way is to introduce the so-called *excess* thermodynamic functions [1, 6, 8].

The widely used definitions of excess functions are based on the Gibbs model of the system, in which a flat interface is regarded as a mathematical dividing plane (the *Gibbs dividing surface*—GDS) [1, 6]. The two phases α and β in contact are assumed to remain homogeneous up to the GDS (Fig. 6.1b depicts such a model). Since the Gibbs model provides a complete description of the heterogeneous system in physico-chemical equilibrium, the formal thermodynamic study of interfacial phenomena is commonly based on this approach. Compared to bulk phases, the thermodynamic expressions for the interface contain additional terms relating to *interfacial tension* and *adsorption* of chemical species. This model has the advantage of leading rapidly to the principal thermodynamic relationships between the interfacial quantities (e.g., the so-called *Gibbs adsorption equation*) [1, 6].

Nevertheless, the Gibbs formalism has some serious drawbacks. Firstly, the interfacial properties (i.e., the Gibbs excess functions) adopt different values depending on the position of the GDS and, consequently, have no direct experimental significance. For dilute solutions, this imperfection may be removed through introducing the so-called *relative interfacial quantities*. Secondly, the Gibbs surface has zero

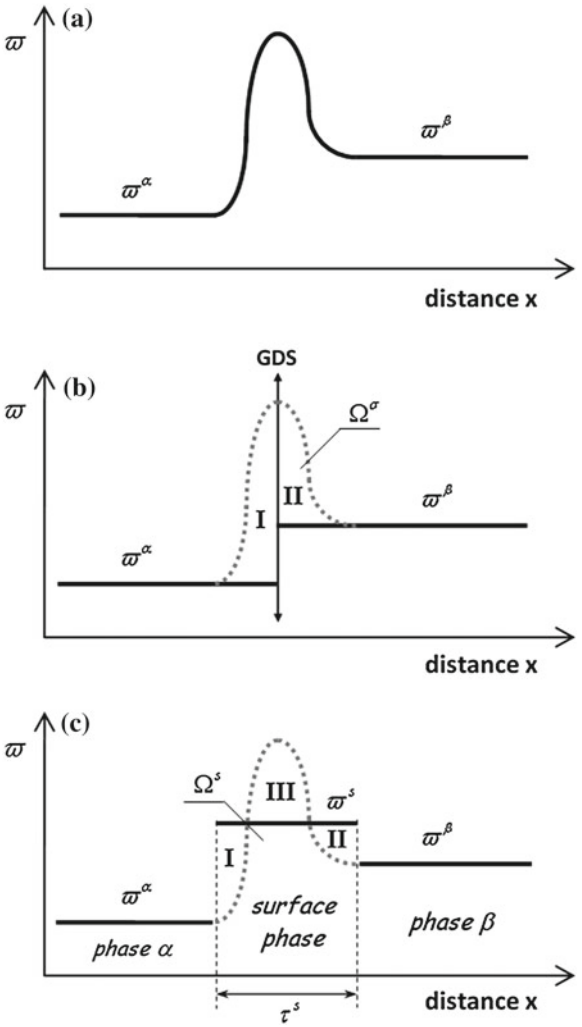

Fig. 6.1 A hypothetical profile of the density ϖ of some extensive property Ω (e.g., number of moles, internal energy, free energy, enthalpy, Gibbs energy, entropy) in the heterogeneous system as a function of the distance x perpendicular to the planar interface. (**a**) Real system: values of ϖ^{α} and ϖ^{β} are determined at such a distance from the interfacial region that the two phases have their bulk properties, (**b**) Gibbs model of the interface: value of the interfacial excess Ω^{σ} is given by a sum of areas I and II [1, 6]; (**c**) Surface phase model of the interface: interfacial property Ω^{s} is defined such that areas I, II and III compensate for one another [6, 8]

thickness and volume and this is at variance with the obvious physical picture of an interface. Furthermore, the physical meaning of the Gibbs excess functions is difficult to translate into molecular terms.

The alternative *surface phase* model popularized by Guggenheim is conceptually simpler since the interfacial region is approximated by a thin, homogeneous layer having an arbitrary thickness [6, 8]. This is illustrated in Fig. 6.1c where the two phases α and β remain homogeneous up to the imaginary planes which constitute the boundaries of the surface phase. This representation may be directly used for the purpose of constructing molecular models of the interface. The related interfacial properties have a real physical significance and are compatible with the experimentally measured quantities. For systems containing a *thermodynamically inert* solid in contact with a pure liquid or a dilute solution, one of the separating planes is chosen to coincide with the surface of the solid. Therefore, the area A of the interface (i.e., its cross-sectional area) is identified with the surface area of the solid phase accessible to the liquid. In practice, the main challenge is always to evaluate correctly the thickness τ^s of the interfacial region.

In the Guggenheim convention [8], the value of any *extensive property of the surface phase*, per unit area of the interface, may be expressed as

$$\Omega^s = \tau^s \cdot \varpi^s = \frac{1}{A}\left[\Omega - \left(\varpi^\alpha V^\alpha + \varpi^\beta V^\beta\right)\right] \tag{6.1}$$

where Ω is the total extensive property of the whole system; ϖ^α, ϖ^β and ϖ^s are the densities of Ω, respectively, in the two bulk phases and in the surface phase of thickness τ^s and surface area A; V^α and V^β represent the volume of the bulk phases α and β. The interfacial enthalpy H^s, interfacial Gibbs energy G^s, and interfacial entropy S^s are defined in such a manner.

It is satisfactory to define the *interfacial tension* γ as the work required to create isothermally and reversibly a unit area of an interface [1, 8]: γ_{SG} (Solid-Gas interface), γ_{SL}(Solid-Liquid interface), and γ_{LG}(Liquid-Gas interface). Since γ is referred to as an energy per unit area in this formulation, the privileged SI unit is J m^{-2}. Nevertheless, interfacial tensions reported in J m^{-2} and N m^{-1} have the same numerical value. Usually more convenient is the submultiple mJ m^{-2} or mN m^{-1} (numerically equivalent to the previously used c.g.s. units). Conceptually, the interfacial tension can be also seen as a new excess quantity that is attributed to the surface phase (or to the GDS) for the Guggenheim (or Gibbs) model to be *thermodynamically* equivalent to the real system [1, 8]. In heterogeneous systems where adsorption does not occur, like those containing the interface between one-component liquid and gas phases, interfacial tension is numerically equal to interfacial Gibbs energy G^s (per unit area of the interface). Otherwise, adsorption takes place with a change in interfacial tension.

From a mechanical standpoint, the interface between a pure liquid and its own equilibrium vapour (or air, *as adsorption is to be neglected here*) behaves as a membrane of infinitesimal thickness stretched uniformly and isotropically by a force exerted tangential to it. Rapid relaxation towards equilibrium is the hallmark of liquid surfaces: when the viscosity of the liquid is not too high, the freshly formed area has enough time to relax completely and the equilibrium interfacial tension will attain the same value in all surface parts. It is important to realise that, owing

to non-equilibrated cohesive forces operating in the interfacial region, the liquid squeezes itself together until it has the locally lowest surface area possible. Therefore, γ_{LG} is regarded as a force (per unit length of surface edge) which opposes any attempt to increase the surface area. The terms *surface* and *interfacial tensions* are used interchangeably for γ_{LG}. The surface tension of most liquids (against equilibrium vapour or air) near room temperature ranges between 10 and 80 mJ m^{-2}, and decreases in a nearly linear fashion as the temperature rises. The description of the common experimental methods with comments on their suitability may be found in Refs. [4, 9].

In pure water, the collective action of intermolecular hydrogen bonds together with classical Van der Waals forces make water molecules stay close to one another (one water molecule is capable of forming four hydrogen bonds since it can accept two and donate two hydrogen atoms). When pure water is in contact with air, the great surface tension tends to minimize the area of hydrophobic-hydrophilic contact: the experimental value of γ_{LG} at 298.15 K is equal to 71.99 ± 0.05 mJ m^{-2} [10]. In the temperature range 273.15–323.15 K, the effect of temperature on the surface tension of water against air is given by [11, 12]:

$$\gamma_{LG} = 75.716 - 0.1416 \cdot (T - 273.15) + \\ - 0.25054 \times 10^{-3} \cdot (T - 273.15)^2 \tag{6.2}$$

Figure 6.2 illustrates the temperature dependence of the surface tension and the numerical procedure leading to the estimate of the surface enthalpy H^s_{LG} of water at room temperature.

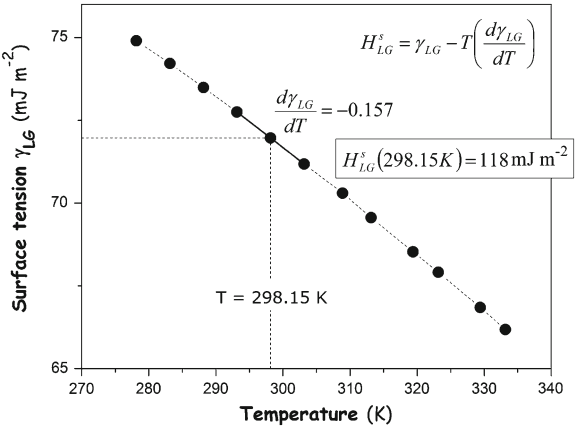

Fig. 6.2 Temperature dependence of the surface tension γ_{LG} of water in contact with air [13] and the numerical determination of the surface enthalpy H^s_{LG} at 298.15 K. The surface entropy S^s_{LG} at 298.15 K is equal to 0.157 mJ m^{-2} K^{-1}

The value of γ_{LG}, which is still equal to 58.9 mN m^{-1} at T = 373.15 K, approaches zero in the vicinity of the critical temperature T = 647.4 K, where there is no longer an interface between the liquid and the vapour.

In the case of solids, the term *surface tension* is used only to designate the interfacial tension γ_{S0} operating at the boundary between the solid phase and the surrounding vacuum. The determination of γ_{S0} for solid surfaces by stretching the surface area against the surface stress is not possible, since the latter is not equal to γ_{S0}. Solids do not deform reversibly and are capable of retaining their non-equilibrium shapes for a long time [4]. The determination of γ_{S0} is sometimes possible from the calculation of reversible work of cleaving a crystal, i.e., by creating fresh surface having the same properties as the original. Several known examples are given in Table 6.1. These results are, however, subject to considerable uncertainty, because the cleavage technique is not entirely reversible [14]. Furthermore, the different crystallographic faces have somewhat different surface tensions owing to the differences in packing density of the atoms.

6.2.2 Adhesion and Cohesion

Adhesion between a pure liquid and a solid may be described in terms of the interfacial and surface tensions [18]. Consider the reversible process of splitting a unit area of the Solid-Liquid interface in such a way as to create a unit area of the Solid-Vacuum interface and a unit area of the Liquid-Gas interface (as shown in Fig. 6.3a).

Adhesion between the two phases is defined as the reversed process and the *Gibbs energy of adhesion* is given, at fixed P and T, by the Dupré equation [4, 19–21]

$$\Delta_{adh} G_{SL} = \gamma_{SL} - \gamma_{S0} - \gamma_{LG}, \textit{per unit area of the interface} \tag{6.3}$$

where γ_{SL} is the interfacial tension between both phases; γ_{S0} and γ_{LG} are the individual surface tensions of the solid against vacuum and the liquid against its equilibrium vapour (or air). For a single solid or liquid phase an analogous procedure (as shown in Fig. 6.3b) yields the *Gibbs energy of cohesion* (per unit area of the interface)

$$\Delta_{coh} G_S = -2\gamma_{S0} \quad \text{or} \quad \Delta_{coh} G_L = -2\gamma_{LG} \tag{6.4}$$

Table 6.1 Surface tensions of several solid crystals against vacuum, as obtained from the work of cleavage, $w_{cliv} = 2 \cdot \gamma_{S0}$ [14–17]

Solid	Cleavage plane	γ_{S0} (mJ m^{-2})
Mica	–	4500
MgO	(100)	1200
CaF_2	(111)	450
LiF	(100)	340
$CaCO_3$	(001)	230
NaCl	(100)	110

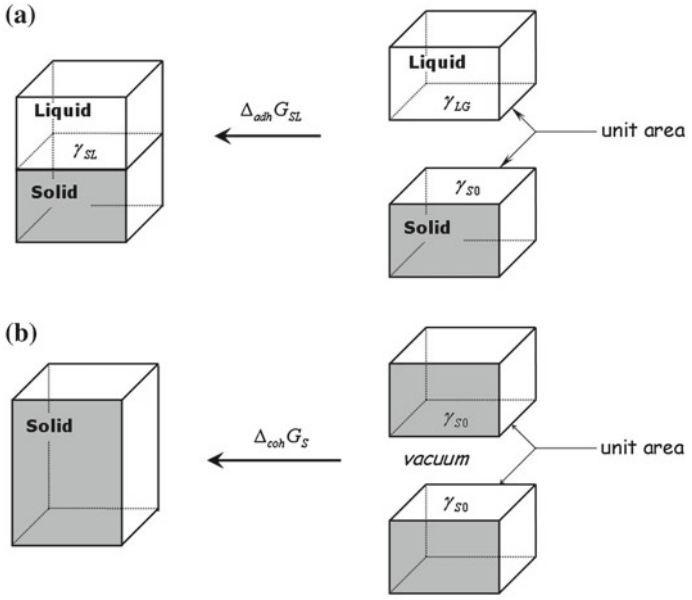

Fig. 6.3 Schematic illustration of the reversible process of (**a**) adhesion and (**b**) cohesion

Combination of Eqs. (6.3) and (6.4) yields

$$\gamma_{SL} = \Delta_{adh}G_{SL} - \frac{1}{2}\left(\Delta_{coh}G_S + \Delta_{coh}G_L\right) \tag{6.5}$$

In a sense, the right-hand side of Eq. (6.5) may be considered as a generalised Gibbs energy of mixing. If the two phases mix spontaneously in all proportions, the Gibbs energy will decrease during such a process, thereby rendering γ_{SL} negative. In thermodynamic terms this means that there is no stable interface. When the phases are immiscible, separation is spontaneous and the interfacial tension becomes positive. In that case, the interface is stable.

In broad outline, the *cohesion* of molecules (atoms, ions) to form the bulk phase of matter is due to long-range physical interactions (mainly of the van der Waals type) and short-range chemical forces (giving rise to covalent, ionic, metal, or hydrogen bonds). Amongst these various types of interactions encountered more or less frequently in interfacial phenomena involving liquid and solid phases, the London (dispersion) forces and the Lewis acid-base ones are really crucial in the construction of a thermodynamic treatment of interfaces [19, 21–23]. Solid and liquid substances may be classified according to their capacity of forming Lewis acid-base bonding. Materials that can be both Lewis acids (electron acceptors) and Lewis bases (electron donors) are termed *bipolar*. The *monopolar acidic* or *monopolar basic* substance can act exclusively as a Lewis acid or a Lewis base (the other property is negligible).

Inert materials, capable of neither acid nor base interactions, are called *apolar*. It should be noted here that this nomenclature [22, 23] has nothing in common with polarity of molecules per se, as measured by their respective dipole moments.

Dispersion forces are universal because they attract all molecules together, regardless of their specific chemical nature. The potential energy of dispersion attraction between two isolated molecules decays with the sixth power of the separation distance. Based on the so-called *Hamaker theory* (i.e., the method of pair-wise summation of intermolecular forces) or the more modern Lifshitz macroscopic treatment of strictly additive London forces, it is possible to develop the so-called Lifshitz-Van der Waals expression for the *macroscopic interactions* between macroscopic-in-size objects (i.e., macrobodies) [19, 21]. Such an expression strongly depends on the shapes of the interacting macrobodies as well as on the separation distance (non-retarded or retarded interaction). For two portions of the same phase of infinite extent bounded by parallel flat surfaces, at a distance h apart, the potential energy of macroscopic attraction is:

$$U(h) = -\frac{A_{11}}{12\pi \cdot h^2} \tag{6.6}$$

where A_{11} is the so-called *Hamaker constant* which depends on the chemical nature of the molecules (atoms, ions) constituting the phase under consideration and the number of molecules per unit volume in two interacting bodies. The more gradual fall-off of the potential energy (6.6) with distance compared to the molecule-molecule interaction indicates that macroscopic attractions are of a more long-range type and they are expected to make a significant contribution to the total energy of attraction even at longer distances.

The values of A_{11} for the various substances interacting across vacuum or across a medium can be found in Refs. [24, 25]. It should be noted that Hamaker constants for interaction across a medium are usually much lower in comparison with the related values under vacuum (e.g., in the case of two macroscopic bodies of quartz at short distances apart, A_{11}equals 41.3×10^{-20} J for interaction across vacuum and 1.3×10^{-20} J for interaction across water [25]).

The macroscopic effect of cohesion due to dispersion forces is usually calculated from the Lifshitz-Van der Waals expression (6.6), providing that the separation distance h is known. Israelachvili [21, 22] has proposed a universal value of 0.165 nm to describe the effective spacing h between molecular planes in all liquids with molecules interacting solely through dispersion forces. In this case, the Gibbs energy of cohesion may be evaluated as

$$\Delta_{coh}G_L \approx 9.74 \times 10^{17} A_{11}\, in\, Jm^{-2}, \quad for\ apolar\ liquids \tag{6.7}$$

where A_{11} is the Hamaker constant for the liquid substance. In general, considerable theoretical and experimental evidence is consistent with the postulate that the Keesom-Debye contribution to the Gibbs energy of cohesion is very small and has no significant importance between macroscopic bodies in the condensed systems [21, 26]. As a result, the Lifshitz-Van der Waals (LW) component $\Delta_{coh}G^{LW}$ of the

Gibbs energy of cohesion for any liquid or solid material is commonly identified with the dispersion contribution.

According to Eq. 6.4, the apolar component of the surface tension of a solid against vacuum or a liquid against its equilibrium vapour (or air) becomes:

$$\gamma_{S0}^{LW} = -\frac{1}{2}\Delta_{coh}G_S^{LW} \quad \text{or} \quad \gamma_{LG}^{LW} = -\frac{1}{2}\Delta_{coh}G_L^{LW} \tag{6.8}$$

Lewis acid-base interaction between molecules (atoms, ions) differs from a classical covalent bond in that only one of the partners supplies the pair of electrons [27]. Electron pair donors (EPD) are molecules which donate the lone pair of nonbonding electrons (n-EPD), the electron pair of a σ-bond (σ-EPD), or the pair of π-electrons (π-EPD). Electron pair acceptor (EPA) molecules may use a vacant valence orbital (n-EPA), a nonbonding σ-orbital (σ-EPA), or a π-bond system with electron-withdrawing substituents (π-EPA). The combinations between all the above donor and acceptor types result in nine types of EPD-EPA complexes, with the bond strength ranging from high values for n-EPD/n-EPA associations to very week π-EPD/π-EPA interactions between neutral molecules. Formally, Lewis acid-base interaction includes a hydrogen bond which is usually situated at the lower end of the chemical bond range.

It has long been an operational premise that the Gibbs energy of cohesion for any *non-metallic* liquid or solid phase can be split into two contributions: an *apolar* one $\Delta_{coh}G^{LW}$ originating chiefly from dispersion forces and a *polar* one $\Delta_{coh}G^{AB}$ arising from the Lewis acid-base interaction between the constituent molecules (atoms, ions). Several semi-empirical methods have been proposed in the literature, e.g., [18, 26, 28–30], to determine both contributions. The results can be collated for different liquids and solids and subsequently used to predict the behaviour of new interfaces. Nevertheless, it is important to understand the approximate nature of this approach and to consider the resulting conclusions with caution.

In consequence, the total surface tension of a given *non-metallic* material against vacuum or its own equilibrium vapour is expressed by the sum of the Lifshitz-van der Waals (LW) and Lewis acid-base (AB) contributions [19, 22]

$$\gamma_{S0} = \gamma_{S0}^{LW} + \gamma_{S0}^{AB} = -\frac{1}{2}\left(\Delta_{coh}G_S^{LW} + \Delta_{coh}G_S^{AB}\right) \tag{6.9a}$$

$$\gamma_{LG} = \gamma_{LG}^{LW} + \gamma_{LG}^{AB} = -\frac{1}{2}\left(\Delta_{coh}G_L^{LW} + \Delta_{coh}G_L^{AB}\right) \tag{6.9b}$$

The change of Gibbs energy during *adhesion* between two phases is the macroscopic outcome of interactions between the microscopic constituents of the different phases. According to the empirical *Berthelot principle* [21], the London energy of attraction between two dissimilar macrobodies is a geometric mean of the mutual interactions between similar objects, so that

$$A_{12} \approx \sqrt{A_{11}A_{12}} \tag{6.10}$$

where A_{12} is the Hamaker constant referring to macroscopic interaction between two different phases.

To obtain the apolar (LW) contribution to the Gibbs energy of adhesion $\Delta_{adh}G_{SL}^{LW}$ between a solid and a liquid, it is assumed that expressions analogous to that given by Eq. 6.7 are still valid. The Berthelot principle Eq. 6.10 may be therefore used to evaluate $\Delta_{adh}G_{SL}^{LW}$. The combining rule for this component of $\Delta_{adh}G_{SL}$ is given by the Good-Girifalco-Fowkes relation [18, 31]:

$$\Delta_{adh}G_{SL}^{LW} = \sqrt{\Delta_{coh}G_{S}^{LW} \cdot \Delta_{coh}G_{L}^{LW}} = -2\sqrt{\gamma_{S0}^{LW} \cdot \gamma_{LG}^{LW}} \tag{6.11}$$

If one of the condensed phases is apolar, dispersion forces are the only important type of interaction operating across the interface and $\Delta_{adh}G_{SL} = \Delta_{adh}G_{SL}^{LW}$. The apolar (LW) surface tension component of any solid can be thus determined by the measurement of the Gibbs energy of adhesion between this material and an apolar probe substance. The latter may be a liquid alkane, methylene iodide, or α-bromonaphthalene, for which the surface tension $\gamma_{LG} = \gamma_{LG}^{LW}$ has already been measured.

The two-condensed-phase analog of Eq. 6.9a, 6.9b is:

$$\Delta_{adh}G_{SL} = \Delta_{adh}G_{SL}^{LW} + \Delta_{adh}G_{SL}^{AB} \tag{6.12}$$

The polar (AB) contributions to the surface tension and Gibbs energy of adhesion are sometimes expressed in terms of Van Oss-Chaudhury-Good parameters [18, 19, 22, 32]

$$\gamma^{AB} = 2\sqrt{\gamma^{A} \cdot \gamma^{B}} \tag{6.13a}$$

$$\Delta_{adh}G_{SL}^{AB} = -2\sqrt{\gamma_{S0}^{A} \cdot \gamma_{LG}^{B}} - 2\sqrt{\gamma_{S0}^{A} \cdot \gamma_{LG}^{B}} \tag{6.13b}$$

where γ^{A} and γ^{B} are the Lewis acid and Lewis base parameters of surface tension γ, respectively. This approximation leads to the following interesting conclusions: the polar (AB) surface tension component of a pure substance is equal to zero, if the substance is monopolar or apolar. There is no acid-base interaction across the interface, i.e., $\Delta_{adh}G_{SL}^{AB} = 0$, if one of the components is apolar or if the two components are monopolar in the same sense, i.e., both being monofunctional acids or both monofunctional bases.

The Lewis acid and base contributions to the surface tension of solids can be derived from measurements of the Gibbs energy of adhesion between the material and a polar probe liquid. At least two different polar liquids (e.g., water and appropriate monofunctional liquid) must be used as probes, provided that their surface components γ_{LG}^{LW}, γ_{LG}^{A}, γ_{LG}^{B} are known.

6.2.3 Wetting in Solid–Liquid Systems

Wetting includes the spreading of a pure liquid over the surface of a solid, displacing the gas (or vapour) initially in contact with that surface [18, 33]. Hence the phenomenon involves three interfaces, namely Solid-Gas, Solid-Liquid, and Liquid-Gas ones. The *spreading coefficient* W_S is defined as [4, 33]

$$W_S = \gamma_{SG} - (\gamma_{SL} + \gamma_{LG}) \tag{6.14}$$

where γ_{SG}, γ_{SL} and γ_{LG} are the appropriate interfacial tensions for the three interfaces at equilibrium. When a portion of the liquid is placed on a uniform, perfectly flat, and non-deformable solid surface and the two phases are allowed to come to equilibrium with the surrounding gas phase, one of the two events may happen:

1. When W_S is positive or zero, the liquid wets the solid material, i.e., spreads out spontaneously over its surface, providing there is enough liquid to eliminate a unit area of the Solid-Gas interface while exposing a corresponding amount of the Solid-Liquid and Liquid-Gas interfaces.
2. When W_S is negative, the liquid remains as a drop having, at equilibrium, a definite angle of contact with the solid surface (the liquid does not wet the solid). This case is illustrated in Fig. 6.4.

The equilibrium *contact angle* Θ between the liquid and the solid phases is determined by the following balance of interfacial tensions [4, 33, 34]:

$$\cos\Theta = \frac{\gamma_{SG} - \gamma_{SL}}{\gamma_{LG}} \tag{6.15}$$

known as Young's equation. This relation applies for contact angles Θ less than, equal to, or greater than 90°. In the limiting case where $\Theta = 0$, the liquid wets out the solid.

The classical form of Young's equation, which describes the equilibrium balance of forces meeting at the three-phase contact line in the plane of the solid surface (see Fig. 6.4), is one of the most controversial expressions in Surface Science and there is

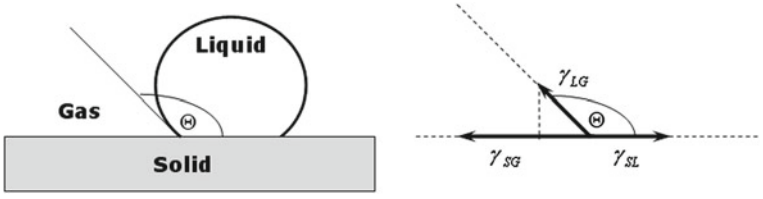

Fig. 6.4 A drop of a non-spreading liquid on a flat solid surface together with the traditional representation of the vectorial equilibrium between respective interfacial tensions viewed as forces acting along the perimeter of the drop

a long list of objections to it (e.g., see Refs. [4, 33, 34] for details). In spite of that, it is still very widely encountered in the literature. To derive it, one must assume an ideal solid: chemically homogeneous, thermodynamically inert (e.g., it cannot swell under the action of the liquid neither can dissolve in the liquid), and flat at an atomic scale. In practice, appreciable hysteresis of the contact angle is observed in real systems (chemical heterogeneity and roughness of solid surfaces), depending on whether the liquid is advancing or receding across the solid surface [33]. Advancing contact angles are larger than receding angles, and the difference may be sometimes as much as 20°–30°. A very detailed critical discussion of the various methods for measuring contact angles can be found in Ref. [34]. The contact angles of powdered solids (e.g., clay minerals) are technically important but are difficult to measure. In the case of numerous fine-grained minerals, which do not occur as large, perfect single crystals with well-developed faces, the contact angles are determined indirectly by column and thin layer wicking [35, 36].

If the liquid is volatile, the gas phase will contain its vapour. In consequence, even though both the fluid phases are nominally pure components, there is in general finite adsorption at the Solid-Gas interface. The equilibrium value of γ_{SG} for this interface will be, therefore, lower than its pure-component value γ_{S0} by an experimentally determinable quantity, which is called the *two-dimensional* or *surface pressure* π_{SG} [4, 5]. For the one-component gas phase under the conditions of sufficiently low pressures in contact with an inert solid adsorbent, the value of π_{SG} can be evaluated using the adsorption isotherm for the vapour of the liquid on the solid surface:

$$\pi_{SG} = \gamma_{S0} - \gamma_{SG}\left(p^*\right) = RT \int_0^{p*} \Gamma^s d \ln p \quad \mathrm{T, P = const} \tag{6.16}$$

where R is the molar gas constant; Γ^s denotes the number of moles of gas adsorbed per unit area of the solid adsorbent related to the equilibrium bulk pressure p in the bulk gas phase, at constant temperature T and pressure P; p^* is the equilibrium pressure at which the actual adsorbed film has been formed on the solid surface: the integration of the adsorption isotherm $\Gamma^s = \Gamma^s\,(p)$ is carried out over a p-range from 0 to p^*. On applying Eq. 6.16 to the solid surface saturated with the vapour, i.e., when the latter forms an equilibrium, physically adsorbed film on the available adsorbent surface at p equal to the saturation vapour pressure p_{sat}, the surface concentration Γ^s and the surface pressure π_{SG} are found to reach their (positive) maximum values, Γ^s_m and π^m_{SG}, respectively.

In the case of solids having relatively small values of surface tension γ_{S0} against vacuum (usually less than 100 mN m^{-1} [2]), the effect of gas adsorption is thought to be of little importance. Polymers and many other solid organic compounds are usually given as examples of this category of substrates. Solid materials for which π^m_{SG} is small for any adsorbate are named the *low-energy solids*. For *high-energy solids* (e.g., mineral oxides, metal sulphides, inorganic salts), the decrease in surface tension due to adsorption is significant [30, 37, 38].

Equations 6.3, 6.15, and 6.16 may be combined to give the Gibbs energy of adhesion between the solid and liquid phases

$$\Delta_{adh}G_{SL} = -\gamma_{LG}\,(1 + \cos\Theta) - \pi^{m}_{SG} \tag{6.17}$$

This is a very useful relation, in which γ_{LG}, $\cos\Theta$, and π^{m}_{SG} can be measured and calculated quite easily and accurately. Therefore, the operating procedures for the adhesion experiment are usually based on Eq. 6.17.

6.2.4 Hydrophobic and Hydrophilic Substances

Commonly the distinction between hydrophobic and hydrophilic substances is based on the analysis of interactions between their molecules and water as a solvent. A more precise classification of liquid and solid substances as hydrophobic and hydrophilic may be constructed basing on the apolar (LW) and polar (AB) components of their surface tensions. This three-parameter approach is of great importance for the understanding of surface behaviour [22, 32, 39, 40]. A non-metallic substance is *hydrophobic* if it interacts with water by exhibiting only LW character. It has very little (or none at all) Lewis acid or Lewis base character. Typical substances at the hydrophobic end have low γ^{LW} surface parameters and their γ^{A} and γ^{B} components are equal to zero. *Hydrophilic* substances have non-zero γ^{LW} components of the surface tension and at least one of their γ^{A} and γ^{B} parameters is significant.

The values of surface tension components that have been derived from the appropriate measurements of the Gibbs energy of adhesion for numerous liquids and solids are listed in Table 6.2. The determination of a set of γ^{A}_{LG} and γ^{B}_{LG} values for probe liquids is based on the choice of the first reference liquid. For this purpose, Van Oss et al. [39] assumed that $\gamma^{A}_{LG} = \gamma^{B}_{LG}$ for water. In consequence, all of acid-base parameters in Table 6.2 are relative to those of water.

6.3 Calorimetry Applied to Evaluate Surface Properties of Solids

The determination of the apolar and polar components of the surface tension of liquids and solids may be a powerful tool for classification of various substances with respect to their hydrophobic-hydrophilic character. In the case of solids, this macroscopic approach provides important information about the potential "global" behaviour of their surfaces against a given environment, however, giving no direct indication in regard with the heterogeneity of the solid surface. In consequence, it cannot replace methods based on the adsorption of probe molecules from the gas phase, but it does complement them by providing a different level of surface scanning.

Table 6.2 Surface tension parameters (in mJ m^{-2}) of some liquids and polymers [23, 32, 39]

Substance	γ^{LW}	γ^{A}	γ^{B}	γ_{S0}/γ_{LG}
Water	21.8	25.5	25.5	72.8
Liquids				
n-Heptane	20.1	0	0	20.1
n-Decane	23.8	0	0	23.8
Chloroform	27.15	3.8	0	27.15
n-Hexadecane	27.5	0	0	27.5
α-Bromonaphthalene	44.4	≈0	≈0	44.4
Methylene iodide	50.8	≈0	≈0	50.8
Ethylene glycol	29.0	1.92	47.0	48.0
Formamide	39.0	2.28	39.6	58.0
Glycerol	34.0	3.92	57.4	64.0
Polymers				
Poly(methylmethacrylate), cast film	39–43	≈0	9.5–22.4	39–43
Poly(vinylchloride)	43	0.04	3.5	43.72
Poly(oxyethylene):				
PEG 6000	45	≈0	66	45
Cellulose acetate	35	0.3	22.7	40.2
Cellulose nitrate	45	0	16	45
Poly(styrene)	42	0	1.1	42

In practice, the experimental procedure is quite long and fastidious referring to the successive determinations of the Gibbs energy of adhesion $\Delta_{adh}G_{SL}$ between a given solid and an apolar or polar liquid, which requires, in accordance with Eq. 6.17, measurement of the surface tension γ_{LG}, contact angle Θ, and vapour adsorption isotherm (to calculate π^{m}_{SG}) for each solid-liquid couple. To make matters worse, the very precise measurement of Θ is possible only for atomically smooth surfaces. Finally, the additive approximation expressed by Eqs. 6.9a, 6.9b and 6.12 is better suited to calculation of the enthalpy term than to that of the free energy, since the interactions may have both mechanical and entropic contributions [41].

The determination of the related surface enthalpy terms H^{s}_{S0} and H^{s}_{LG} from direct calorimetry measurements provides an alternative way to evaluate the hydrophobic-hydrophilic character of a solid surface [38, 42–44], since the following deconvolution procedures may be proposed for the surface enthalpy in analogy with those holding for the Gibbs energy (Eqs. 6.8–6.13a, 6.13b):

- surface enthalpy of a non-metallic solid against vacuum:

$$H^{s}_{S0} = H^{LW}_{S0} + H^{AB}_{S0} = H^{LW}_{S0} + 2\sqrt{H^{A}_{S0} \cdot H^{B}_{S0}} \tag{6.18a}$$

- surface enthalpy of a non-metallic liquid against its equilibrium vapour (or air):

$$H^{s}_{LG} = H^{LW}_{LG} + H^{AB}_{LG} = H^{LW}_{LG} + 2\sqrt{H^{A}_{LG} \cdot H^{B}_{LG}} \tag{6.18b}$$

- Solid-Liquid interfacial enthalpy (*Berthelot principle*):

$$H^{s}_{SL} = H^{LW}_{SL} + H^{AB}_{SL} = H^{s}_{S0} + H^{s}_{LG} + \\ - 2\left(\sqrt{H^{LW}_{S0} \cdot H^{LW}_{LG}} + \sqrt{H^{A}_{S0} \cdot H^{B}_{LG}} + \sqrt{H^{B}_{S0} \cdot H^{A}_{LG}}\right) \tag{6.18c}$$

where H^{LW}_{S0}, H^{LW}_{LG} and H^{AB}_{S0}, H^{AB}_{LG} are, respectively, the apolar (LW) and polar (AB) contributions to the appropriate surface enthalpy; H^{A}_{S0}, H^{A}_{LG} denote the Lewis acid and H^{A}_{S0}, H^{A}_{LG} the Lewis base components of the surface enthalpy ; the H^{LW}_{SL}, H^{AB}_{SL} components refer to the Solid-Liquid interface.

It should be always remembered that the global treatment of surface hydrophobicity-hydrophilicity based on surface and interfacial enthalpies does not include the entropy effects.

For liquids and solids, specific orientation and conformation of *unsymmetrical* molecules (ions) in the interfacial regions result not only in the maximization of their interaction energy, but also yield entropy effects that cannot be neglected. For example, molecular dynamics calculations of the intermolecular potential function points to a predominant orientation of the water dipoles at the Liquid-Gas interface [45]. Other examples are an icelike structuring of water molecules in the vicinity of crystalline solid surfaces [46] and a specific orientation of the alcohol molecules in the interface between a liquid *n*-alkanol and water [47].

Immersional and wetting calorimetry is an important method for studying interactions at the Solid-Liquid interface [48–50], especially in the case of finely divided and porous solids where the direct measurements of contact angle are hardly possible.

6.3.1 Enthalpy Changes in the Thermodynamic Cycle of Immersion-Adsorption–Wetting

Consider a simple experiment in which a clean solid surface (free of adsorbed liquid and vapour impurities) is immersed in an excess of pure liquid (Path 1 in Fig. 6.5). If thermal effects arising from absorption, solubility, and swelling of a solid may be eliminated, the whole enthalpy change on *immersion* is ascribed only to the interface. Sometimes the immersion of a solid in a liquid is accompanied by the formation of an electrical double layer. For mineral oxide-water systems [51, 52], the double-layer effects (i.e., generation of surface charge by protonation or deprotonation of some surface hydroxyl groups, and adsorption of counterions in the Stern or/and diffuse layers) are clearly secondary in comparison with the basic wetting (this contribution is 10–15 % of the total heat effect, at the most).

The total enthalpy change, at constant P and T, is then written as

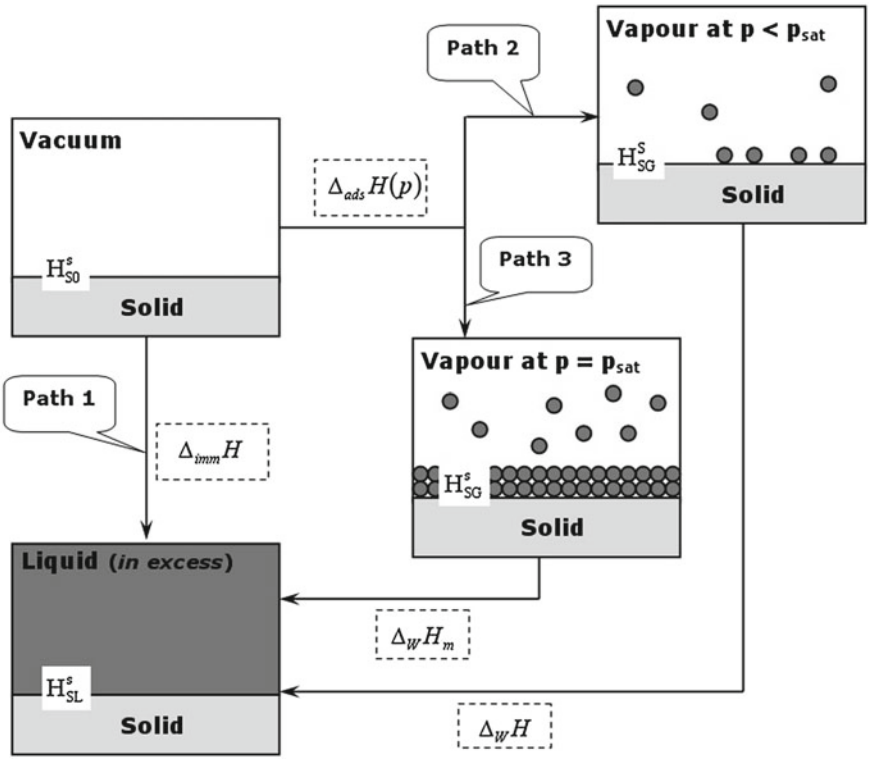

Fig. 6.5 Schematic representation of the difference between immersion (clean solid surface) and immersional wetting (solid surface pre-covered with vapour); the excess of liquid is high enough for the enthalpy change in the bulk liquid phase during adsorption or immersion to be neglected

$$\Delta_{imm} H = A_{SL} \cdot \Delta_{imm} H^* = A_{SL} \left(H^s_{SL} - H^s_{S0} \right) \tag{6.19}$$

where $\Delta_{imm} H$ is called the *enthalpy of immersion*; A_{SL} is the area of the Solid-Liquid interface (often identified with the surface area of a non-microporous solid); H^s_{SL} and H^s_{S0} are the interfacial enthalpies per unit area for the Solid-Liquid and Solid-Vacuum interfaces, respectively.

The experiment of immersion is sometimes performed under completely different conditions. The solid may be first put in equilibrium with the vapour of the immersional liquid at a given equilibrium pressure p (Paths 2 or 3 in Fig. 6.5). The adsorbed gas may be at submonolayer, monolayer or multilayer coverage, depending chiefly on the value of p, but also on the nature of liquid and solid. When the solid is subsequently immersed in the liquid, the measured enthalpy change, called the *enthalpy of immersional wetting*, $\Delta_W H$, will be different from $\Delta_{imm} H$. The various stages of the immersion-adsorption-wetting cycle are shown in Fig. 6.5.

In the case of ideal wetting (this means that the contact angle among the solid, immersional liquid, and vapour of this immersional liquid $\Theta = 0$), the final state is

always the same, irrespective of the path followed. Therefore, one can write for Path 2 in Fig. 6.5:

$$\begin{aligned}\Delta_W H &= A_{SL} \cdot \Delta_W H^* = A_{SL}\left[H^s_{SL} - H^s_{SG}(p)\right] \\ &= \Delta_{imm} H - \Delta_{ads} H(p)\end{aligned} \tag{6.20}$$

where $H^s_{SG}(p)$ is the interfacial enthalpy for the Solid-Gas interface at equilibrium pressure p. The area of the Solid-Gas interface is taken to be identical with A_{SL} (the accessibility of the solid surface does not change when passing from the vapour to the liquid phase).

The enthalpy change

$$\Delta_{ads} H(p) = A_{SL}\left[H^s_{SG}(p) - H^\sigma_{S0}\right] \tag{6.21}$$

refers to the formation of an adsorbed film onto solid in equilibrium with the current gas phase and is therefore named the *enthalpy of adsorption* from vapour.

Since adsorption at the solid-gas interface is in general exothermic, $\Delta_W H$ increases (becomes less negative) monotonously with precoverage from the initial value $\Delta_{imm} H$ at p = 0 to a limiting steady value $\Delta_W H_m$ at $p = p_{sat}$. Examples of such curves are presented in Fig. 6.6.

As far as the enthalpy is concerned, the interface between the saturated (multilayer) film on the solid surface and the equilibrium vapour phase at $p = p_{sat}$ may be identified with the interface between the liquid and its own vapour [49, 54, 55]. Therefore,

$$\Delta_W H_m = A_{SL}\left[H^s_{SL} - H^s_{SG}(p_{sat})\right] = -A_{SL} H^s_{LG} \tag{6.22}$$

where H^s_{LG} is the surface enthalpy of the immersional liquid.

6.3.2 Immersional and Wetting Calorimetry Experiments

Measurements of the enthalpy changes accompanying the immersion and wetting phenomena may be performed with a Tian-Calvet type differential calorimeter [49, 54]. The experimental procedure includes several intermediate stages which may take much time, especially when the wetting enthalpy is measured as a function of the surface coverage by the vapour of the immersional liquid.

The first stage corresponds to the sample preparation during which a solid sample of a given mass is placed in a bulb made of high temperature glass and closed by a brittle tail (Fig. 6.7a). The subsequent sample evacuation and pre-coverage steps are performed with the solid enclosed in this bulb, as represented schematically in Fig. 6.7. The bulb fixed to the end of a glass tube is placed in the outgassing rig where the sample is evacuated at a high temperature to remove all adsorbed impurities from its surface. Then the tube is sealed off a few cm from the bulb end, fixed to the end

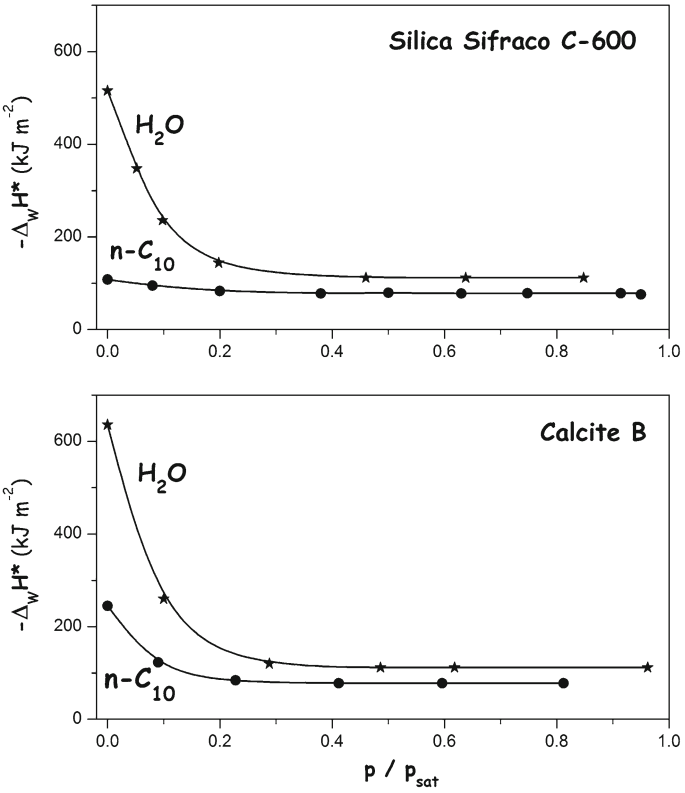

Fig. 6.6 Enthalpy of immersional wetting per unit surface area $\Delta_W H^*$ (taken with the opposite sign) as a function of the surface pre-coverage for two powdered solid samples in two immersional liquids: water (H_20) and *n*-decane (n-C_{10}) [53]

of glass rod and transferred to the calorimeter. Prior to wetting experiment, the solid sample is outgassed in a glass bulb and then brought into contact with the vapour of the immersional liquid at a given pressure and at constant temperature T_M. The equilibrium pressure of the pre-coverage step is controlled by the temperature T_b of the thermostated bath (T_b must be lower than ambient temperature and T_M).

The Tian-Calvet type calorimeter system contains a massive calorimetric bloc which acts as a heat sink (its temperature is constant) and a removable calorimetric cell made of stainless steel and designed to fit in a cylindrical hole inside the calorimetric bloc. The instrumental signal is obtained by measuring the heat flux between the cell and the bloc. The temperature signal is derived from a sensor in the bloc: two symmetrical thermal flux meters, each constructed by a series of thermocouples surrounding a cylindrical hole for the measurement cell. The electric signal delivered by the difference in output voltage of the two flux meters is proportional to the temperature difference θ between the bloc and the cell. The electric signal is directly fed into a computer; the digitized signal is recorded on the computer hard disk and

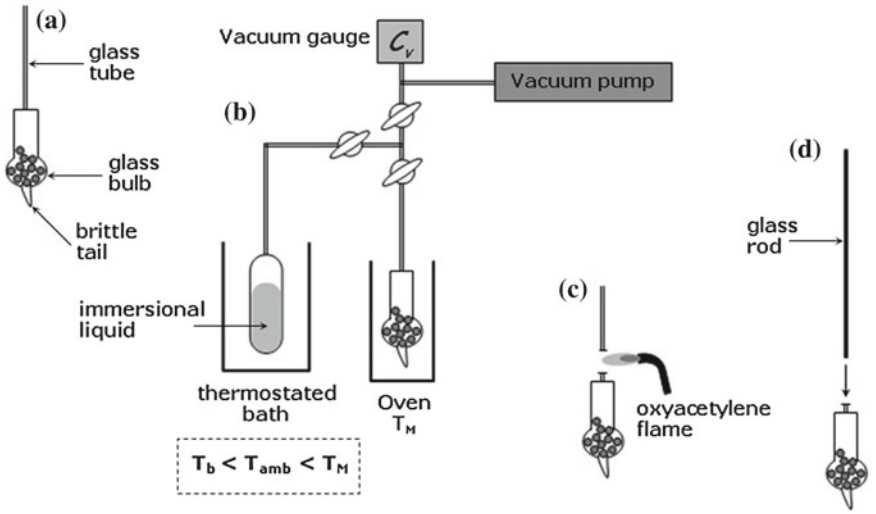

Fig. 6.7 Schematic representation of the sample preparation stage in immersional and wetting calorimetry experiments: (**a**) solid sample enclosed in the glass bulb, (**b**) sample evacuation and pre-coverage, (**c**) sealing the end of the tube, (**d**) assembling

then processed using special software. To control the heat evolvement (or absorption) during each calorimetric run, a pen recorder may be used in analog recording of the signal; here, the vertical pen deflection Δl perpendicular to the direction of feed of the recording chart is proportional to the temperature difference θ. The scheme of the calorimetric cell is shown in Fig. 6.8, together with a trace showing a representative thermal profile for immersion.

According to the theoretical equation of Tian [56–59] for a conduction calorimeter working under ideal conditions (e.g., the thermal delay between the temperature change θ in the calorimetric cell and the response of the sensor is to be neglected), the total heat effect occurring in the calorimetric cell during the time of experiment t_{exp} is given by the following expression:

$$Q_{\text{exp}} = \int_0^{t_{\text{exp}}} P(t)dt = \frac{\lambda}{g}\int_0^{t_{\text{exp}}} \Delta dt + \frac{\Lambda}{g}\int_{\Delta_1}^{\Delta_2} d\Delta \tag{6.23}$$

where *P(t)* is the heat generation (absorption) rate at time t, λ is the thermal conductivity of conducting surface separating the calorimetric cell and the calorimetric bloc, Λ is the heat capacity constant of the calorimetric cell with its content, Δ is the voltage signal produced by the sensor at time t, and g is the proportional constant in the relation $\Delta = g \cdot \theta$; Δ_1 and Δ_2 denote the initial (t = 0) and final ($t = t_{exp}$) sensor indications, respectively. The first term on the right hand side of Eq. 6.23 represents the heat exchange between the bloc and the cell *monitored by the sensor during the*

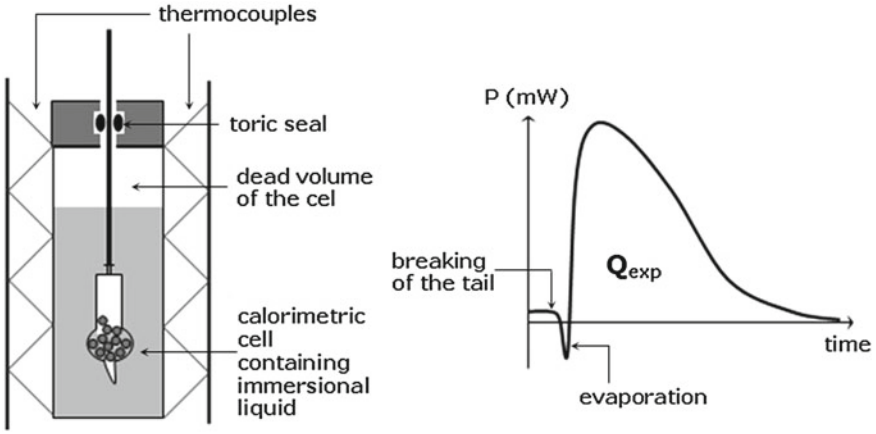

Fig. 6.8 Scheme of the calorimetric cell in a Tian-Calvet type differential calorimeter and a trace showing a representative thermal profile for immersion. Q_{exp} is the overall thermal effect recorded

experiment, whereas the second term corresponds to the temperature rise (decrease) in the calorimetric cell. When the duration of the experiment t_{exp} is chosen such that $\Delta_1 = \Delta_2$ (i.e., the sensor signal returns to the baseline), this second term is always equal to zero and the total heat effect Q_{exp} is determined by integrating the sensor record $\Delta = \Delta(t)$ from Δ_1 to Δ_2:

$$Q_{\text{exp}} = \frac{\lambda}{g} \int_0^{t_{\text{exp}}} \Delta dt = K \int_0^{t_{\text{exp}}} \Delta dt \tag{6.24}$$

The calorimeter constant $K = \frac{\lambda}{g}$ is evaluated during the *calibration run*. Calibration of the area under each thermal peak in the *thermogram* $\Delta = \Delta(t)$ is carried out by dissipating a known amount of energy in the cell (heating through Joule effect). For this purpose, a special calibration resistor is placed in a glass bulb and introduced into the calorimetric cell under the conditions of real experiment. The operator decides both the power dissipated in the resistor $I^2 \cdot R$(I—current flowing through the resistor and R—its resistance) and the duration of the calibration step t_{cal}. The integration of the resulting thermal peak allows the calibration constant K to be calculated as follows:

$$K = \frac{A_{cal}}{I^2 \cdot R \cdot t_{cal}} \tag{6.25}$$

where A_{cal} is the area under the calibration peak.

The standard operating procedure for heat measurement is as follows [49, 54]. The glass bulb containing the solid sample after the sample evacuation (and pre-coverage) stage is introduced into the calorimetric cell, which has been previously filled with

the immersional liquid (usually about 15cc). A large part of the glass rod remains outside when the cell is closed. Complete gas-tightnest of the cell is ensured by a special toric seal placed around the rod. At a given temperature, there is still some vapour of the immersional liquid occupying the dead volume inside the calorimetric cell. Then the calorimeter is left overnight to come to thermal equilibrium, giving a steady baseline on the recorder.

After attaining thermal equilibrium, the glass rod is pushed gently down and the glass tail of the bulb is broken against the bottom side of the cell. The immersional liquid penetrates into the bulb and comes into contact with the solid sample. Thermal effects accompanying the related exothermic and endothermic phenomena induce changes in the temperature inside the calorimetric cell and the concomitant heat flux between the bloc and the cell. The global thermal effect is recorded as a thermal peak A_{exp} which can be integrated and transformed to the heat quantity Q_{exp} (Fig. 6.8) making use of the calibration constant K:

$$Q_{\text{exp}} = K \cdot A_{\text{exp}} \tag{6.26}$$

To extract the net enthalpy of immersion $\Delta_{imm}H$ or net enthalpy of wetting $\Delta_W H$, several correction terms have to be subtracted from Q_{exp}. These correction terms are related to (i) breaking the tail of the glass bulb inside the calorimetric cell, (ii) changes in the dead volume of the calorimetric cell and the bulb during the experiment, (iii) evaporation of the immersional liquid and condensation of its vapour, (iv) decrease in the adsorbent mass during the evacuation step. They may be determined in a blank test recording. Nevertheless, only two of them were found to give a noticeable contribution to the total heat effect [43, 54].

When a given volume of the immersional liquid enters the bulb, the liquid level in the cell is lowered and there is some evaporation of the liquid to equilibrate the vapour pressure in the dead volume. This phenomenon yields an endothermic effect which is proportional to the dead volume V_0 of the bulb:

$$Q_{cor} = -V_0 \cdot \Delta_{vap}h \tag{6.27}$$

where $\Delta_{vap}h$ is the evaporation enthalpy per unit volume measured in a blank run with an empty bulb (without a solid sample). The values of $\Delta_{vap}h$ obtained for some immersional liquids are given in Table 6.3.

The second correction term of great importance concerns the loss of the adsorbent mass during the evacuation step [43]. Prior to immersion and wetting measurements, the solid sample is subjected to thermal treatment in the glass bulb under vacuum. The total mass of the sample certainly decreases, depending on the amount of liquid and vapour impurities pre-adsorbed on its surface. The present experimental procedure does not allow the actual mass to be determined precisely because the bulb containing the sample cannot be weighed at the end of the outgassing process. In consequence, the measured enthalpy values may be underestimated, especially if the weight loss is significant (e.g., hydrophilic solids with a high specific surface area may contain much water vapour adsorbed on the surface). The most reliable way of quantifying

Table 6.3 Enthalpies of evaporation per unit volume $\Delta_{vap}h$ for selected immersional liquids, as measured in a blank calorimetry run with an empty bulb [60]

Immersional liquid	Δ_{vap} h(mJ cm^{-3})
n-heptane	126
Isooctane	59
Chloroforme	254
Benzene	249
Water	78
Formamide	24
l-butanol	160

the mass decrease is to carry out the outgassing procedure separately under the same conditions as those used in the calorimetry experiment (the outgassed sample may be weighed and the mass difference calculated).

Finally, the enthalpy change upon immersion of a solid in a given liquid per unit surface area of the solid is calculated as follows:

$$\Delta_{imm}H^* = \frac{\Delta_{imm}H}{A_{SL}} = -\frac{1}{m_S \cdot S}\left(Q_{\exp} - V_0 \cdot \Delta_{vap}h\right), \text{ in mJ m}^{-2} \qquad (6.28)$$

where m_S and S are the mass and the specific surface area of the "dry" solid sample, respectively.

6.3.3 Hydrophilic-Hydrophobic Series and Harkins-Jura Method

Using approximation Eq. 6.18c to express the interfacial enthalpy H^s_{SL} in terms of the apolar (LW), Lewis acid (A) and Lewis base (B) components of the surface enthalpy for the solid and immersional liquid, the final explicit form for the enthalpy of immersion is as follows [42–44]:

$$\Delta_{imm}H = H^s_{LG} - 2 \cdot \left(\sqrt{H^{LW}_{S0} \cdot H^{LW}_{LG}} + \sqrt{H^{A}_{S0} \cdot H^{B}_{LG}} + \sqrt{H^{B}_{S0} \cdot H^{A}_{LG}}\right) \qquad (6.29)$$

Provided that the surface enthalpy components for the liquids, i.e., H^{LW}_{LG}, H^{A}_{LG}, H^{B}_{LG} are known, the apolar (H^{LW}_{S0}), Lewis acid (H^{A}_{S0}), and Lewis base (H^{B}_{S0}) contributions to the surface enthalpy of solids can be derived from measurements of the enthalpy of immersion. At least one apolar liquid and two polar liquids must be used. The values of H^{LW}_{LG}, H^{A}_{LG}, H^{B}_{LG} for selected immersional liquids, i.e., apolar *n*-heptane, bifunctional water, and monofunctional basic formamide, are given in Table 6.4.

The examples of the use of apolar *n*-heptane, bifunctional water, and monofunctional basic formamide to study the surface hydrophobic-hydrophilic character of several solids are shown in Figs. 6.9, 6.10, and 6.11 [38, 43, 44, 60]. *n*-heptane

Table 6.4 Surface enthalpy components for *n*-heptane, water and formamide [43]

Liquid	H_{LG}^{LW} mJ m^{-2}	H_{LG}^{A} mJ m^{-2}	H_{LG}^{B} mJ m^{-2}	H_{LG}^{s} mJ m^{-2}
n-heptane	54.5	0	0	54.5
Water	35.0	41.5	41.5	118.0
Formamide	55.6	3.25	56.4	82.6

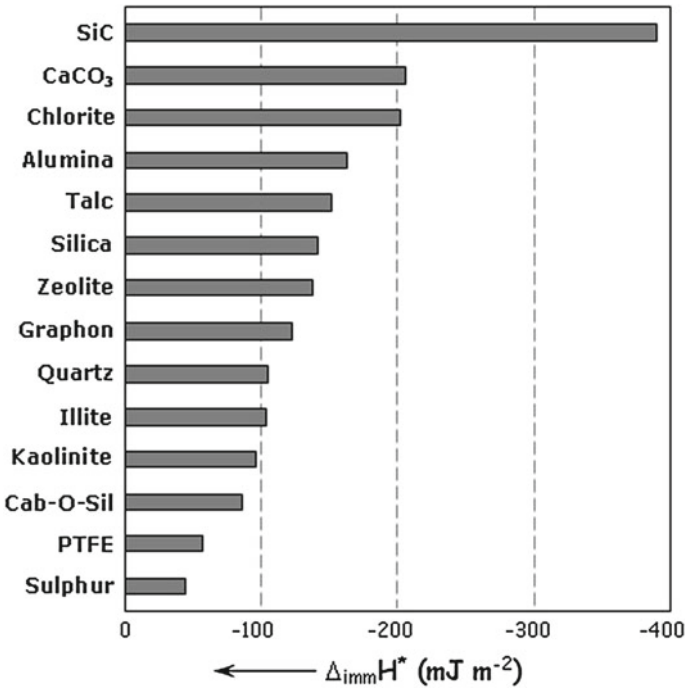

Fig. 6.9 Enthalpy of immersion per unit surface area of the solid $\Delta_{imm} H^*$ for several solid materials in *n*-heptane

and formamide (Merck HPLC grade materials with purity exceeding 99 %), were additionally dried with 3A zeolite molecular sieves. *This purification procedure to remove even traces of water from organic solvents is of great importance and strongly recommended for all immersion experiments*. Water was deionised and purified with a Millipore Super Q System.

The immersion experiment was repeated three times for each solid sample and the average value taken. The amount of immersional liquid penetrating into the glass bulb upon immersion was determined by weighing the bulb after every run (to evaluate the correction term 6.27). Reproducibility of the calorimetry measurement in regard to the enthalpy of immersion expressed by weight of the solid was within 3 %. To obtain the enthalpy of immersion per unit surface area of the solid $\Delta_{imm} H^*$,

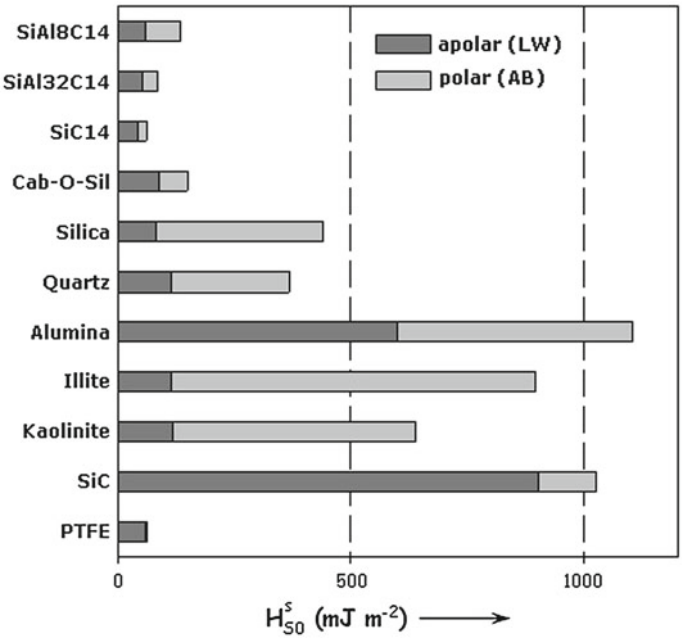

Fig. 6.10 Apolar (LW) and polar (AB) contributions to the surface enthalpy for a series of solids, as derived from measurements of the enthalpy of immersion $\Delta_{imm}H^*$ of each solid in *n*-heptane, water and formamide

the experimental enthalpy values were divided by the corresponding BET specific surface areas (the adsorption model of Brunauer, Emmet, and Teller applied to the experimental results of gaseous nitrogen adsorption at 77 K taking a cross sectional area of 0.162 nm^2 per N_2 molecule), i.e., $S = S_{BET}$. Finally, each solid was separately outgassed under the same conditions as those used in the immersion experiment with the purpose of quantifying the mass of dried sample. Then the immersion data were corrected for the mass loss during outgassing (following Eq. 6.28). In consequence of all these additional steps, the uncertainty in the enthalpy determination increased, but was, on average, better than 5 %.

Figure 6.9 shows the experimental values of $\Delta_{imm}H^*$ for one series of solids immersed in *n*-heptane. Here the interfacial phenomenon involves only van der Waals interactions between the immersional liquid and the solid, irrespective of the actual *surface hydrophobic-hydrophilic balance* (SHB) of the latter. Based on the enthalpy results obtained, it is possible to classify these solids with respect to hydrophobic character of their surface.

According to the criteria of hydrophobicity given in Sect. 6.2.4, the most hydrophobic substance has the lowest H^{LW}_{S0} (more precisely γ^{LW}_{S0}) surface parameter. Therefore, its enthalpy of immersion in *n*-heptane per unit area of the solid should have the smallest value. Among the solids presented in Fig. 6.9, only sulphur and

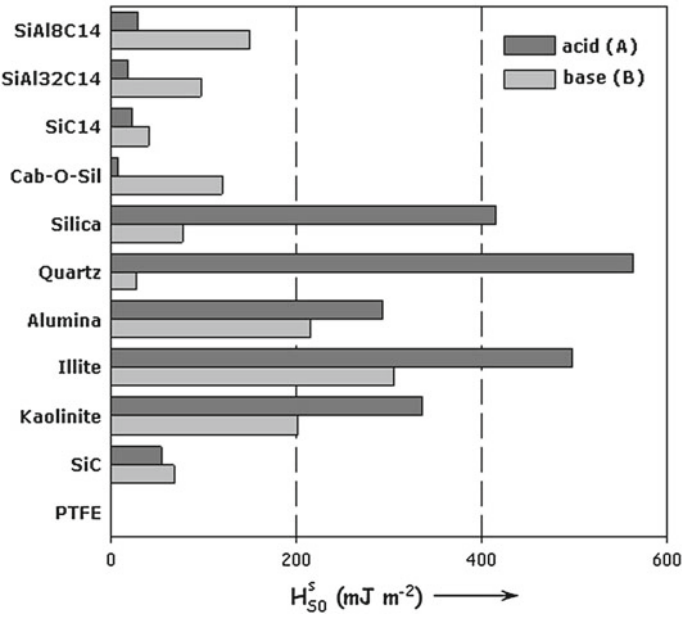

Fig. 6.11 PLewis acid (**A**) and Lewis base (**B**) contributions to the surface enthalpy for a series of solids, as derived from measurements of the enthalpy of immersion $\Delta_{imm}H^*$ of each solid in *n*-heptane, water and formamide

polytetrafluoroethylene (PTFE) appear clearly at the hydrophobic end. Such mineral oxides as clay minerals with a lamellar structure (kaolinite, illite, talc, chlorite), precipitated amorphous SiO_2 (silica), crystalline SiO_2 (quartz), amorphous Al_2O_3 (alumina), or crystalline aluminosilicates (zeolite) are known to be more or less hydrophilic (commonly, the presence of numerous functional groups with a polar character in the surface of these materials is advanced as a typical argument). The comparison of the $\Delta_{imm}H^*$ values reported in Fig. 6.9 indicates that the overall intensity of Lifshitz-Van der Waals interactions between apolar *n*-heptane and a unit area of the solid surface is not the same for various solids. This means that all microscopically unsaturated structures which may be encountered in solid surfaces differ also in "apolar character" and, consequently, the apolar (LW) component to the surface enthalpy H^{LW}_{S0} is a solid-dependent parameter. Surprisingly, non-porous graphitized carbon black (Graphon), regarded as a weakly hydrophilic solid, yield $\Delta_{imm}H^*$ greater than those of kaolinite, illite, or quartz which certainly possess more polar groups per unit surface area. Of course, it may be argued that graphitic basal planes in the surface of Graphon act as electron pair donors, thereby participating in π-EPD/π-EPA or π-complexation interactions with the foreign molecules. Nevertheless, it is more reasonable to evaluate both the apolar (LW) and the polar (AB) components to the surface enthalpy H^s_{S0} in order to compare the differences in the SHB among various solids.

It is worth noting that any arrangement of solid surfaces by hydrophobic character, as well as any ordering or ranking of solids in regard to their SHB may be used only for comparative purposes and do not give the "absolute ranking position" of a given solid within the class of hydrophobic and hydrophilic substances.

Figure 6.10 shows examples of several hydrophobic and hydrophilic solids, together with their H_{S0}^{LW} and H_{S0}^{AB} parameters obtained on the basis of Eq. 6.29. SiC14, SiAl32C14, and SiAl8C14 are mesoporous silica-based materials of the MCM-41 type prepared by a surfactant-assisted synthesis and doping with aluminium (e.g., abbreviation "SiAl32" refers to a molar Si-to-Al ratio of 32). Only PTFE is a clearly hydrophobic substance since it has low H_{S0}^{LW} and zero H_{S0}^{AB} component. Amorphous fumed SiO_2 (Cab-O-Sil) and mesoporous MCM-41 silica or aluminosilicates can be reckoned among low-energy solids possessing surfaces with a weakly hydrophilic character. For high-energy solids with surface enthalpy H_{S0}^{s} greater than 500 mJ m^{-2}, the ratio between H_{S0}^{AB} and H_{S0}^{LW} varies from 7 (illite) to 0.2 (SiC); alumina is characterized by an intermediate SHB value of 0.8.

Figure 6.11 illustrates the Lewis acid-base character of the solid surfaces presented in Fig. 6.10. The Lewis acid H_{S0}^{A} and Lewis base H_{S0}^{B} components are related to the polar (AB) contribution to the surface enthalpy of each solid: $H_{S0}^{AB} = 2\sqrt{H_{S0}^{A} \cdot H_{S0}^{B}}$. Crystalline SiO_2 (quartz) and, to a smaller extent, amorphous precipitated SiO_2 (silica) provide strongly acidic surfaces, whereas the surfaces of MCM-41 mesoporous silicas and Cab-O-Sil have a predominantly basic character.

The *Harkins-Jura method* for estimating the specific surface area S_{HJ} of a solid available to a given immersional liquid is based on Eq. 6.22 [20, 54, 55]. In practice, water is by far the most frequently used liquid because of the small size of its molecules (the van der Waals diameter of a water molecule is about 0.28 nm). The specific surface area of a hydrophilic solid is thus calculated as follows:

$$S_{HJ} = -\frac{\Delta_W H_m}{m_S \cdot H_{LG}^{s}} = -\frac{\Delta_W h_m}{H_{LG}^{s}} = -\frac{\Delta_W h_m}{0.118} \tag{6.30}$$

where $\Delta_W h_m$, expressed in J g^{-1}, denotes the minimum value of the specific enthalpy of immersional wetting, i.e., wetting enthalpy per unit mass of the solid sample $\Delta_W h_m = \frac{\Delta_W H_m}{m_S}$. This enthalpy value is determined from the plot of $\Delta_W h$ against the relative pressure $\frac{p}{p_{sat}}$ at which surface pre-coverage with water vapour has been carried out (Fig. 6.12).

The application of the above procedure is limited only to non-microporous materials, for which the solid surface area available to water is equal to the area of the interface between the adsorbed water film on the surface and the equilibrium water vapour phase. It is always necessary to check the condition of the ideal wetting. Water does not spread on hydrophobic surfaces, like the surface of the Graphon, and the value of $\Delta_W H$ decreases (becomes more negative) as the surface adsorbs more water vapour [20]. This proves that the empty surface has less affinity for water than has the surface of the adsorbed water. Equations 6.22 and 6.30 cannot be applied to such a system.

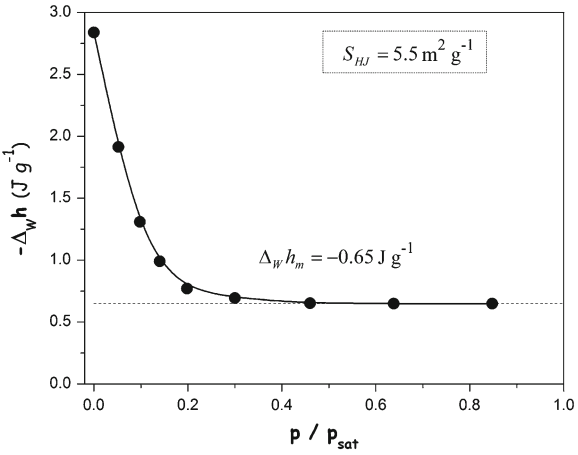

Fig. 6.12 Specific enthalpy of immersional wetting $\Delta_W h$ (taken with the opposite sign) in water for silica SIFRACO C-600 pre-covered with water vapour as a function of the relative vapour pressure [60]. The resulting HJ specific surface area is also given ($S_{HJ} = 5.5\ m^2 g^{-1}$)

6.4 Enthalpy Changes Accompanying Competitive Adsorption from Dilute Solution

The *competitive aspect* of the phenomenon, nowadays commonly accepted, shows up most clearly in adsorption from concentrated solutions (e.g., mixtures of completely miscible liquids) [6]. In dilute solution, only a very detailed analysis of the adsorption system may reveal that the phenomenon is indeed competitive. In this context, calorimetry has proven very useful in studying the competitivity of adsorption from dilute solution onto solids.

The *driving force* of competitive adsorption from binary solution onto solids is a macroscopic outcome of intermolecular forces belonging to the following categories: (i) interactions of the solute and the solvent with the solid surface, (ii) interactions among the solution components in the interfacial region, and (iii) solute—solvent, solvent—solvent, and solute—solute interactions in the bulk solution. In numerous adsorption systems, a considerable enhancement of the amount adsorbed is often the result of *co-operative effects* involving various interaction types. The most spectacular examples are related to the adsorption of amphiphilic substances (e.g., surfactants and polymers) that exhibit reduced water solubility [61, 62]. The general behaviour of amphiphilic molecules in aqueous solution reflects the opposing tendencies of the hydrophobic portion of the molecule to escape from the aqueous environment while the hydrophilic moiety tends to remain immersed in the water. Depending on the surface hydrophilic-hydrophobic character of the solid particules immersed in the solution, such molecules can be compelled to accumulate in an oriented fashion at the Solid-Solution interface or to associate between themselves within the solution (i.e., *micellization*). Aggregation of surfactant units both at the Solid-Solution

interface and in the bulk solution is mainly governed by *hydrophobic bonding*, which refers to the apparent attraction between hydrophobic moieties being much stronger in water than it is in non-aqueous media [26, 61, 63]. Hydrophobic bonding is a typical example of the so-called thermodynamic interactions having both mechanical and entropic contributions.

Adsorption experiment may be carried out in two different ways: as (1) *immersion* of a dry adsorbent in a binary solution of a given composition or (2) *displacement* of the solvent from the solid-solvent interface by the adsorbing solute supplied in a stock solution [6, 64, 65]. Additionally, the effects of displacement are determined either in a batch displacement or in a flow displacement experiment. Depending on the experimental procedure applied, the accompanying changes of macroscopic properties differ to a great extent. The amount adsorbed and enthalpy change on adsorption can be precisely defined in operational terms by considering models of the immersion and displacement experiments.

6.4.1 Thermal Properties of Dilute Solutions

A dilute solution typically means a solution containing no more than about 10^{-2} mol l^{-1} of solute. For the solvent, a convenient reference state is its own pure liquid state at 1 bar. However, a more useful *reference state for the solute*, including aqueous solutions of electrolytes and non-electrolytes, is that of *infinite dilution in the solvent* [66, 67].

The general form of the chemical potential of a real solute in a binary solution of non-electrolytes is therefore [66, 67]

$$\mu_2 = \mu_2^* + RT \ln\left(\frac{m_2}{1} \cdot f_2\right), \; f_2 \to 1 \text{ as } m_2 \to 0 \tag{6.31a}$$

$$\mu_2 = \mu_2^* + RT \ln\left(\frac{c_2}{1} \cdot f_2\right), \; f_2 \to 1 \text{ as } c_2 \to 0 \tag{6.31b}$$

where μ_2^* is the standard chemical potential of the solute; m_2 is the molality of this component and c_2 the corresponding molar concentration. The unity on the right-hand side is written to remind the reader that the molality (the molar concentration) is expressed in mol kg^{-1} (mol L^{-1}), whereas the activity is dimensionless. The employment of concentration units is often discouraged because the concentration of a given solution varies with temperature, while the molality is independent of temperature. The latter also allows the composition determination to be achieved with greater precision, since any solution may be prepared by weighing the solute and solvent, or the stock solution and solvent (dilution of the stock solution).

The interactions between ions contained in an ionic solution are so strong that the solution approaches ideality in the sense of obeying Henry's law only at very low values of total ion concentration, usually less than 10^{-3} mol kg^{-1} [68, 69]. In precise considerations, ion activities must be used. In the case of strong electrolytes

in aqueous solution, the total Gibbs energy (and any other extensive property) of the solute is the sum of the partial molar Gibbs energies for the individual ions produced by the solute. Suppose that a strong electrolyte M_pX_q dissociates into ions according to the following reaction

$$M_pX_q = p \cdot M^{z+} + q \cdot X^{z-} \quad , \quad p \cdot z_+ = q \cdot z_- \tag{6.32}$$

where p and q are the number of ions of M and X type, respectively; z_+ and z_- represent the valencies of the respective ions (positive number for cations and negative number for anions). The chemical potential of the solute j in a real solution may be written as [68, 69]

$$\mu_j = \mu_j^* + (p+q)RT \ln m_\pm + (p+q)RT \ln f_\pm \tag{6.33a}$$

where the mean ionic molality $m_\pm$ and the mean ionic activity coefficient $f_\pm$ are defined as follows:

$$m_\pm = \left[(m_+)^p (m_-)^q\right]^{\frac{1}{p+q}} \quad \text{and} \quad f_\pm = \left[(f_+)^p (f_-)^q\right]^{\frac{1}{p+q}} \tag{6.33b}$$

Now both types of ion share equal responsibility for the non-ideality.

Strong and long-range Coulombic forces acting between ions are primarily responsible for the departures from ideality (the activity coefficients are lowered) and dominate all other contributions. The effect has been evaluated in the Debye-Hückel theory and there exist several equations, which are useful in estimating the mean activity coefficient [68, 69]. The latter is related to the *ionic strength* of the solution:

$$I = \frac{1}{2} \sum_j z_j^2 \cdot m_j \tag{6.34}$$

where the sum extends over all ions present in the solution; m_j is the molality of the jth ion. For example, the value of $f_\pm$ can be calculated from the Debye-Hückel limiting law

$$\log f_\pm = -A \, |z_+ \cdot z_-| \cdot \sqrt{\frac{I}{1}} \tag{6.35a}$$

where A is the dimensionless constant characteristic of the solvent at the specified temperature and pressure ($A = 0.5085$ for an aqueous solution at 298.15 K [68, 69]).

The approximation (6.35a) is in good agreement with the experiment at very low molalities: less than 0.01–0.001 mol kg^{-1}, depending on charge type (the range of validity becomes narrower when divalent or multivalent ions are present in the solution). Nevertheless, when the departures from the experimental results are large, the activity coefficient may be estimated from the extended Debye-Hückel law

$$\log f_{\pm} = -\frac{A\,|z_+ \cdot z_-| \cdot \sqrt{\frac{I}{1}}}{1 + B \cdot \sqrt{\frac{I}{1}}} \tag{6.35b}$$

where B is an adjustable empirical parameter (which involves numerical factors, the dielectric constant, the temperature and the mean distance of nearest approach of the ions [68, 69]).

In thermodynamics of solutions, the partial molal quantity and the apparent molal quantity for a component are usually defined [66]. In the properties of enthalpy, one deals with quantities which cannot be measured in an absolute sense. It is thus necessary to use a reference state from which to make the evaluations. Since the state of infinite dilution of the solute in the solvent is taken as reference, the specification of the composition of the solution by means of the molality m_2 of the solute is consequently most convenient for the calculation of enthalpy.

If the enthalpy H of a two-component solution is expressed as a function of the composition, at constant pressure and temperature, the *partial molal enthalpy* $\overline{h}_2$ for the solute is defined as the rate of change of the enthalpy H with change in the number of moles of this component, with the number of moles of the solvent being held constant; that is

$$\overline{h}_2 = \left(\frac{\partial H}{\partial n_2}\right)_{T,P,n_1} \tag{6.36}$$

The basic partial molal equation for the total enthalpy of the binary solution is

$$H = \sum_{j=1}^{2} n_j \cdot \overline{h}_j \quad , \mathrm{T, P} = \mathrm{const} \tag{6.37}$$

where n_j is the number of moles of the jth component in the solution.

The partial molal enthalpy of the solute in a solution may not always be conveniently measured experimentally with the required precision. Usually, the apparent molal property for the solute is most used in connection with dilute solutions. For a solution of two components, the *apparent molal enthalpy* of the solute Φ_H is

$$\Phi_H = \frac{\Delta H}{n_2} \quad , \ \mathrm{T, P} = \mathrm{const} \tag{6.38}$$

whereΔH is the enthalpy change produced when the solution is formed by adding n_2 moles of solute to n_1 moles of pure solvent.

The total enthalpy of the solution may be conveniently expressed in terms of the apparent molal enthalpy of the solute as

$$H = \frac{M_1}{10^3} m_2 \Phi_H + M_1 h_1^* \tag{6.39}$$

where M_1 is the total mass of the solvent in the solution and h_1^* is the specific enthalpy (per unit mass) of the pure solvent.

In the infinitely dilute solution, the value of the molal enthalpy for the solute is identical with the corresponding value of the partial molal enthalpy, namely

$$\Phi_H(\infty) = \overline{h}_2(\infty) \quad \textit{at infinite dilution} \tag{6.40}$$

For any other solution, the partial molal enthalpy of the solute referred to the state of infinite dilution may be calculated if the apparent molal enthalpy is known as a function of the composition. In such a case,

$$\overline{h}_2 - \overline{h}_2(\infty) = \Phi_H - \Phi_H(\infty) + m_2 \frac{d\left[\Phi_H - \Phi_H(\infty)\right]}{dm_2} \tag{6.41}$$

It frequently happens that the apparent molal enthalpy is expressible as an appropriate function of the composition in order to obtain a curve which does not depart greatly from a simple function and which has not too great a curvature over the given range. For aqueous solutions of strong electrolytes, the value of Φ_H is sometimes linear with the square root of the molality, over a given range of molality [68]. Converting Eq. 6.41 to the slope of Φ_H against $\sqrt{m_2}$, one obtains

$$\overline{h}_2 - \overline{h}_2(\infty) = \Phi_H - \Phi_H(\infty) + \frac{1}{2}\sqrt{m_2}\frac{d\left[\Phi_H - \Phi_H(\infty)\right]}{d\left(\sqrt{m_2}\right)} \tag{6.42}$$

The difference $\Phi_H - \Phi_H(\infty)$, called the *relative apparent molal enthalpy*, is the quantity most readily evaluated from calorimetric measurements of enthalpies of dilution. For the following reaction of dilution:

$$\left(\frac{\mathrm{M}_1^0}{10^3}\mathrm{m}_2^0 \times \text{solute} + \mathrm{M}_1^0 \times \text{solvent}\right)(\text{liq}) + \left(\infty - \mathrm{M}_1^0\right) \times \text{solvent(liq)}$$
$$\rightarrow \left(\frac{\mathrm{M}_1^0}{10^3}\mathrm{m}_2^0 \times \text{solute} + \infty \times \text{solvent}\right)(\text{liq}) \tag{6.43}$$

the change in the enthalpy is equal to

$$\Delta_{dil}H\left(m_2^0 \rightarrow \infty\right) = -\frac{M_1^0}{10^3}m_2^0\left[\Phi_H - \Phi_H(\infty)\right] \tag{6.44}$$

where M_1^0 denotes the initial mass of the solvent and m_2^0 the initial molality of the solute. Values of the relative apparent molal enthalpy may be obtained by measuring enthalpy changes $\Delta_{dil}H$ for the dilution of a given stock solution of molality m_2^0 to a series of different molalities m_2,

$$\Delta_{dil}H\left(m_2^0 \rightarrow m_2\right) = -\frac{M_1^0}{10^3}m_2^0\left[\Phi_H\left(m_2^0\right) - \Phi_H\left(m_2\right)\right] \tag{6.45}$$

and suitably extrapolating the curve $\Delta_{dil}H = \Delta_{dil}H\left(m_2\right)$ to infinite dilution.

6.4.2 Macroscopic Description of Competitive Adsorption

Compared to interfacial phenomena occurring at the boundary between a solid and a pure liquid, Coulombic forces constitute an additional type of interaction that should be taken into account when analysing the adsorption phenomenon at an electrified interface from solution containing free charges (ions and electrons) and associated charges (dipolar molecules and polarised atoms). In such systems, there is a variation in the charge density across the interfacial region and an *electric double layer* forms [70–72] (the Gouy-Chapman-Stern-Grahame model of the EDL is shown in Fig. 6.13).

Transfer of the individual ionic species between the interface and the solution leads to a thermodynamic equilibrium at which *the interface is electrically neutral as a whole* (and so is the equilibrium bulk solution).

Based on isothermal reversible work done in transferring one mole of ions of the solute 2 from infinity (*in vacuum*) to a given part in the interfacial region which has a non-zero average charge and where the electrostatic potential is Ψ, it is possible to define the so-called *electrochemical potential* of component 2 [70]

$$\mu_2 = \mu_2 + z_2 \cdot \mathsf{F} \cdot \Psi \quad , \mathrm{T}, \mathrm{P} = \mathrm{const} \tag{6.46}$$

where μ_2 is the chemical potential of the solute, z_2 is the valency of an ion of the solute, and F is the Faraday constant (F is a product of the Avogadro number L and the elementary charge e). If the transferred species carries no net charge, i.e., $z_2 = 0$, the electrochemical potential $\overline{\mu}_2$ becomes simply the chemical potential μ_2. The new potential $\overline{\mu}_2$ is now the quantity which must have *the same value everywhere in the system for thermodynamic equilibrium to be established* at constant temperature and pressure [70].

According to the surface phase model (cf., Sect. 6.2.1), when the concentrations of the components of the binary solution β in the solid phase α are to be neglected, i.e., $c_j^{\alpha} = 0$ (j =1,2), the *interfacial concentration* Γ_j^s of component j is given by [6, 8]

$$\Gamma_j^s \equiv \frac{n_j^s}{A} = \tau^s \cdot c_j^s = \frac{1}{A}\left(n_j - c_j^{\beta}V^{\beta}\right), \quad (\mathrm{j} = 1, 2) \tag{6.47}$$

where c_j^{β} and c_j^s are the concentrations (in moles per unit volume of solution) of the jth component in the bulk solution β and in the surface phase of thickness τ^s and surface area A; V^{β} represents the volume of the bulk phase β in the surface phase model. The subscripts 1 and 2 denote the solvent and the solute, respectively; this notation will be used throughout the present chapter.

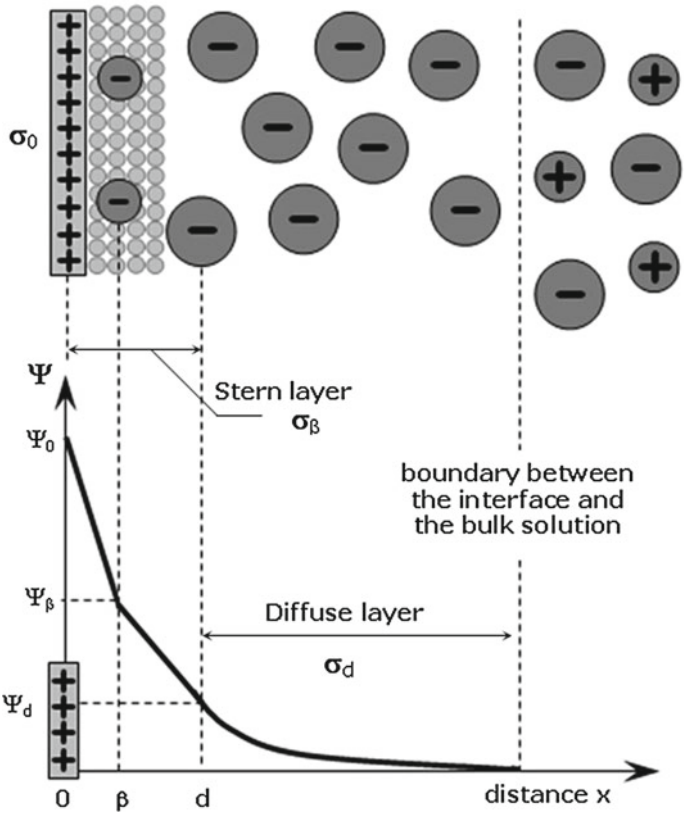

Fig. 6.13 Schematic representation of the structure of the electric double layer according to the Gouy-Chapman-Stern-Grahame model and variations of the interfacial electric potential Ψ across the interfacial region. By convention, the potential Ψ of any part of the electrified interface is defined with respect to the solution at infinite distance where the average charge is zero. The distance x is measured in reference to the position of a plane containing *solid surface charge* σ_0. The solution part of the EDL with an excess of counter-ions is composed of two distinct regions: a thin *Stern layer* (next to the surface charge plane) including specifically adsorbed (Coulombic and other non-electrostatic forces) counter-ions which may be partially dehydrated and an extended *diffuse layer* where the hydrated counter-ions are distributed non-uniformly according to the combined action of electrostatic forces and random thermal motion. Electroneutrality of the charged interface requires that $\sigma_0 + \sigma_\beta + \sigma_d = 0$; σ_β and σ_d represent the charge densities of the Stern and diffuse layers, respectively [70]

The case of $\Gamma_j^s > 0$ defines the preferential *adsorption* of component j at the Solid-Liquid interface. In a given adsorption system, the interfacial concentration Γ_j^s is a function of both the actual composition of the bulk solution (i.e., c_1^β and c_2^β) and the relative affinities of the components for the interface (chiefly, for the solid surface). Contrary to the case of adsorption at the Solid-Gas interface, the interfacial region is always completely filled with molecules of solvent and solute. Further

consideration will be based on the *preferential adsorption* of solute against solvent, taking the interface between the solid and the pure solvent as a starting point for thermodynamic treatment of competitive adsorption. In such a case, the adsorption equilibrium can be represented schematically as follows:

$$\mathrm{r} \cdot \mathrm{n}_2^{\beta} + \mathrm{n}_1^{\mathrm{s}} \rightleftarrows \mathrm{r} \cdot \mathrm{n}_2^{\mathrm{s}} + \mathrm{n}_1^{\beta} \tag{6.48}$$

where r is the *molar ratio of displacement* introduced to account for unequal molecular sizes of both the components. It is worth noting that the same formalism may be applied in the treatment of adsorption at the interface between a binary liquid solution and a gas phase.

When the pure liquid phase is replaced by a binary liquid solution β, the interfacial tensions γ_{SL} and γ_{LG} will be lowered owing to the preferential adsorption of the solute at the Solid-Liquid and Liquid-Gas interface. The relationship between the extent of adsorption and the resulting interfacial (surface) tension change (T, P = const) is given by the following equation developed by Guggenheim [6, 8]

$$\begin{aligned} d\gamma &= -\left[\Gamma_2^s - \Gamma_1^s\left(\frac{c_2^{\beta}}{c_1^{\beta}}\right)\right] d\mu_2 = -\left[\Gamma_2^s - \Gamma_1^s\left(\frac{n_2^{\beta}}{n_1^{\beta}}\right)\right] d\mu_2 \\ &= -\left[\Gamma_2^s - \left(\frac{M_1^s}{10^3 A}\right) \cdot m_j^{\beta}\right] d\mu_2 \end{aligned} \tag{6.49}$$

where μ_2 is the chemical potential of solute in the bulk solution β: at equilibrium, μ_2 is the same throughout the system; when expressing the solution composition in terms of the molality m_2^{β} (in moles per kilogram of solvent), M_1^s is the mass of solvent in the surface phase. It is worth noting that Eq. 6.49 is formally analogous to the Gibbs adsorption isotherm for a binary solution [6, 8].

6.4.3 Competitive Adsorption Measurements

The amount of solute molecules preferentially adsorbed from dilute solution onto a given solid can be measured in a separate adsorption experiment, independently of the calorimetry measurement. In the case of the titration calorimetry procedure, this is even the only possibility to determine the amount adsorbed after each injection step and subsequently calculate the differential molar enthalpy of adsorption. The main difficulty here, contributing to a significant uncertainty of the experimental result, is related to *the necessity of reproducing strictly the same experimental conditions in both types of experiment* (i.e., the same solid surface-to-solution volume ratio, evolution of the pH and ionic strength in the equilibrium bulk solution, charging behaviour of the solid surface, etc.).

The quantity of adsorption is usually measured by means of the *solution depletion method* [6] in glass stoppered tubes or flasks (Fig. 6.14). A known mass of the solid

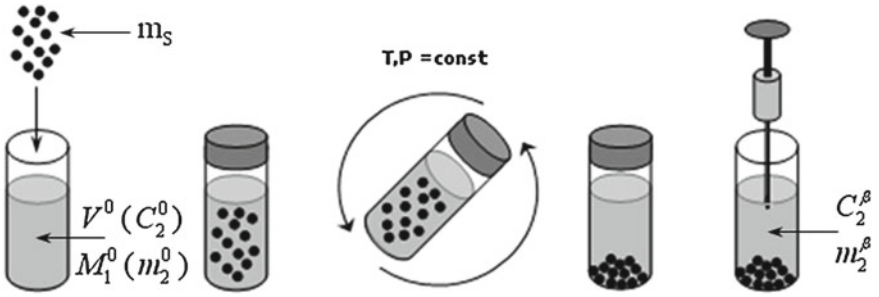

Fig. 6.14 Schematic representation of the solution depletion technique. The solid particles are separated from the supernatant solution by centrifugation or filtration. The way of calculating the quantity of adsorption depends on whether the solution composition is expressed in terms of molality m_2^β or the molar concentration C_2^β

sample and a certain amount of dilute binary solution of given composition are put into each tube or flask, and the mixture is shaken at a constant temperature (e.g., in a thermostated box) for a period of time necessary to attain the adsorption equilibrium. Then the solid particles are separated from the supernatant by centrifugation or filtration (special attention should be paid during fitration to avoid the retention of the solute on the filtration membrane). After centrifugation when the solid particles have been precipitated at the bottom of the tube or flask, a sample of the supernatant may be collected by using a special syringe with a long needle. The equilibrium composition of the supernatant is determined by referring to the appropriate analytical technique (UV spectroscopy, refractometry, total carbon analysis, etc).

The amount n_2^s of solute adsorbed at the Solid-Liquid interface is calculated by means of the following formulas:

$$\frac{n_2^s}{m_S} = \frac{V^0}{m_S}\left(C_2^0 - C_2^\beta\right) \quad \text{or} \quad \frac{n_2^s}{m_S} = \frac{M_1^0}{10^3 \cdot m_S}\left(m_2^0 - m_2^\beta\right) \tag{6.50}$$

where m_S is the mass of the solid sample in a given tube or flask; C_2^0 and m_2^0 are respectively the molarity and the molality of the initial solution (before adsorption); C_2^β and m_2^β are respectively the molarity and the molality of the supernatant solution β (after the attainment of adsorption equilibrium); V^0 denotes the volume of the solution put initially into the tube or flask and M_1^0 is the total mass of the solvent in the heterogeneous system. When the specific surface area of the solid S_{BET} or S_{HJ} is known, it is even possible to calculate the interfacial concentration Γ_2^s of the solute. It should be realised that expressions 6.50 hold only for dilute binary solutions containing a solute that is preferentially adsorbed at the Solid-Liquid interface.

For a given adsorption system, the amount of solute adsorbed at equilibrium depends on the temperature T, the pressure P, and the composition of the equilibrium solution phase β. The experimental results of adsorption measurements are usually reported in the form of *individual adsorption isotherms* showing the quantity $\frac{n_2^s}{m_S}$ or

Γ_2^s as a function of the solution composition:

$$\frac{n_2^s}{m_S} = \frac{n_2^s}{m_S}\left(C_2^\beta\right) \quad \text{or} \quad \frac{n_2^s}{m_S} = \frac{n_2^s}{m_S}\left(m_2^\beta\right), \text{T, P} = \text{const} \tag{6.51a}$$

$$\Gamma_2^s = \Gamma_2^s\left(C_2^\beta\right) \quad \text{or} \quad \Gamma_2^s = \Gamma_2^s\left(m_2^\beta\right), \text{T, P} = \text{const} \tag{6.51b}$$

Figure 6.15 shows three selected shapes of adsorption isotherms at the Solid-Liquid interface for various charged and uncharged solutes exhibiting a limited solubility in the solvent employed. In general, typical adsorption curves present the amount adsorbed as a smooth, monotonically increasing function of the solute content in the equilibrium bulk solution. Many adsorption isotherms end up in an upper composition range at a constant amount adsorbed (a *plateau* of the isotherm).

The appearance of an adsorption plateau region at equilibrium concentrations (molalities) approaching the solubility limit indicates that the phenomenon involves only single solute species that are individually dissolved in the solvent. When the adsorption plateau is observed at lower concentrations (molalities), it is usually argued that surface sites of a given type have been saturated by the adsorbing solute species.

The experimental adsorption isotherms may be plotted on different scales, thereby allowing a more detailed analysis of the subsequent adsorption stages to be made. When the adsorption of homologous substances onto the same solid is due only to their different solubilities in the solvent, the use of a *reduced concentration (molality)*

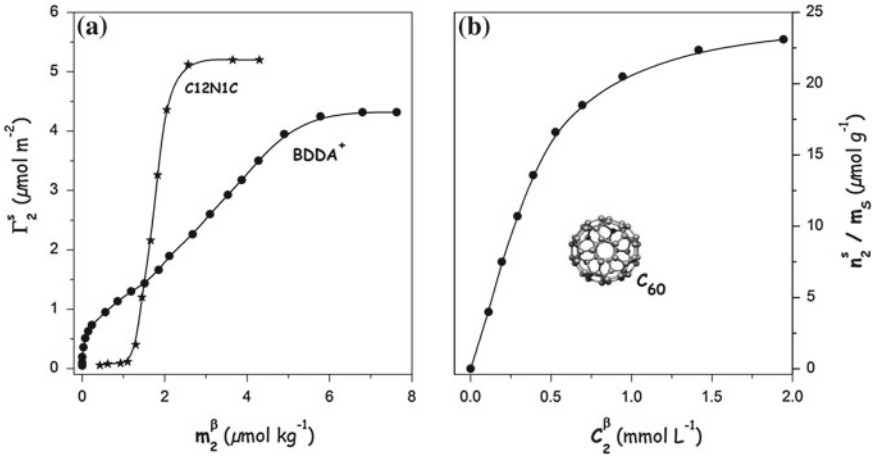

Fig. 6.15 Adsorption isotherms of (**a**) zwitterionic (C12N1C), and cationic ($BDDA^+$) surfactants from aqueous solutions onto non-porous negatively charged silica at 298 K [73, 74], (**b**) buckminsterfullerene C_{60} from its tollune solutions onto mesoporous activated carbon at 293 K [75]; C12N1C and $BDDA^+$ denote (dodecyldimethylammonio)ethanoate and benzyldimethyldodecylammonium cation, respectively

scale to represent the corresponding isotherms results in a single adsorption curve. Any changes in the adsorption mechanism with increasing bulk concentration (molality) show up most clearly in *double logarithmic* (log-log) plots. The transitions between such adsorption regions are obviously more gradual in reality than they seem to be on a log-log scale. The plateau adsorption region markedly manifests itself only on a *double linear* (lin-lin) scale. In the *linear-logarithmic* (lin-log) plot, it is difficult to observe the effects of surface heterogeneity and co-operative adsorption at low bulk concentrations (molalities) but the top parts of the isotherm become clearer.

By analogy to Eq. 6.16, the surface pressure per unit surface area of the Solid–Liquid interface may be determined as follows:

$$\pi_{SL}\left(C_2^*\right) = \gamma_{SL1} - \gamma_{SL}\left(C_2^*\right) = \frac{RT}{m_S \cdot S} \int_{C_2=0}^{C_2^*} n_2^s d \ln C_2 \tag{6.52}$$

where γ_{SL1} is the interfacial tension of the solid in equilibrium with the pure solvent; S is the specific surface area of the solid (i.e., $S = S_{BET}$ or $S = S_{HJ}$); C_2^* denotes the equilibrium bulk concentration taken into consideration.

6.4.4 Immersion in Dilute Solutions

The solution depletion procedure can be generalised to construct a simplified model of immersion experiment [64, 65]. This model is very useful to define the measurable enthalpy quantities, which does not necessarily mean that they can be easily obtained experimentally. The immersion process is schematically represented in Fig. 6.16.

Before immersion the system separately contains an outgassed solid sample of a given mass m_S and a given surface area S in vacuum and a binary solution of molality m_2^0 consisting M_1^0 grams of the solvent, all at constant temperature T and pressure P. Then the solid is immersed in the solution under conditions of constant T, P. The phenomenon of adsorption induces an uneven partition of solvent and solute molecules between the solid-solution interface and the bulk solution. After attaining the adsorption equilibrium, the molality of the solute in the bulk of the solution (sufficiently far from the solid-liquid interface) becomes equal to m_2^β. Since absorption, dissolution and swelling effects are not taken into consideration, the adsorbent is considered as *thermodynamically inert*, i.e., its mass, specific surface area and bulk phase properties do not change during adsorption. Furthermore, the adsorption of the solute at the Solution-Gas interface and the relative surface enthalpy for this interface are omitted for convenience: changes of both effects during immersion in an excess of dilute solution are negligible small.

The balance of enthalpy in the initial (init) and final (fin) states of the model system can be written as follows (cf. Sect. 6.4.1):

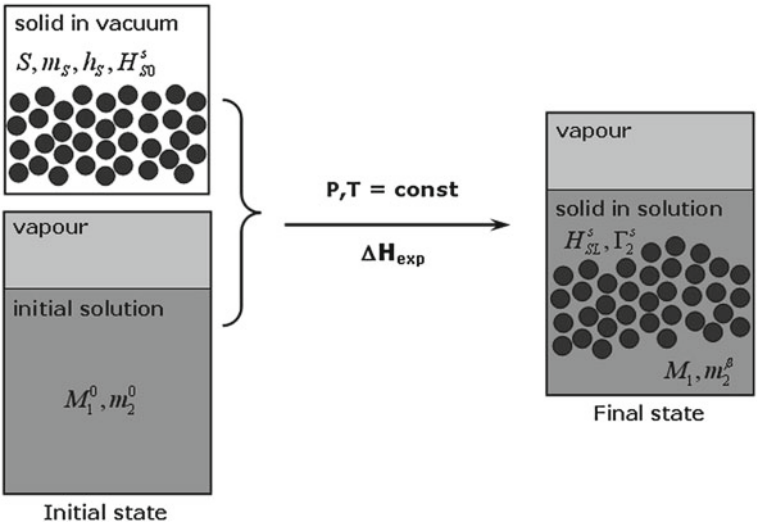

Fig. 6.16 Schematic representation of the immersion experiment (explanation of the symbols in the text). The adsorption phenomenon is assumed not to affect the enthalpy of the bulk of solid, $m_S \cdot h_S$; changes in the mass of the solvent are to be neglected when immersion is carried out in a sufficient excess of dilute solution containing a preferentially adsorbed solute (i.e., $M_1 = M_1^0$)

$$H^{init} = m_S \cdot S \cdot H^s_{S0} + m_S \cdot h_S + M_1^0 \cdot h_1^* + \frac{M_1^0}{10^3} m_2^0 \cdot \Phi_H \left(m_2^0\right) \tag{6.53a}$$

$$H^{fin} = m_S \cdot S \cdot H^s_{SL} + m_S \cdot h_S + \frac{M_1^0}{10^3} m_2^\beta \cdot \Phi_H \left(m_2^\beta\right) + M_1^0 \cdot h_1^* \tag{6.53b}$$

where H^s_{S0} and H^s_{SL} are the interfacial enthalpies for solid in vacuum and for Solid-Liquid interface in equilibrium with a bulk solution of molality m_2^β, respectively; h_S is the specific (per unit mass) enthalpy of the bulk of the solid phase; $\Phi_H\,(m_2)$ is the value of the apparent molal enthalpy of the solute in a binary solution corresponding to the molality m_2; h_1^* is the specific enthalpy (per unit mass) of the pure liquid solvent. Equation (6.53b) has been developed based on the hypothesis that changes in the mass of the solvent can be neglected during immersion in excess solution.

The total thermal effect of the immersion experiment is:

$$\Delta H_{\text{exp}} = H^{fin} - H^{init} = m_S \cdot S \cdot \left(H^s_{SL} - H^s_{S0}\right) + \frac{M_1^0}{10^3}\left[m_2^\beta \cdot \Phi_H\left(m_2^\beta\right) - m_2^0 \cdot \Phi_H\left(m_2^0\right)\right] \tag{6.54a}$$

Taking into account the reference state for the solute defined in Sect. 6.4.1 and using Eqs. (6.40), (6.47), and (6.50), this expression may be transformed as follows:

$$\Delta H_{\text{exp}} = m_S \cdot S \cdot \left(H^s_{SL} - H^s_{S0}\right) - m_S \cdot S \cdot \Gamma^s_2 \cdot \overline{h}_2\,(\infty) + \\ - m_S \cdot S \cdot \Gamma^s_2 \left[\Phi_H\left(m^\beta_2\right) - \Phi_H\,(\infty)\right] - \frac{M^0_1}{10^3} m^0_2 \left[\Phi_H\left(m^0_2\right) - \Phi_H\left(m^\beta_2\right)\right] \tag{6.54b}$$

Since the adsorption of the solvent is here considered negligible (i.e.,$M_1 = M^0_1$), the first two terms on the right hand side of Eq. (6.54b) represents the *enthalpy of immersion in a binary solution (1+2)* with respect to the bulk solution at infinite dilution taken as the reference state [64]; the third term corresponds to the enthalpy of dilution of $m_S \cdot S \cdot \Gamma^s_2$ moles of the solute from molality m^β_2 to infinite dilution in the solvent (cf., Eq. 6.44) and it is often incorporated into the previous enthalpy contribution to give the enthalpy of immersion $\Delta_{imm} H_{12}\left(m^\beta_2\right)$ of the solid in excess solution of molality m^β_2 [48, 76, 77]. The last term represents the dilution effects in the bulk solution: $\frac{M^0_1}{10^3} m^0_2$ moles of the solute are diluted from molality m^0_1 to molality m^β_2. Finally,

$$\Delta H_{\text{exp}} = \Delta_{imm} H_{12}\left(m^\beta_2\right) + \Delta_{dil} H\left(m^0_2 \rightarrow m^\beta_2\right) \tag{6.55}$$

When the dilution term is evaluated independently in appropriate dilution experiment, the enthalpy of immersion $\Delta_{imm} H_{12}\left(m^\beta_2\right)$ can be determined experimentally by means of the same calorimetry equipment as that used to measure the enthalpy of immersion in a pure liquid (Sect. 6.3.2). However, great difficulties may be encountered when evaluating the usual correction terms in case of solutes which are volatile or surface-active (the composition of the vapour occupying the dead volume of the bulb is unknown). This method is also tedious. For systems containting electrified interfaces, the effects of EDL formation additionally contribute to the complexity of the adsorption phenomenon. Here the displacement experiment yields the enthalpy data easier to interpret.

6.4.5 Model of Flow Calorimetry Experiment

Liquid-flow microcalorimetry is a reliable method to measure simultaneously the enthalpy changes and amounts of adsorption under dynamic conditions. Calorimetry experiments may be carried out in two different ways by following a *pulse* or *saturation operating mode* [64, 78–83]. In the pulse mode, small aliquots of a stock solution at a known concentration are injected into the carrier liquid (pure solvent) flowing through the adsorbent bed placed inside the calorimetric cell. In this case, the calorimetric system contains an additional loop injection facility (a manual injection valve with appropriate injection loops). The interpretation of the enthalpy data obtained is straightforward only when the whole amount of the solute injected is irreversibly adsorbed on the solid surface.

The saturation mode (*continuous-flow method*) is more frequently used. Here changes in enthalpy and amount adsorbed of the solute correspond to the formation of a Solid-Liquid interface being in thermal and material equilibrium with the percolating stock solution of a given composition. Repeated adsorption and desorption cycles with the liquid phase in contact with the solid surface for a time required to reach equilibrium can be used to assess reversibility of the phenomenon, and quantify the reversible and irreversible adsorption components [79, 80]. In addition, the same equipment allows probing for some active sites in the solid surface.

The physical meaning of thermodynamic quantities measured in the flow calorimetry experiment, may be discussed based on a simplified model of the system (Fig. 6.17). The model system is composed of three parts: (i) a reservoir R containing a given volume of the stock solution of molality m_2^0, (ii) a cell C with the solid sample of mass m_S, in contact with the solvent or the stock solution, (iii) a trap T for the effluent [65, 78].

Initially, the outgassed solid sample is immersed in M_{1C}^0 grams of pure solvent and the total quantity of stock solution in the reservoir is given by the mass of solvent M_{1R}^0; the trap is empty. Then the flow of stock solution from the reservoir is directed to the cell under constant liquid-flow conditions. The temperature and pressure are assumed to be uniform throughout the system and there is neither loss of energy nor loss of matter between the reservoir, the cell and the trap. As the stock solution

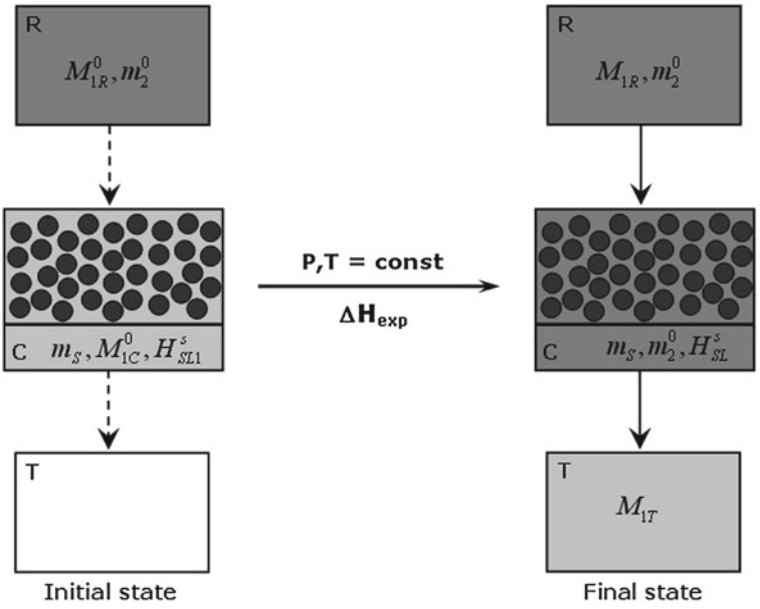

Fig. 6.17 Schematic representation of the flow calorimetry experiment (explanation of the symbols in the text). The model system is composed of three parts: *R* Reservoir, *C* Calorimetric cell, *T* Trap

flows through the cell with the adsorbent, the boundary between the solution and the solvent remains sharp, and the effects of adsorption and desorption change its position according to the *ideal chromatographic behaviour*. In practice, this means that the change of liquid composition should be sufficiently small for heat of mixing contribution to be neglected. The final state is achieved just before the front of the stock solution reaches the trap. At this point, the trap is filled with M_{1T} grams of pure solvent and the equilibrium molality of the solute within the cell (far from the solid surface) is equal to m_2^0. The composition of the stock solution in the reservoir does not change but its amount decreases; the final mass of the solvent is M_{1R}.

For the initial state, the amount of the solute n_2^{init} in the model system and the total enthalpy of the system H^{init} are given by (cf. Sect. 6.4.1):

$$n_2^{init} = \frac{M_{1R}^0}{10^3} m_2^0 \tag{6.56a}$$

$$H^{init} = m_S \cdot S \cdot H_{SL1}^s + m_S \cdot h_S + M_{1C}^0 \cdot h_1^* + \frac{M_{1R}^0}{10^3} m_2^0 \cdot \Phi_H\left(m_2^0\right) + M_{1R}^0 \cdot h_1^* \tag{6.56b}$$

where H_{SL1}^s is the interfacial enthalpy for the solid-solvent interface; other quantities have been introduced previously (cf., Eqs. 6.53a, 6.53b).

Applying the law of mass conservation to the solvent in the system, the corresponding quantities in the final state may be written as follows:

$$n_2^{fin} = m_S \cdot S \cdot \Gamma_2^s + \frac{M_{1R}}{10^3} m_2^0 + \frac{M_{1R}^0 + M_{1C}^0 - M_{1R} - M_{1T}}{10^3} m_2^0 \tag{6.57a}$$

$$H^{fin} = m_S \cdot S \cdot H_{SL}^s + m_S \cdot h_S + \frac{M_{1R}}{10^3} m_2^0 \cdot \Phi_H\left(m_2^0\right) + M_{1R} \cdot h_1^* + \frac{M_{1R}^0 + M_{1C}^0 - M_{1R} - M_{1T}}{10^3} m_2^0 \cdot \Phi_H\left(m_2^0\right) + \left(M_{1R}^0 + M_{1C}^0 - M_{1R} - M_{1T}\right) \cdot h_1^* \tag{6.57b}$$

where H_{SL}^s refers to the interfacial enthalpy for the solid-solution interface in equilibrium with a bulk solution of molality m_2^0. The comparison of expressions (6.56b) and (6.57b) indicates that the adsorbent is considered as thermodynamically inert, i.e., its parameters m_S, S, and h_S do not change during adsorption.

The law of mass conservation applied to the solute gives rise to the following relation:

$$\Gamma_2^s = \frac{\left(M_{1T} - M_{1C}^0\right)}{10^3 \cdot m_S \cdot S} m_2^0 \tag{6.58a}$$

This relation shows that the quantity of adsorption for the solute may be directly measured in the flow calorimetry experiment if the values of M_{1C}^0 and M_{1T} are known. When the solid bed in the cell contains a non-adsorbing solid, the difference

$M_{1T} - M_{1C}^0$ is equal to zero; the value of M_{1C}^0 can thus be measured in the appropriate "blank" run. Otherwise, this difference depends on how much longer the solute is retained by the adsorbent. In the model flow experiment, the concentration curves obtained with a non-adsorbing and adsorbing solid represent obviously square profiles (Fig. 6.18a).

If the feed solution flow rate d_{pump} is constant and the solvent migrates at the same velocity throughout the whole system, the mass of solvent entering the trap is directly proportional to the retention time τ_A:

$$M_{1T} = \frac{10^3 \cdot d_{pump}}{10^3 + m_2^0 \cdot M_{solute}} \cdot \tau_A \tag{6.58b}$$

where M_{solute} is the molar mass of the solute. The amount of solute adsorbed onto solid sample can be thus calculated from the *corrected retention time*, i.e., $\tau_A - \tau_{NA}$ (Fig. 6.18a). In a real calorimetry run, the shape of the m_2 *vs.* time plot depends on the underlying equilibrium isotherm of solute adsorption, as well as diffusion and mass-transfer kinetics. This results in a breakthrough curve, as shown in Fig. 6.18b. The quantity of solute adsorption is calculated from the difference between the areas over the breakthrough curves obtained with a non-adsorbing and adsorbing solid [79, 80].

When using a pen recorder, the retention measurements are made in terms of chart distances and the area difference is determined by graphical integration. In modern systems, this theoretically correct analysis is also easy to perform when the digitized signal is recorded on the computer hard disk. In practice, the calculation of the areas always includes signal noise and it is very sensitive to the integration limits (the mass transfer is often slow and the plateau concentration m_2^0 is reached slowly, thereby resulting in significant systematic errors). Therefore, it is easier and better to handle

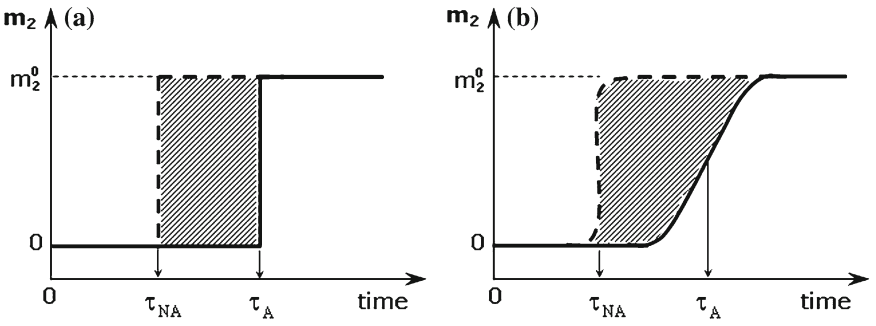

Fig. 6.18 Square profiles of the solute concentration obtained in the model flow experiments (**a**) and breakthrough curves of the solute registered during real flow calorimetry runs (**b**). The *dashed lines* refer to the profiles obtained with a non-adsorbing solid; τ_A and τ_{NA} are the retention times of the retained solute and the completely unretained solute, respectively. The *dashed areas* represent the amount of solute adsorbed (the calibration factor is needed)

the retention times (chart distances) defined by characteristic points method (e.g., the retention parameters derived from the inflection point or the half-height [84]).

The thermal balance in the flow calorimetry experiment can now be expressed in the following way:

$$\Delta H_{\text{exp}} = H^{fin} - H^{init} = m_S \cdot S \cdot \left[\left(H^s_{SL} - H^s_{S0} \right) - \Gamma^s_2 \cdot \Phi_H \left(m^0_2 \right) \right] + - m_S \cdot S \cdot \left(H^s_{SL1} - H^s_{S0} \right) \tag{6.59a}$$

Taking into account the discussion in Sect. 6.4.4, the first term on the right hand side represents the enthalpy of immersion $\Delta_{imm} H_{12} \left(m^0_2 \right)$ of the solid in excess solution of molality m^0_2 and one obtains:

$$\Delta H_{\text{exp}} = \Delta_{imm} H_{12} \left(m^0_2 \right) - \Delta_{imm} H_1 = \Delta_{dpl} H \tag{6.59b}$$

where $\Delta_{dpl} H$ denotes the *integral enthalpy of displacement* [64], which is the main enthalpy effect measured in the liquid-flow calorimetry experiment.

The *molar integral enthalpy* of displacement is calculated as follows:

$$\Delta_{dpl} h = \frac{\Delta H_{\text{exp}}}{m_S \cdot S \cdot \Gamma^s_2} \tag{6.60}$$

This quantity provides information about the excess of component-adsorbent interactions averaged over all surface domains from which the solvent has been displaced by the adsorbing solute species. In consequence, it is not easy to monitor subtle changes in the adsorption mechanism based on usually small variations of the $\Delta_{dpl} h$ values with increasing quantity of adsorption. Compared to the differential molar enthalpy of displacement, the enthalpy $\Delta_{dpl} h$ is less sensitive to the energetic heterogeneity of the solid surface.

6.4.6 Model of Batch Calorimetry Experiment

Liquid titration calorimetry is a *microcalorimetric batch technique* most often used to study the mechanism of solute adsorption onto solids from binary dilute solution [83, 85, 86]. It differs from the flow variant in that a stock solution is injected into the calorimetric cell where the solid sample is kept in homogeneous suspension in a liquid (solvent or solution). The possibility of measuring the pseudo-differential molar enthalpy effects is the most important advantage of this technique. The differential enthalpy is very sensitive to various partial processes of adsorption occurring at the Solid-Liquid interface, thus allowing changes in the interfacial properties with surface coverage to be continuously monitored. From this standpoint, calorimetric data are very useful for theoretical consideration and modelling. Additionally, titration

calorimetry may be an important analytical tool for determining the enthalpy effects accompanying the dilution of solutions with given compositions.

A typical operational procedure involves injection of a stock solution by small steps into the calorimetric cell containing either dilute solution (*dilution experiment*) or suspension of powder solid sample in a dilute solution (*adsorption experiment*). Serious drawbacks to the use of this calorimetry technique in studying the adsorption phenomena are due to the difficulty of direct evaluation of the related amounts adsorbed and to insufficient control of the environment of the liquid phase (e.g., the pH and ionic strength cannot be maintained constant through the whole run) [73, 87]. The progress in the adsorption quantity during successive injections of the adsorbate to the cell is quantified from the adsorption isotherm measured separately under *exactly the same* experimental conditions. For the adsorption of ionic solutes at electrified interfaces, it is impossible to well reproduce the charging behaviour of the adsorbent at a constant pH since this parameter cannot be re-adjusted during injections.

The model of dilution experiment is depicted in Fig. 6.19. Prior to injection sequence, there is M_1^0 grams of pure solvent in the calorimetric cell. Then, small aliquots of the stock solution of molality m_2^0 are injected by the syringe pump operating at a constant flow rate d_{pump}. When the time of injection t_{inj} is maintained constant, the amount of the solute n_2^{inj} introduced into the calorimetric cell is always the same. As a result, the equilibrium solution in the cell becomes more and more concentrated, i.e., $m_2^i \rightarrow m_2^0$. The dilution data may be further processed in two different ways, by calculating either *differential molar* or *cumulative molar* enthalpy changes.

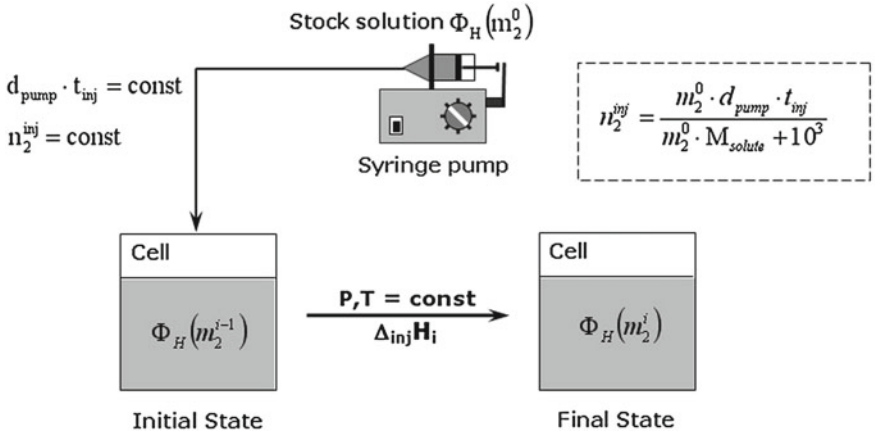

Fig. 6.19 Schematic representation of an injection step in the batch dilution experiment. The flow rate d_{pump} of the pump and the time t_{inj} of injection are kept constant during the experiment. The equation shows how to calculate the number of moles of the solute injected; m_2^0 and M_{solute} are the molality of the stock solution in the syringe and the molar mass of the solute, respectively; Φ_H (m_2) is the value of the apparent molal enthalpy of the solute in a binary solution corresponding to the molality m_2

The total enthalpy change during the ith injection *per mole of the solute* is expressed as follows [73, 74, 88]:

$$\frac{\Delta_{inj} H_i}{n_2^{inj}} = \Phi_H\left(m_2^i\right) + (i-1)\cdot n_2^{inj} \cdot \frac{\left[\Phi_H\left(m_2^i\right) - \Phi_H\left(m_2^{i-1}\right)\right]}{n_2^{inj}} + \\ - \Phi_H\left(m_2^0\right) \tag{6.61a}$$

where n_2^{inj} depends on d_{pump}, t_{inj}, and m_2^0, according to the formula given in Fig. 6.19.

The equilibrium molality of the solution m_2^i in the cell after this injection is calculated by means of the following expression:

$$m_2^i = \frac{10^3 \cdot i \cdot n_2^{inj}}{M_1^0 + \frac{10^3 \cdot i \cdot n_2^{inj}}{m_2^0}} \tag{6.61b}$$

The determination of all $\frac{\Delta_{inj} H_i}{n_2^{inj}}$ terms in function of m_2^{i-1} and m_2^i yields the results in the form of a histogram, as shown in Fig. 6.20. Referring to the general definition of the partial molal enthalpy $\overline{h}_2$ and apparent molal enthalpy Φ_H for any particular

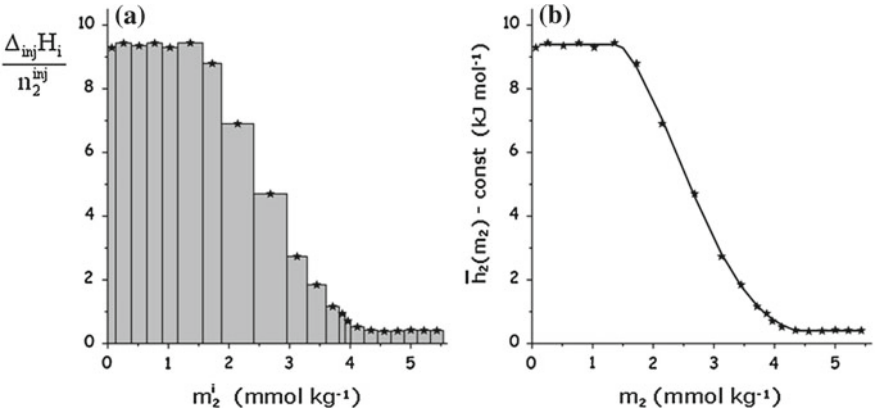

Fig. 6.20 Titration calorimetry of successive dilutions of a 0.028 mol kg^{-1} aqueous solution of benzyldimethyldodecylammonium bromide (BDDAB) in the presence of 0.01 mol kg^{-1} NaBr at 298 K [89]: (**a**) histogram of the molar enthalpy change during the *i*th injection as a function of the equilibrium solution molality, (**b**) plot of the partial molal enthalpy of the solute against its bulk molality. The solution is regarded as a binary system: the solute ions $BDDAB^+$ and Br^- form together the mean solute, whereas NaBr is included in the mean solvent. The smooth curve of $\overline{h}_2$ against the equilibrium solution molality m_2 is achieved by choosing the value of m_2 to lie in the middle of interval $\left[m_2^{i-1}, m_2^i\right]$

solute in a solution of two components (Eqs. 6.36 and 6.39), it is to be noted that, for the sufficiently small quantities n_2^{inj} of the solute injected during each injection, Eq. (6.61a) can be transformed to give:

$$\frac{\Delta_{inj} H_i}{n_2^{inj}} \approx \lim_{n_2^{inj} \to 0} \frac{H\left(m_2^i\right) - H\left(m_2^{i-1}\right)}{n_2^{inj}} - const = \overline{h}_2\left(m_2\right) - const,$$
$$m_2^{i-1} < m_2 < m_2^i \tag{6.62}$$

where H denotes the enthalpy of a binary solution in the calorimetric cell.

Thus, values of $\overline{h}_2$ may be obtained experimentally by measuring both enthalpy changes $\Delta_{inj} H_i$ and very small quantities n_2^{inj} of the solute injected during successive dilution of the stock solution. It is clear from Eq. (6.62) that the above relation does not hold for the first injection: the first points in the calorimetric curves of dilution should not be taken into consideration.

The thermal effects of successive injections can be also summed up to obtain the molar cumulative enthalpy of dilution $\Delta_{dil} h_{cum}$. After k injections, one obtains:

$$\Delta_{dil} h_{cum} = \sum_{i=1}^{k} \frac{\Delta_{inj} H_i}{n_2^{inj}} = k \cdot \left[\Phi_H\left(m_2^k\right) - \Phi_H\left(m_2^0\right)\right],$$
$$\text{with } m_2 = m_2^k \tag{6.63}$$

The experimentally measured values of $\Delta_{dil} h_{cum}$ are further plotted against the equilibrium solute molality m_2 and only such a representation may have clear physical meaning from a thermodynamic standpoint. Nevertheless, it is sometimes more useful to present the enthalpy of dilution curve in terms of $\Delta_{dil} h_{cum}$ as a function of the injection number k, especially when the dependence of $\Delta_{dil} h_{cum}$ *vs* m_2 is linear or contains several linear portions (cf., Fig. 6.21).

In the adsorption calorimetry experiment, a small amount n_2^{inj} of the stock solution injected during a given injection is diluted in the supernatant liquid inside the cell and some of the resulting species subsequently adsorb onto solid particles. They displace a certain amount of solvent molecules and can exchange with some pre-adsorbed molecules or ions, because of the limited extent of the adsorption space. The effects of desolvation and re-solvation of various compounds taking part in the displacement process contribute to the competitive character of adsorption at the solid-solution interface. The flow chart of the batch displacement experiment is shown in Fig. 6.22. Since the enthalpy effects accompanying dilution of the stock solution inside the cell should be known, both the dilution and adsorption experiments are carried out under the same conditions (cf., Fig. 6.19).

When the adsorbent is initially immersed in M_1^0 grams of pure solvent and the final state corresponds to the formation of a Solid-Liquid interface in equilibrium with a bulk solution of molality m_2^k, the mass balance inside the cell leads to the following expression for the amount of solute adsorbed at the Solid-Liquid interface:

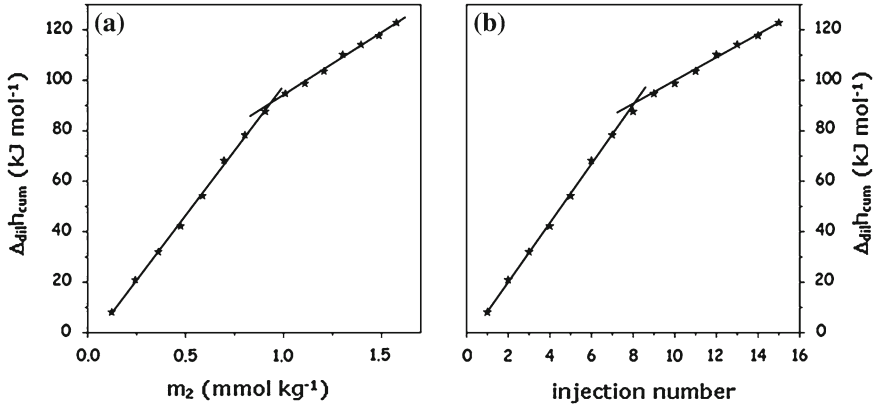

Fig. 6.21 Cumulative enthalpy of dilution of a 0.009 mol kg^{-1} aqueous solution of hexadecyltrimethylammonium bromide (HTAB) at 303 K as a function of (**a**) the solute molality and (**b**) the injection number [88]. The solution is regarded as a binary system: the solute ions HTA^+ and Br^- form together the mean solute. Plot **a**: the intersection of the two linear portions provides estimate of the critical micelle concentration for HTAB; Plot **b**: the enthalpy of HTAB micellisation is determined directly from the difference between the slopes of the two linear regression segments

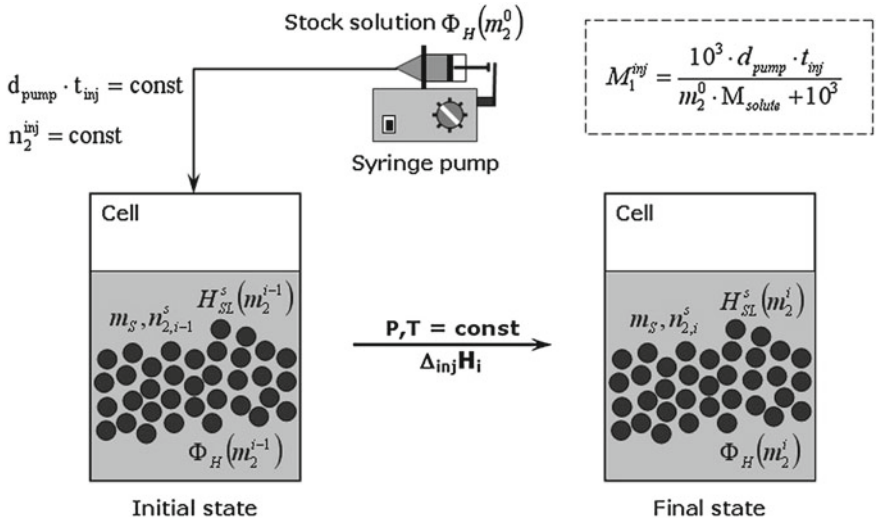

Fig. 6.22 Schematic representation of an injection step in the batch adsorption experiment. The values of d_{pump}, t_{inj}, n_2^{inj}, and m_2^0 are the same as those in Fig. 6.19. The equation shows how to calculate the mass of solvent injected with the stock solution. H_{SL}^s (m_2) refers to the Solid-Liquid interface in equilibrium with a bulk solution of molality m_2

$$n_{2,k}^{s} = n_2^{s}\left(0 \rightarrow m_2^{k}\right) = \sum_{i=1}^{k} n_2^{inj} - \frac{m_2^{k}}{10^3}\left(M_1^{0} + \sum_{i=1}^{k} M_1^{inj}\right) \tag{6.64}$$

where M_1^{inj} is the mass of solvent introduced into the calorimetric cell during one injection of the stock solution (see the appropriate equation in Fig. 6.22).

Equation 6.64 represents the so-called *calorimetric line*, since the amount adsorbed $n_{2,k}^{s}$ varies linearly with m_2^{k} between two characteristic points: (P1) the whole amount of the solute injected is retained by the adsorbent surface and $m_2^{k} = 0$; (P2) the whole amount of the solute injected remains in the bulk solution and $n_{2,k}^{s} = 0$. In practice, it is impossible to measure directly the values of n_2^{s} for all injections (it would not be reasonable to interrupt the calorimetry run after each injection and remove the calorimetric cell in order to analyse its content). Nevertheless, the partition of the solute between the adsorbed and bulk phases is strictly determined by the adsorption equilibrium at a given temperature and does not depend on the path by which the adsorption system passes from its initial state to the equilibrium. Hence, the values of m_2^{k} and $n_{2,k}^{s}$ are evaluated from the intersection between the calorimetric line (6.64) and the experimental isotherm $\Gamma_2^{s} = \Gamma_2^{s}\left(m_2^{\beta}\right)$, obtained under *exactly the same* experimental conditions (Fig. 6.23).

The total change in enthalpy during the *i*th injection in the adsorption experiment may be written as follows:

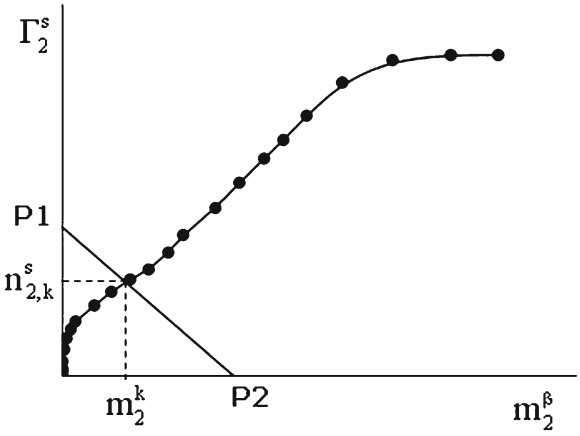

Fig. 6.23 Graphical determination of the amount adsorbed $n_{2,k}^{s}$ after a given injection step in the titration calorimetry run and the related molality of the equilibrium bulk solution m_2^{k} from the intersection between the calorimetric line 6.64 (*passing through two characteristic points P1 and P2*) and the experimental adsorption isotherm measured under the same conditions

$$\Delta_{inj}H_i = m_S \cdot S \cdot \left[H_{SL}^s\left(m_2^i\right) - H_{SL}^s\left(m_2^{i-1}\right)\right] - n_{2,i}^s \cdot \Phi_H\left(m_2^i\right) + \\ + n_{2,i-1}^s \cdot \Phi_H\left(m_2^{i-1}\right) + \\ + n_2^{inj} \cdot \left\{\Phi_H\left(m_2^i\right) + (i-1) \cdot n_2^{inj} \cdot \frac{\left[\Phi_H\left(m_2^i\right) - \Phi_H\left(m_2^{i-1}\right)\right]}{n_2^{inj}} - \Phi_H\left(m_2^0\right)\right\} \tag{6.65a}$$

where S is the specific surface area of the adsorbent; $H_{SL}^s(m_2)$ is the interfacial enthalpy for a Solid-Liquid interface in equilibrium with a bulk solution of molality m_2. The above equation has been developed by neglecting any changes in the enthalpy of the bulk of the adsorbent $m_S \cdot h_S$. The comparison with Eqs. (6.54a, 6.54b) and (6.59a, 6.59b) in Sects. 6.4.4 and 6.4.5 indicates that the first three terms on the right hand side of Eq.(6.65a) represent the difference in the enthalpy of displacement $\Delta_{dpl}H\left(m_2^i\right) - \Delta_{dpl}H\left(m_2^{i-1}\right)$ when passing from m_2^{i-1} to m_2^i. The forth term has the same form as the overall enthalpy change recorded in the dilution experiment (cf., Eq. 6.61a). For small n_2^{inj} values accompanied by small increments in the amount adsorbed n_2^s, the batch adsorption experiment allows measuring the *differential enthalpy of displacement per mole of the solute* adsorbed at the Solid-Liquid interface, since:

$$\Delta_{dpl}h_{diff} = \lim_{\Delta n_2^s \to 0} \frac{\Delta_{dpl}H\left(m_2^i\right) - \Delta_{dpl}H\left(m_2^{i-1}\right)}{n_{2,i}^s - n_{2,i-1}^s} \\ \approx \frac{\Delta_{dpl}H\left(m_2^i\right) - \Delta_{dpl}H\left(m_2^{i-1}\right)}{n_{2,i}^s - n_{2,i-1}^s} = \\ = \frac{\Delta_{inj}H_i - n_2^{inj} \cdot \left[\overline{h}_2\left(m_2^\beta\right) - const\right]}{n_{2,i}^s - n_{2,i-1}^s} \tag{6.65b}$$

where the equilibrium molality m_2^β is located in the middle of interval $\left[m_2^{i-1}, m_2^i\right]$.

The experimental procedure and data processing leading to a smooth curve of $\Delta_{dpl}h_{diff}$ as a function of the amount adsorbed n_2^s include the following stages: the quantity of the solute injected n_2^{inj} and the successive enthalpy changes $\Delta_{inj}H_i$ are measured in the adsorption calorimetry experiment; the limit molality values m_2^{i-1} and m_2^i for each injection class and the related increments in the amount adsorbed $n_{2,i-1}^s$ and $n_{2,i}^s$ are evaluated with the aid of the adsorption isotherm; based on the "differential" enthalpy curve obtained in the dilution experiment, the correction terms for dilution, $n_2^{inj} \cdot \left[\overline{h}_2\left(m_2^\beta\right) - const\right]$, are determined for the values of m_2^β taken as the middle of appropriate intervals $\left[m_2^{i-1}, m_2^i\right]$; with small increments $\Delta n_2^s =$

$n^s_{2,i} - n^s_{2,i-1}$, the differential displacement terms $\Delta_{dpl}h_{diff}$ are finally calculated and ascribed to the n^s_2 values in relation with the equilibrium molalities m^β_2. It should be noted again that the enthalpy value corresponding to the first injection cannot be considered as the differential molar enthalpy of displacement and has to be removed from the experimental curve.

6.5 Calorimetry Applied to Study Competitive Adsorption from Dilute Solution

The integral and differential enthalpies of displacement can be measured directly using calorimeters of the isothermal type. Such instruments either are produced and marketed by some manufacturers of high-performance calorimetric systems for different applications (e.g., SETARAM Instrumentation, LKB-ThermoMetric, TA Instruments, Microscal Ltd), or are home-mode prototypes based on original work carried out in university laboratories and therefore documented in considerable detail in scientific publications. This section focuses on the properties of two calorimetry systems used by the author to study the competitive adsorption from dilute solution.

6.5.1 Flow Calorimetry System

A liquid-flow calorimetry system (commercialised by Microscal Ltd) is represented schematically in Fig. 6.24 [79, 80]. Here the calorimetric cell is simply a cylindrical cavity inside the calorimetric bloc and its volume is limited by two removable tubes. The outlet tube is also used as a holder for a powdered solid sample. Prior to each calorimetry run, the inlet and outlet tubes are taken away from the calorimeter and the calorimetric cell is cleaned.

The measuring termistors detect the temperature of the cell content *via* a PTFE cell wall membrane which protects them from chemical attack. A separate temperature sensor is installed in the calorimetric block to permit the digital display of block temperature. The thermistor sensors are part of a Wheatstone bridge, which has the advantage that only temperature differences between the calorimetric cell and the block will put the bridge out of balance. When the solution containing a preferentially adsorbing solute or the pure solvent reaches the adsorbent bed there is an exothermic or endothermic displacement with resultant evolution or absorption of heat. This causes a small resistance change to the measuring thermistors and the effect is registered in the form of a thermal peak, the area of which is proportional to the heat measured.

It is necessary to have an evenly packed adsorbent bed in the calorimetric cell and a smooth, steady flow of liquid to pass through the bed so as to obtain reproducible results. Since the volume of the cell is limited (about 0.17 mL), a suitable volume

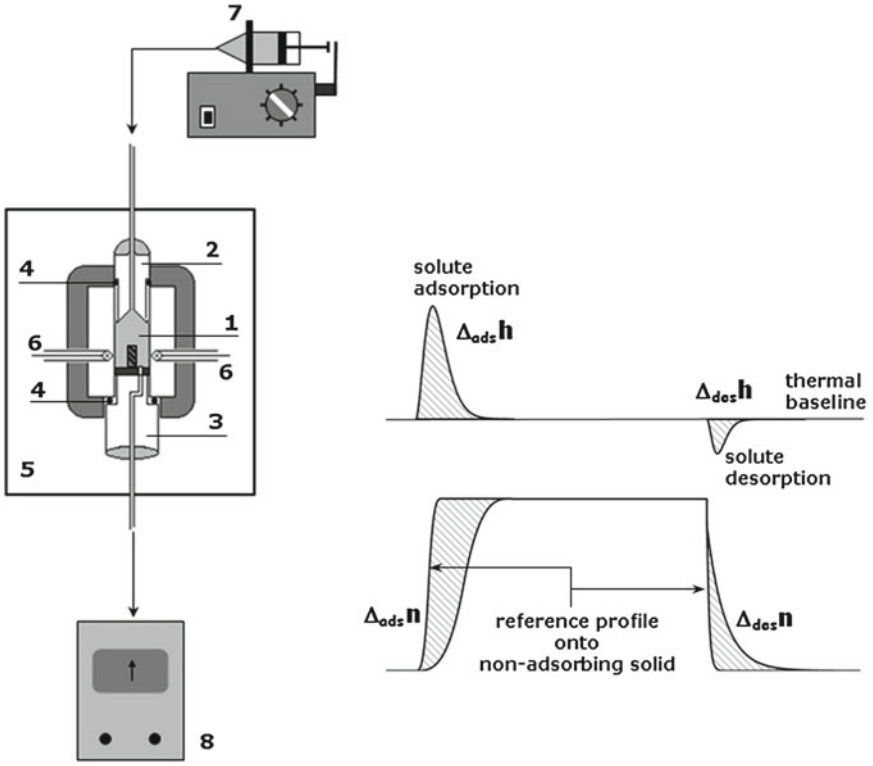

Fig. 6.24 Schematic representation of a liquid-flow microcalorimetry system operating in continuous-flow mode, together with traces showing the thermal and mass exchange profiles for adsorption of solute from its solution in the solvent, followed by the desorption of the solute by flow of pure solvent: *1* adsorbent bed, *2* inlet tube, *3* outlet tube, *4* toric seals, *5* aluminium block, *6* measuring thermistors, *7* syringe pomp, *8* downstream detector

of powder or granular solid is weighed out in a special measuring tube provided by the manufacturer. Then the outlet tube is fitted in the calorimeter and the powder is poured into the sample holding space by means of an extended stainless steel funnel. Contrary to appearances, this operation is crucial for further measurements. Sometimes, the sample should be gently crushed to decrease the dead volume of the adsorbent bed. The use of monodispersed particles can be beneficial. When the particles are agglomerates of much finer material, they should not disintegrate in the liquid flow through the adsorbent. For solids having significant differences in their dry and wet packing densities (e.g., solids swelling in carrier liquids), the sample volume placed in the cell must take account of the volume change occurring on sample evacuation and immersion with the liquid. It is still possible to check whether the quantity of solid sample introduced and its packing in the cell are correct by fitting the inlet tube carefully. Any adsorbed species can be subsequently removed from the sample surface by evacuation, making use of a vacuum pump connected to the

outlet tube. The temperature may be raised on evacuation by heating the calorimetric block with the aid of a stabilised D.C. power supply. The temperature limit depends on the thermal resistance of the materials of construction used. The efficiency of the evacuation step can be enhanced by flushing the adsorbent bed with the carrier liquid.

Further operating procedure for adsorption studies includes establishing a steady flow of the solvent used as a carrier liquid, awaiting thermal equilibrium, and setting the sensitivity controls. Different flow rates should be usually tested to optimise the operation for peak height, shape, sensitivity and duration. It should be remembered that the pump flow rate is limited by the syringe volume (normally 10 or 20 mL), compressibility of the solvent utilised, size of the solid particles, and their packing density in the sample holding space: the most commonly applicable flow rates are included in the range 0.05–0.1 mL per minute. Moreover, all occluded air should be carefully removed from the syringe and the whole line purged. As the equilibration proceeds, the thermal signal in function of time approaches a straight line asymptotically and this state is the criterion by which to judge the equilibration and to set the sensitivity of the calorimeter.

After attaining thermal equilibrium in the system, the flow of carrier liquid solvent is replaced with the identical flow rate of the solution of adsorbate at defined concentration by means of a changeover valve. The solution is fed by a syringe pump other than the one directing the solvent *via* the valve to the calorimeter. The progress of solute adsorption is monitored by the evolution or absorption of heat measured by thermistors sensing temperature changes in the calorimetric cell and simultaneously adsorbate transfer from the bulk phase to the Solid-Liquid interface is monitored by measuring composition changes in the effluent leaving the adsorbent and passing through the downstream detector. The principle of detection (UV, refer-actometry, thermal conductivity) and thus the choice of the detector depend on the chemical nature of both the solute and the solvent, the flow rates to be used, as well as the technical specification of the detector (e.g., operating parameters, sensitivity of detection, linearity of the signal with concentration, baseline stability, ease of operation). The adsorbent bed and the solution are allowed to remain in contact until heat evolution or absorption ceases (the signal returns to the thermal baseline) and no further change in the effluent composition is detected (the recorder trace shows a straight line), as illustrated in Fig. 6.24.

Since the calorimetric system is particularly well adapted to the study of the thermodynamic reversibility of the adsorption phenomenon, it is always worth carrying out the first desorption stage under exactly the same experimental conditions, just by returning to the flow of the carrier liquid through the adsorbent bed. The reader should be reminded that the heat effects of adsorption and desorption are opposite in sign. When the thermal and detector signals return to those of pure solvent, the adsorption-desorption cycle can be repeated to test the attainment of adsorption reversibility (e.g., the heat effects of adsorption and desorption are equal and repeatable). For some porous materials, the desorption process may last longer than the corresponding adsorption due to the slower mass transfer kinetics and the

peak tailings effects are observed, thereby reducing the measurement accuracy and repeatability.

Calibration of the instrument is required at some stage for the particular operating conditions employed. Calibration of the areas under the thermal peaks is carried out by dissipating a known amount of energy in the adsorbed bed with the aid of a calibration probe incorporated into the outlet tube and encapsulated in PTFE. The related "exothermic" peak may be integrated making use of appropriate software facilities to process the digitized signal recorded on the computer hard disk. The data processing is the same as that described in Sect. 6.3.2 for immersional and wetting calorimetry. The downstream detector provides a plot of the effluent composition, the profile of this curve being influenced by the amount of solute molecules retained on the adsorbent surface during adsorption or released from the surface during desorption. To determine the related amount of solute adsorbed or desorbed, this profile is to be compared with composition changes obtained in a "blank" experiment with the use of a "non-adsorbing" solid through which pure solvent and the solution are passed at the same flow rate and temperature as those for the adsorbing sample. Glass or PTFE balls of low specific surface areas are usually used as non-adsorbing adsorbents, but the main difficulty here is to reproduce the same flow conditions of liquids through the adsorbent bed in the blank run (e.g., packing density of the solid, hydrophobic-hydrophilic character of its surface, pressure drop over the adsorbent bed). The two types of composition profile can be matched and presented in the form of net mass-transfer for adsorption and desorption. The areas of the segments, resulting from the subtraction of the peaks obtained on adsorbing and non-adsorbing solids, provide a direct measure of the quantity of the solute which either fails to emerge in the effluent solution due to its adsorption by the adsorbent bed in the calorimetric cell or is released to the carrier stream by the flow of pure solvent. The detector calibration factor is determined from the injection of a given volume of the solution into the stream of the solvent percolating through the detector (calibrated injection loop facility).

6.5.2 Measurements of Integral Enthalpy of Displacement

Despite the limited physical meaning of the integral enthalpy of displacement, measuring $\Delta_{dpl}H$ or $\Delta_{dpl}h$ may be very useful in several cases.

The first case certainly corresponds to the study of the thermodynamic reversibility of adsorption onto solids from binary solutions. Liquid-flow calorimetry measurements usually provide clear, unambiguous arguments for irreversible character of the phenomenon in numerous systems. An example of such systems is illustrated in Fig. 6.25. With non-porous Graphon possessing a very small number of surface polar sites, the adsorption of C_{60} fullerene from toluene is completely reversible. In the case of porous active carbons, the phenomenon is only partially reversible, the degree of reversibility being evaluated from the difference between the values of $\Delta_{dpl}h$ measured for the adsorption and desorption stage.

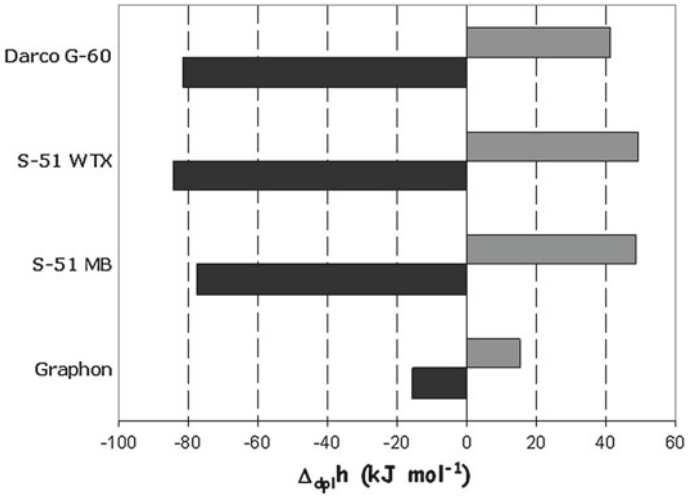

Fig. 6.25 Integral molar enthalpies (in kJ mol^{-1}) of C_{60} fullerene adsorption (*black bars*) and desorption (*grey bars*) obtained in one adsorption-desorption cycle from a 0.5 g L^{-1} toluene solution onto graphitised carbon *black* (Graphon) and three active carbons (S-51 MB, S-51 WTX, Darco G-60) at 293 K [75]

The irreversible enthalpy component may be calculated from the following formula:

$$\Delta_{dpl}h_{IR} = \frac{\Delta_{ads}n \cdot \Delta_{ads}h + \Delta_{des}n \cdot \Delta_{des}h}{\Delta_{ads}n - \Delta_{des}n} \tag{6.66}$$

where $\Delta_{ads}n$ and $\Delta_{des}n$ are positive changes in the number of moles of solute measured during the adsorption and desorption run, respectively; $\Delta_{ads}h$ and $\Delta_{des}h$ are the corresponding molar enthalpies of displacement observed in both stages.

Low sensitivity of the $\Delta_{dpl}H$ or $\Delta_{dpl}h$ values to the surface heterogeneity effects makes the integral enthalpy of displacement useful for probing specific sites on the surface of solid materials. The principle of this method lies in measuring the enthalpy of displacement per unit area of the adsorbent $\Delta_{dpl}H^*$ during adsorption of specific probe species (solute) capable of displacing non-specific solvent molecules from the targeted surface sites. For example, the polar contribution to the interfacial enthalpy H^s_{SL} may be thus approximated by determining the integral enthalpy of displacement of an apolar solvent by a polar solute. Prior to calorimetry measurements, the solution composition should be carefully optimised to ensure monomolecular adsorption of the solute on the solid surface [90, 91].

Figure 6.26 shows the effect of heteroatom incorporation into the framework of ordered mesoporous silica, as inferred from the adsorption of *1*-butanol from *n*-heptane.

When diluted in an apolar solvent, the molecules of *1*-butanol (BuOH) may be regarded as monomer species, potentially acting as both hydrogen-bond donors and

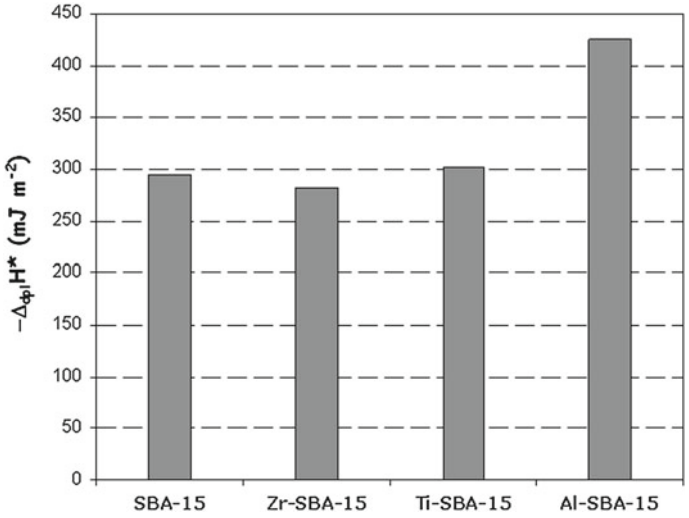

Fig. 6.26 Integral enthalpy of displacement per unit surface area $\Delta_{dpl}H^*$ (taken with the opposite sign) measured in the liquid-flow calorimetry experiment for adsorption of *1*-butanol from a 2 g L^{-1} solution in *n*-heptane at 298 K onto ordered mesoporous silica of the SBA-15 type and three mesoporous silica-based materials doped with various heteroatoms [92]

acceptors. Since the doping procedure aims at isomorphic substitutions of silicon by such heteroatoms as Al, Ti or Zr in the tetrahedral structures, the hydrophilic surface of the four mineral oxides should be dominated by surface hydroxyl groups. Butanol molecules can form hydrogen bonds with these silanols (Si-OH), aluminols (Al-OH), titanols (Ti-OH), or zirconols (Zr-OH). The monolayer adsorption of BuOH is accompanied by simultaneous desorption of apolar heptane molecules. In consequence, the integral enthalpy of displacement per unit area of the adsorbent surface $\Delta_{dpl}H^*$ is a function of the surface density of hydroxyl groups. In the case of materials doped with Ti(IV) and Zr(IV), there is no reason for a marked change in the surface density of hydroxyl groups.

This hypothesis is well illustrated by quite similar (within the experimental error) $\Delta_{dpl}H^*$ values obtained for SBA-15, Zr-SBA-15, and Ti-SBA-15, irrespective of differences in the surface area and porous structure among the samples. The partial replacement of Si(IV) by Al(III) results in additional surface hydroxyls related to the 'bridging' Si(OH)Al hydroxyl structures, thereby enhancing the value of $\Delta_{dpl}H^*$ (Fig. 6.26).

In the liquid-flow calorimetry experiment, the purified adsorbent bed remains in contact with a stock solution of constant composition. It is clear that the environment of the liquid phase does not change during the measurement. This is an important advantage of the flow calorimetry, especially in the case of solid-solution systems containing electrified interfaces. The study of ions adsorption from aqueous solutions

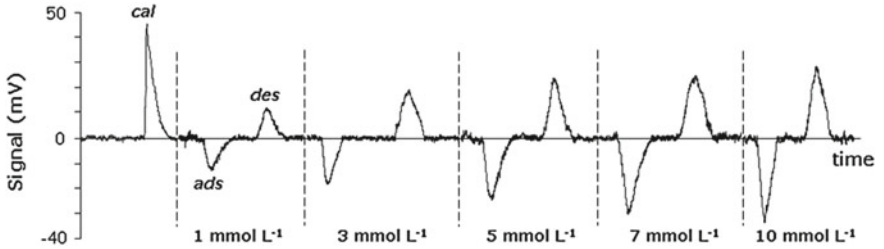

Fig. 6.27 Adsorption of Cd^{2+} cations from $Cd(NO_3)_2$ aqueous solutions of varying concentration at pH 7 onto Spherosil (S_{BET} = 25 m^2g^{-1}) at 298 K [94]: a record of successive saturation and desorption runs showing heat absorption and evolution: calibration (cal), adsorption (ads), and desorption (des). For each concentration of the stock solution m_2^0, the areas under the adsorption and desorption peaks are equal

onto mineral oxides bearing a pH-dependent surface charge always requires constant pH and ionic strength [71, 93].

Figure 6.27 presents the thermogram resulting from adsorption of a heavy metal cation from aqueous solution on the negatively charged surface of Spherosil registered during liquid-flow calorimetry measurements.

For a given concentration of the stock solution m_2^0, continuous percolation of the solution through the calorimetric cell containing the solid sample leads to saturation of the adsorbent with the solute giving rise to a negative heat effect (i.e., adsorption is endothermic) in the form of a peak in which the beginning and the end depend on the solution concentration, flow rate of solution throughout the adsorbent bed, and the kinetics of adsorption. Then the solute is removed from the adsorbent by exchanging the flow of the solution for that of pure solvent. The solute desorption is exothermic and complete in each cycle since the adsorption and desorption enthalpy effects have the same absolute value. Therefore, the successive saturation-desorption cycles can be performed without changing the solid sample in the cell. Although the thermogram in Fig. 6.27 shows that the resulting values of $\Delta_{dpl}H$ increases with increasing concentration, the molar enthalpy $\Delta_{dpl}h$ is proven to be a monotonously decreasing function of m_2^0 [94].

The comparison among thermal displacement effects accompanying the individual adsorption of an alkaline earth metal from aqueous solution is given in Fig. 6.28. The pH and ionic strength of the aqueous phase were identical in the four systems studied.

According to the appropriate speciation diagrams, each metal forms divalent cationic species in aqueous solution under the experimental conditions applied. In spite of the same electric charge of the four cations, the positive enthalpy values are very different, indicating that electrostatic attraction is not the only driving force of adsorption. Since there are Na^+ ions in the heterogeneous system, the total displacement effect should also include ion exchange between sodium and a given divalent cation. Modelling attempts to reproduce the positive displacement effects lead to the conclusion that metal cations may form multidentate complexes with oxygen atoms of ionised silanol groups and changes in the hydration layers of the adsorbing and

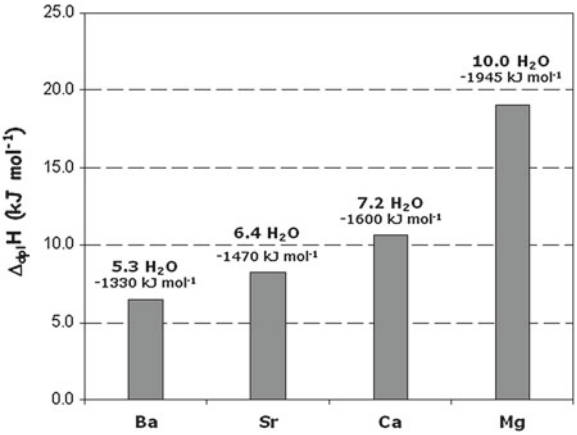

Fig. 6.28 Integral molar enthalpy of displacement related to the adsorption of a metal cation from 10^{-2} M nitrate solution onto Spherosil in the presence of 10^{-1} M $NaNO_3$ at pH 7 and 298 K for various divalent cations [95]. The number of water molecules in the hydration layer and the total enthalpy of hydration are given for each metal cation in aqueous solution

desorbing cations are the main reason for the endothermic character of the overall process [96].

6.5.3 Titration Calorimetry System

Liquid titration calorimeters contain a stirring device, which ensures the homogeneity of the liquid solution or solid suspension in the calorimetric cell, and an injection system permitting the controlled introduction of the reagents from outside the calorimetric cell. Contrary to the flow system, nothing flows out of the calorimeter to the surroundings since the reagents from a stock solution fed to the injection device are collected within the calorimetric cell. The heat detection is usually based on the principles of the isothermal batch or flow microcalorimeters. An example of home-made microcalorimeter [86] designed for study of the enthalpies of mixing of liquid and adsorption from dilute solution onto divided solids is represented schematically in Fig. 6.29.

The variations of temperature in the calorimetric cell induced by dilution or adsorption phenomena, as well as by the electrical calibration are recorded by thermistors arranged as a Wheatstone bridge. The two measuring thermistors, calibration coil and the inlet end of the injection tube are immersed in the solution or suspension. A precision syringe pump injects a stock solution into the cell at a constant rate ranging between 0.01 and 0.2 g min^{-1} without introducing any significant thermal perturbation. The injected solution flows through a heat exchanger tube where it is heated up to attain the temperature of the calorimetric block. The measurement of the

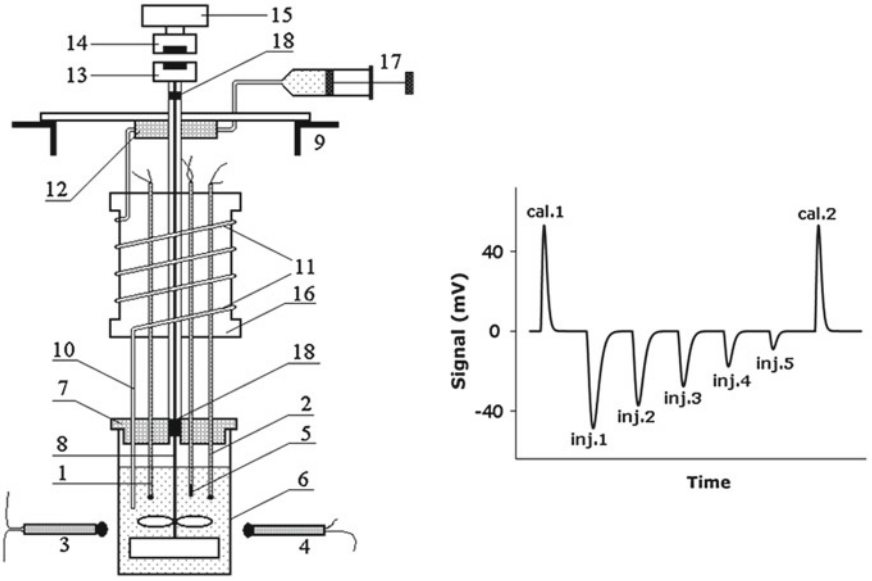

Fig. 6.29 Schematic representation of the calorimetric cell, stirring device, liquid injection and heat effect recording systems of the Montcal titration microcalorimeter [86], together with a thermal record of successive injections of a stock solution by small steps of 0.1 g mn^{-1} into the calorimetric cell: *1*,*2* measuring thermistors, *3*,*4* reference thermistors, *5* calibration coil, *6* stainless steel calorimetric cel (12–30 mL), *7* inert cover for calorimetric cell, *8* stirrer, *9* aluminium calorimetric block, *10* injection tube, *11* heat exchanger tube, *12* pre-heater, *13* magnet attached for stirrer, *14* magnet attached to electric motor, *15* electric motor, *16* aluminium cylinder supporting the exchanger tube, *17* syringe pump, *18* bearing; cal.1, cal.2—calibration peaks, inj.1, …, inj.5—injection peaks

enthalpy changes may be carried out also at higher temperatures (this microcalorimeter has been proven to give satisfactory results at temperatures ranging from 20 and 50°C [86]). For this purpose, an additional power unit provides a stabilised D.C. power supply for heating the calorimetric block to the desired temperature. To reduce the heat loss or temperature variations during injection, it is sometimes necessary to thermostate both the stock solution in the syringe and the injection tube outside the calorimetric block. A horizontal agitator with a variable speed of rotation is driven by a stepper motor fitted through a magnetic transmission.

The dissipation of a known amount of electrical energy inside the calorimetric cell by means of a calibration coil (i.e., the Joule effect) is used to relate the area of the thermal peaks recorded to the enthalpy effects which this represents. The difficulty with this type of calibration in the titration calorimetry systems is related to the fact that the mass of solution in the calorimetric cell is constantly increased by successive injections, thereby changing the calorific capacity of the cell. Therefore, thermal calibration should be regularly repeated after each series of injections in the same calorimetric run.

The calorimetric cell, together with the measuring termistors, stirring device and injection system, can be removed from the calorimetric block to facilitate cleaning and refilling the cell. After the instrument set up and attainment of thermal equilibrium, all steps of the run (injections of the stock solution containing the adsorbate, calibration processing, and recording of the heat effects) are carried out by the appropriate computer system. It is a best practice to weigh the calorimetric cell at the end of each run in order to calculate the real (mean) pump rate. One of the original features of the construction of this calorimeter is also the possibility of easily changing the thickness of the insulating barrier between the calorimetric cell and the metal block. This operation permits the modification of the calorimeter sensitivity and the time of the return of the thermal signal to the baseline.

The titration calorimetry technique presents some limitations due to the necessity of a strict correlation between the dilution and adsorption measurements. A special care must be taken to avoid experimental artefacts and erroneous interpretations in the study of solute adsorption onto solid supports which dissolve to a great extent in solutions or when the quantity of foreign substances released from the solid surface to the bulk solution is significant. In such cases, the composition of the equilibrium supernatant does not correspond to the pure solvent and it may even change constantly with increasing adsorption of the preferentially adsorbed solute [87, 93, 97]. Firstly, this evolution of the supernatant liquid should be monitored thoroughly during adsorption. Then, the evaluation of the correction term for dilution may pose serious problems since the stock solution has to be prepared by dissolving solute in the actual supernatant liquid and not in the pure solvent.

An example of the adsorption system investigated by means of titration calorimetry technique is given in Fig. 6.30 [74]. The experimental adsorption isotherm (Fig. 6.30b) has been determined separately based on the solution depletion method. The solute (dodecyldimethylammonio) butanoate (C12N3C) is a zwitterionic surfactant possessing a dipolar head-group and a linear aliphatic tail. In aqueous solution, the solute molecules self-assemble into aggregates called *micelles*. The concentration of the surrounding aqueous phase at which the surfactant monomers begin to form micelles is known as the *critical micelle concentration* (CMC).

When a micellar stock solution (i.e., its concentration is 10 times the CMC) is injected into a more dilute solution in the calorimetric cell, the constant value of partial molal enthalpy $\overline{h}_2$ in the premicellar region is due to destruction of micelles and dilution of unmicellized species (Fig. 6.30a); the constant $\overline{h}_2$ value in the postmicellar region is ascribed to dilution of micelles.

The molar change in partial molal enthalpy of the surfactant when monomers associate into a micelle at the cmc represents the *standard enthalpy of micellisation* $\Delta_{mic}h^o$ per mole of surfactant monomers [98]. In accordance with the variations of $\overline{h}_2$ as a function of m_2^β in Fig. 6.30a, the enthalpy of micellisation for C12N3C at 298 K is positive, indicating that the micellisation process is endothermic.

The experimental curves describing the adsorption of C12N3C onto Spherosil XOB015 from aqueous solution at 298 K (i.e., Figs. 6.30b and 6.30c) suggest that the phenomenon generally occurs in two stages. At very small quantities of adsorp-

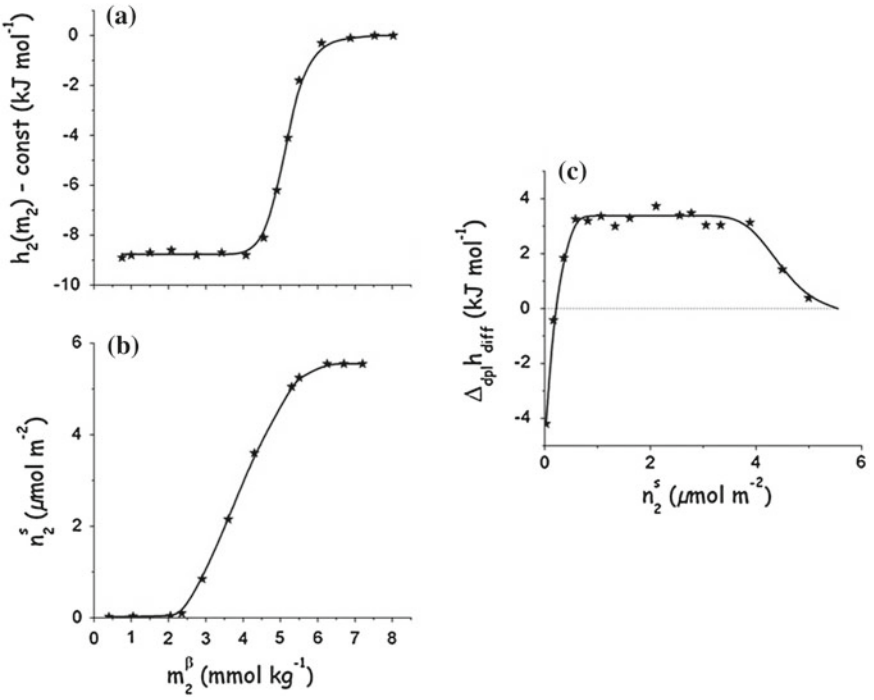

Fig. 6.30 Dilution of aqueous solution of (dodecyldimethylammonio) butanoate (C12N3C) and its adsorption onto Spherosil XOB015 ($S_{BET} = 25 m^2 g^{-1}$) at 298 K: (**a**) enthalpy of dilution, (**b**) adsorption isotherm, (**c**) differential molar enthalpy of displacement. In both types of titration calorimetry experiment, a 0.3 mol kg^{-1} C12N3C solution in pure H_2O was used

tion n_2^s, the values of $\Delta_{dpl} h_{diff}$ are negative so that the phenomenon is exothermic. The negative enthalpies of displacement are usually attributed to individual adsorption of surfactant molecules on an empty surface, where there may be only a few adsorbed molecules, and therefore lateral adsorbate-adsorbate interactions can be neglected [74]. The subsequent adsorption stage is dominated by adsorbate-adsorbate interactions. At moderate and great adsorption amounts, the driving force of adsorption derives from the hydrophobic effect, i.e., lateral chain-chain attractions and the tendency of hydrophobic tails to escape from an aqueous environment. This mode of adsorption is characterised by a constant, positive enthalpy of displacement, showing much similarity to micelle formation in the bulk solution [74]. This surface aggregation is likely controlled by a pseudo nucleation step, i.e., individual adsorption: the first adsorbed monomers act as nucleation centres for future surface-bound surfactant aggregates formed through chain-chain association.

6.5.4 Scanning of Surfactant Aggregation by Titration Calorimetry

Surface-active molecules or ions with an amphiphilic structure are known to have low solubility in water and self-assemble into large aggregates [61]. According to the enthalpy curves presented in Fig. 6.30, surfactant aggregation may occur not only in aqueous solution but also at the Solid-Liquid interface. Since the topic of surfactant aggregation is a well-developed field of research [62, 71, 73, 93, 99, 100], only a brief review of the broad principles is proposed in the present paragraph to better illustrate the contribution of titration calorimetry.

In aqueous solution, the formation of surfactant aggregates is driven by the tendency of the surfactant units to densely pack their tails. The hydrophobic tails remain inside the *liquid-like micellar core* due to unfavourable interactions with water molecules, whereas the polar head-groups, due to favourable interactions with the solvent, form a *hydrophilic outer layer* protecting the hydrophobic core. In the case of ionic surfactants, the Coulombic repulsion among the ionised head-groups is moderated by the specific adsorption of some counter-ions close to them within the Stern part of a curved ionic double layer surrounding the micelle. The micelle morphology and size depend primarily on the nature and relative sizes of the hydrophilic and hydrophobic moieties, as well as on the composition and environment of the aqueous phase [61, 62]. Titration calorimetry may be very useful when studying surfactant micellisation under different experimental conditions. The fundamental thermodynamic parameters, namely the CMC and the standard molar enthalpy of micellisation $\Delta_{mic}h^{\circ}$, can be easily inferred from calorimetric measurements of successive dilutions of a micellar stock solution injected by small steps into aqueous solution having a given composition [73, 74]. Several examples of cationic and zwitterionic surfactants are given in Table 6.5.

It is important to note that the formation of micelles in pure water may be an exothermic, endothermic or even athermic phenomenon, depending on the detailed molecular structure of the surfactant. The CMC value is related to the standard Gibbs energy of micellization, $\Delta_{mic}G^{\circ}$, which always takes negative values. This negative energy results rather from a large increase in entropy, which is ascribed either to structural changes in the solvent, associated with loss of hydration of the hydrophobic tail when the surfactant enters the micelle [61] or to increased freedom of the hydrophobic chain in the interior of the micelle compared to the bulk aqueous medium [101]. Besides the volume and length of the hydrophobic tail, the area per head-group at a curved interface between the micelle core and the aqueous solution σ_{mic} is a critical packing factor having an impact on the ultimate micelle structure [102]. For conventional ionic and zwitterionic surfactants with a single hydrocarbon chain, globular micelles are formed above but near the CMC. A significant increase in the overall surfactant content in aqueous solution may induce a change from spherical micelles to cylindrical (prolate) or disc-like (oblate) aggregates. This change is parralled by a decrease in σ_{mic} which allows a larger number of monomers to be inserted into each aggregate. The maximum cohesion is attained in large lamellar

Table 6.5 Critical micelle concentrations, CMC, and standard enthalpies of micellisation, $\Delta_{mic}h^{\circ}$, per mole of surfactant monomers for selected quaternary ammonium surfactants in pure water at 298 K [73, 74, 88, 97, 103, 104]

Surfactant acronym and formula	CMC mmol kg^{-1}	$\Delta_{mic}h^{\circ}$ kJ mol^{-1}
Zwitterionic surfactants		
C12N1C: $C_{12}H_{25}(CH_3)_2N^+(CH_2)CO_2^-$	1.9	4.6
C12N3C: $C_{12}H_{25}(CH_3)_2N^+(CH_2)_3CO_2^-$	4.6	8.8
C12N3S: $C_{12}H_{25}(CH_3)_2N^+(CH_2)_3SO_3^-$	3.0	3.6
Classical cationic surfactants		
BDDAB: $(C_6H_5)(CH_2)N^+(CH_3)_2(C_{12}H_{25})Br^-$	5.6	−5.3
TTAB: $C_{14}H_{29}N^+(CH_3)_3Br^-$	4.0	−4.7
DTAB: $C_{12}H_{25}N^+(CH_3)_3Br^-$	14.8	−1.6
Gemini cationic surfactants with a hydrophobic spacer		
C12S2C12: $C_{12}H_{25}(CH_3)_2N^+(CH_2)_2N^+(CH_3)_2C_{12}H_{25}Br^-$	0.84	−22
C12S6C12: $C_{12}H_{25}(CH_3)_2N^+(CH_2)_6N^+(CH_3)_2C_{12}H_{25}Br^-$	1.03	−8.5
C12S12C12: $C_{12}H_{25}(CH_3)_2N^+(CH_2)_{12}N^+(CH_3)_2C_{12}H_{25}Br^-$	0.37	−12.2
Gemini cationic surfactants with a hydrophilic spacer		
C12EO3C12: $C_{12}H_{25}(CH_3)_2N^+(C_2H_4O)_3N^+(CH_3)_2C_{12}H_{25}Br^-$	1.02	−6.9
C12EO7C12: $C_{12}H_{25}(CH_3)_2N^+(C_2H_4O)_7N^+(CH_3)_2C_{12}H_{25}Br^-$	1.58	0.0
C12EO12C12: $C_{12}H_{25}(CH_3)_2N^+(C_2H_4O)_{12}N^+(CH_3)_2C_{12}H_{25}Br^-$	1.93	6.3

sheets (flat bilayers) two molecules thick, though surfactant tails never attain such a close-packed arrangement in dilute solutions.

Dimeric or Gemini surfactants (composed of two surfactant units connected by a hydrophobic or hydrophilic chain—*spacer*) usually show a much stronger tendency for micellar growth and self-assemble into larger aggregates with a lower degree of curvature (e.g., linear thread-like and tree-like micelles, or spheroids) [105, 106].

The addition of solid particles (porous or non porous) into aqueous solution induces a decrease in the chemical (or electrochemical) potential of the surfactant solute and, in consequence, the adsorbing surfactant units form, at the solid surface, some periodic adsorbate self-assemblies closely related to the micellar structures encountered in the bulk solution at higher monomer concentrations. Such surface-bound aggregates are spoken of as *interfacial aggregates* or *solloids* [107]. In the general case, the shape and size of solloids are considered to be a compromise between the free curvature, as defined by the energetic, geometrical and packing factors arising from the molecular structure of the surfactant in a given environment, and some influences and constraints imposed, on the one hand, by direct solute-surface

interactions and, on the other hand, by the porosity of the adsorbent. For example, the images of extended aggregate structures showing a closer registry with the underlying surface have been obtained by atomic force microscopy (AFM) on atomically smooth crystalline surfaces [99]. Such solloids have cylindrical and hemi-cylindrical morphologies, depending on the hydrophilic-hydrophobic character of the solid surface. In the case of powders or porous solids, where such microscopy techniques as AFM or ellipsometry have very limited applicability, the titration calorimetry measurements of the differential molar enthalpy of displacement as a function of the surfactant adsorption may provide important information about the self-assembled surfactant structures when compared with the thermal effects of surfactant micellisation in aqueous solution under the same experimental conditions. Nevertheless, calorimetry alone cannot be used to scan for the detailed solloid morphology and appropriate modelling of the adsorption system is necessary.

As far as the adsorption of ionic surfactants on the oppositely charged (and macroscopically flat) surfaces of mineral oxides is concerned, the following three types of solloid are frequently used in the empirical explanation or modelling of the experimental data:

(1) *monolayered hemimicelles*, composed of surfactant units oriented 'head-on' towards the surface, with the surfactant tails forming a hydrophobic film in contact with the equilibrium aqueous solution [108],
(2) *bilayered admicelles*, containing two adsorbed layers of the surfactant monomers directed 'head-on' and 'head-out' with respect to the surface [109],
(3) *small surface micelles*, i.e., spherical isolated aggregates anchored to certain surface sites with aggregation numbers markedly smaller than in bulk micelles [110].

Each of these solloid morphologies is claimed to have a micelle-like character, although the contact area between the water molecules and the hydrophobic surfactant moieties is not always reduced to the minimum.

Typical plots of the differential molar enthalpy of displacement against the amount of the surfactant adsorbed reveal significant variations in the enthalpy value when the adsorption progresses. An example of the enthalpy curve is given in Fig. 6.31. Such trends in $\Delta_{dpl}h_{diff}$ with increasing n_2^s suggest almost continuous evolution of the solloid morphology and size: the aggregates self-assembled from the adsorbing surfactant monomers at equilibrium concentrations in the bulk phase lower than the CMC may grow in the direction parallel and perpendicular to the solid surface. The most successful theoretical attempts to mimic complex shapes of both the experimental adsorption isotherms and enthalpy of displacement curves have been based on the assumption that the adsorbed phase at a given surface coverage can be seen as a mixture of mutually interacting surface-bound monomers, monolayered hemimicelles, and bilayered admicelles varying in size and number [65, 111]. The proportion between the various types of adsorbate species is shown to undergo significant changes with increasing surfactant adsorption, first monomers and monolayered aggregates and then bilayered admicelles dominating on the surface.

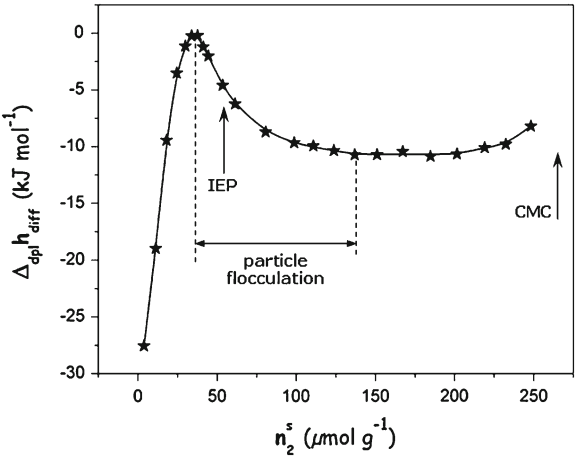

Fig. 6.31 Variations of the differential molar enthalpy of displacement as a function of the adsorption of benzyldimethylammonium bromide (BDDAB) onto silica powder S91-16 (Rhône-Poulenc, France) from aqueous solutions at 298 K at the initial pH 8 [89]. The arrows indicate the critical micelle concentration (CMC) and the isoelectric point (IEP) at which the effective charge of the silica particles together with the specifically adsorbed surfactant cations becomes equal to zero. The region of particle flocculation (where the silica particles covered with the adsorbed species are predominantly hydrophobic) is also shown

When surfactants are adsorbed onto fine-pore solids, the growth of solloids in the direction perpendicular to the pore walls should be limited by the pore volume [93]. For mesoporous ordered mineral oxides, it may be even that the surfactant monomers adsorb only head-on with respect to the hydrophilic surface and the hydrophobic tails of the surfactant units adsorbed on the opposite walls interpenetrate themselves in such a way as to produce "internal" aggregates, which fill the pore space. To check whether the head-out adsorption of surfactant monomers is to be excluded in such systems, one can refer to the micellar solubilisation of water-insoluble, hydrophobic materials as well as polar substances, which dissolve in water only to a limited extent [62, 69, 112, 113]. For low contents in aqueous solution, some small molecules may behave as molecular probes, occupying specific sites in surfactant aggregates without greatly disturbing their morphology and size. The exact locus of a given probe molecule in a micelle reflects the type of forces operating between the aggregate and the solubilised material. This justifies the use of titration calorimetry to study micellar solubilisation. One of the possible methodologies is to lump water and the additive together into the mean solvent and investigate the micellisation of the surfactant in this new medium. The molar enthalpies of micellisation for several cationic surfactants in the absence and the presence of phenol at various additive contents are compared schematically in Fig. 6.32.

On the addition of phenol to the aqueous phase, the enthalpy of micellisation per mole of the surfactant becomes more negative (and the CMC value is decreased), thereby indicating more favourable phenol-surfactant interactions after the transfer

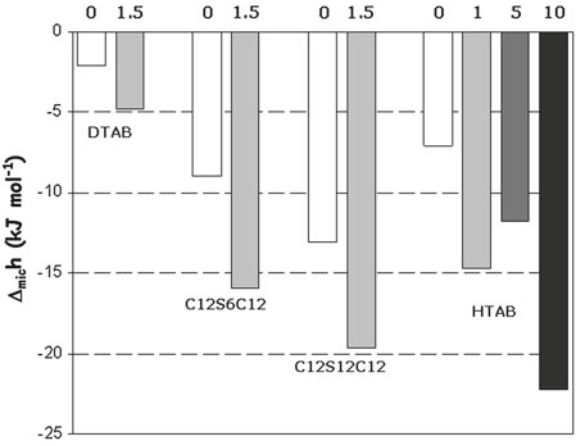

Fig. 6.32 Molar enthalpies of micellisation, $\Delta_{mic}h$, for selected quaternary ammonium surfactants in pure water and in the presence of phenol molecules in the aqueous phase at 298 K [88, 114, 115]. The overall phenol (PhOH) content (in mmol kg^{-1}) is reported on the X-axis. The surfactant acronyms are explained in Table 6.5. For hexadecyltrimethylammonium bromide (HTAB), the calorimetry measurements were carried out at 303 K safely above the Krafft point

of the additive to the micellar phase. Therefore, phenol molecules are preferentially located in the outer portions of cationic micelles close to the surfactant head-groups, without involving much rearrangement of the micelle structure. When the phenol concentration increases (e.g., PhOH-HTAB systems), the existence of an endothermic contribution to $\Delta_{mic}h$ may be deduced from the evolution of the enthalpy value. To better understand this positive enthalpy component, one may refer to the detailed analysis of ^{1}H NMR spectra recorded with the various PhOH-HTAB solutions: additional phenol units penetrate deeper into the micelle core producing unfavorable interactions with cationic micelles of HTAB [88]. Consequently, if phenol is to be used as a molecular probe for detecting the presence of the head-out adsorbed surfactants at the Solid-Liquid interface, the overall additive content in the system should remain low.

Based on the assumption that surfactant aggregation on the solid surface is a prerequisite for the uptake of phenol and the aromatic molecules can be located only close to the "free" head-groups of the surfactant units within the interfacial aggregates, it may be helpful to compare the curves presenting the differential enthalpy of displacement as a function of the surface coverage by the surfactant adsorbate in the absence and in the presence of the additive. Figure 6.33 illustrates such a comparison for a cationic surfactant adsorbed onto ordered mesoporous aluminosilicate of the MCM-41 type.

The difference between the two curves is clearly pronounced at higher surface coverage ratios where surface aggregation is considered to be the predominant sorption mode. With a small amount of phenol added to the aquous phase, the displacement phenomenon is more exothermic in this region: the related portion of the enthalpy

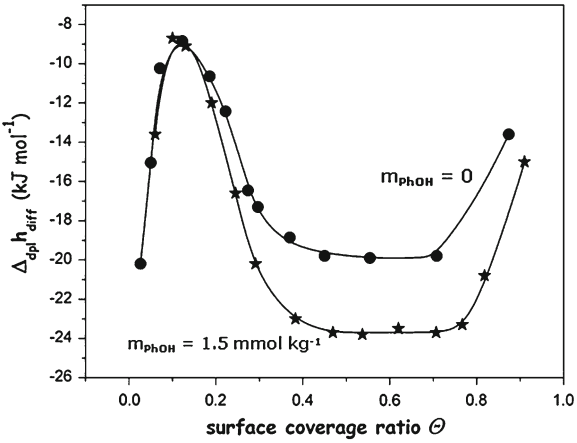

Fig. 6.33 Effect of phenol addition on the differential molar enthalpy of displacement upon adsorption of cationic Gemini C12C12C12 onto ordered mesoporous aluminosilicate of the MCM-41 type (S_{BET} = 860 m^2g^{-1}, mean pore diameter = 5 nm, Si:Al = 32) from aqueous solution at 298 K and the initial pH 8 [114]. The $\Delta_{dpl}h_{diff}$ enthalpy is plotted against the adsorption coverage of the solid surface by the surfactant cations

curve can be viewed as shifted towards more negative values by a constant value in comparison with the curve corresponding to the system without phenol. Similar enthalpy behaviour of this surfactant has been observed during its micellisation in aqueous solution (cf., Fig. 6.32). This analysis provides strong indication for phenol incorporation in the interfacial aggregates having their head-groups oriented outwards. Therefore, the image of all surfactant units interacting directly with the negatively charged surface and their hydrophobic tails filling the whole pore space available is rather to be excluded.

The coexistence of hydrophilic and hydrophobic nano-domains separated in space, with a local order and fluidity typical of liquids, confer to supramolecular surfactant structures remarkable properties, which are advantageous in applications involving molecular confinement within nanoscopic regions and reactivity in microheterogeneous media. Micelle-mediated reactions constitute the basis of the so-called micellar catalysis [62, 116], admicellar catalysis [117] or admicellar polymerisation [118] in which reaction mechanisms may be controlled at a molecular level to save energy and raw materials, as well as to avoid lengthy post-reaction purification and analytical steps.

6.6 Concluding Remarks

The intention of the present chapter was to present mostly the prospective advantages, but also some limitations, of the use of isothermal calorimetry at the Solid-Liquid interface as a powerful tool in the study of interactions between solid surfaces and

the surrounding liquid phase. The operating principles and examples of applications were described for three calorimetry techniques frequently used to date in Surface Science and Technology: (i) wetting and immersional calorimetry, (ii) liquid flow calorimetry, (iii) titration batch calorimetry. The interested reader is encouraged to search for other outstanding examples of commercial or home-made instruments and their specific uses which have not been included here.

Wetting and immersional calorimetry may be employed to determine surface properties of catalysts, adsorbents and other solid materials in contact with liquids. Based on the calorimtery measurements of the various contributions to the total surface enthalpy of a solid, it is possible to evaluate the hydrophobic-hydrophilic character of its surface. The Harkins-Jura method for the evaluation of the specific surface area of a solid based on enthalpy changes in the so-called immersion-adsorption-wetting cycle gives the surface area of contact between this solid and a pure liquid or a solution, thereby sheding light on the availability of the solid surface under real experimental conditions.

Liquid flow or batch titration calorimetry techniques offer an opportunity for studying the macroscopic outcome of the various interactions involved in interfacial phenomena occurring at the Solid-Liquid Interface. The enthalpy changes appear very sensitive to the partial mechanisms through which a given phenomenon can occur. In particular, the effects of heterogeneity of a solid surface (i.e., surface sites with different adsorption energies, "confinement effects" due to adsorbent porosity) show up more clearly in heat quantities than in adsorption isotherms, thereby allowing easier interpretation of the phenomenon studied. The assessment of the thermodynamic reversibility of competitive adsorption from multicomponent solutions is one of the different possibilities of isothermal calorimetry. Self-assembled surfactant structures, defined by the regular assembly of small molecular entities into larger supra-molecular structures either in aquous solution or at the Solid-Liquid interface, may be thermodynamically described based on the results of titration calorimetry measurements. Here the next step would be to use high sensitivity isothermal calorimeters to determine the thermal effects of micelle-mediated reactions in micellar or admicellar catalysis.

In spite of many advantages, Solid-Liquid calorimetry alone is not capable of solving satisfactorily many detailed problems concerning the resulting interfacial mechanisms. It certainly cannot provide much information on entropy changes. In consequence, calorimetric measurements have to be always supplemented by other experimental studies reported on the system so as to obtain a more complete description of the phenomenon

References

1. R. Defay, I. Prigogine, A. Bellemans, D.H. Everett, *Surface Tension and Adsorption* (Longmans, London, 1966)
2. P.C. Hiemenz, *Principles of Colloid and Surface Chemistry*, 2nd edn. (Marcel Dekker, New York, 1986)

3. R.J. Hunter, *Foundations of Colloid Science,*, vol. 1 and 2, (Oxford University Press, Oxford, 1989)
4. A.W. Adamson, *Physical Chemistry of Surfaces*, 5th edn. (Wiley-Interscience, New York, 1990)
5. J. Lyklema, *Fundamentals of Interface and Colloid Science*, vol. 1–3, (Academic Press, London, 1991–2000)
6. D.H. Everett, Reporting data on adsorption from solution at the solid/solution interface (Recommendations 1986). Pure Appl. Chem. **58**(7), 967–984 (1986). doi:10.1351/pac198658070967
7. W. Rudzinski, D.H. Everett, *Adsorption of Gases on Heterogeneous Surfaces* (Academic Press, London, 1992)
8. E.A. Guggenheim, *Thermodynamics*, 5th edn. (North Holland Publishing Co., Amsterdam, 1967)
9. J.F. Padday, in *Surface Tension. II. The Measurement of Surface Tension*, vol 1, ed. by E. Matijevic, F. Eirich. Surface and Colloid Science, vol 1 (Wiley-Interscience, New York, 1969), pp. 101–149
10. N.R. Pallas, Y. Harrison, An automated drop shape apparatus and the surface tension of pure water. Colloids Surf. **43**(2), 169–194 (1990). doi:10.1016/0166-6622(90)80287-E
11. R. Cini, G. Loglio, A. Ficalbi, Temperature dependence of the surface tension of water by the equilibrium ring method. J. Colloid Interface Sci. **41**(2), 287–297 (1972). doi:10.1016/0021-9797(72)90113-0
12. G. Loglio, A. Ficalbi, R. Cini, A new evaluation of the surface tension temperature coefficients for water. J. Colloid Interface Sci. **64**(1), 198–198 (1978). doi:10.1016/0021-9797(78)90352-1
13. R.C. Weast (ed.), *Handbook of Chemistry and Physics*, 45th edn. (CRC, Cleveland, 1964)
14. A.R.C. Westwood, T.T. Hitch, Surface energy of 100 potassium chloride. J. Appl. Phys. **34**(10), 3085–3089 (1963)
15. S. Boffi, M. Ricci, On the cleavage energy of magnesium oxide. Mater. Chem. **1**(4), 289–296 (1976). doi:10.1016/0390-6035(76)90030-4
16. J.J. Gilman, Direct measurements of the surface energies of crystals. J. Appl. Phys. **31**(12), 2208–2218 (1960)
17. E. Orowan, Die Zugfestigkeit von Glimmer und das Problem der technischen Festigkeit. Z. für Phys. A Hadrons Nuclei **82**(3), 235–266 (1933). doi:10.1007/bf01341490
18. R.J. Good, Contact angle, Wetting, and Adhesion: a critical review, in *Contact Angle*, ed. by K.L. Mittal, Wettability and Adhesion (VSP, Utrecht, 1993), pp 3–36
19. C.J. Van Oss, M.K. Chaudhury, R.J. Good, Interfacial Lifshitz-van der Waals and polar interactions in macroscopic systems. Chem. Rev. **88**(6), 927–941 (1988). doi:10.1021/cr00088a006
20. A.C. Zettlemoyer, Hydrophobic surfaces. J. Colloid Interface Sci. **28**(3–4), 343–369 (1968). doi:10.1016/0021-9797(68)90066-0
21. J.N. Israelachvili, *Intermolecular and Surface Forces*, 2nd edn. (Academic Press, London, 1991)
22. J.C. Berg, The Role of Acid-Base Interactions in Wetting and Related Phenomena, in *Wettability*, ed. by J.C. Berg (Marcel Dekker, New York, 1993), pp. 75–148
23. C.J. Van Oss, M.K. Chaudhury, R.J. Good, Monopolar surfaces. Adv. Colloid Interface Sci. **28**, 35–64 (1987). doi:10.1016/0001-8686(87)80008-8
24. D.B. Hough, L.R. White, The calculation of Hamaker constants from Liftshitz theory with applications to wetting phenomena. Adv. Colloid Interface Sci. **14**(1), 3–41 (1980). doi:10.1016/0001-8686(80)80006-6
25. J. Visser, On Hamaker constants: a comparison between Hamaker constants and Lifshitz-van der Waals constants. Adv. Colloid Interface Sci. **3**(4), 331–363 (1972). doi:10.1016/0001-8686(72)85001-2
26. C.J. Van Oss, R.J. Good, M.K. Chaudhury, The role of van der Waals forces and hydrogen bonds in "hydrophobic interactions" between biopolymers and low energy surfaces. J. Colloid Interface Sci. **111**(2), 378–390 (1986). doi:10.1016/0021-9797(86)90041-X

27. R.S. Drago, Quantitative evolution and prediction of donor-acceptor interactions. Struct. Bond. (Berlin) **15**, 73–139 (1973)
28. F.M. Fowkes, Quantitative characterization of the acid-base properties of solvents, polymers, and inorganic surfaces. in *Acid-Base Interactions—Relevance to Adhesion Science and Technology* ed. by K.L. Mittal, H.R.J. Anderson (VSP, Utrecht, 1991), pp. 93–115
29. M.K. Chaudhury, Interfacial interaction between low-energy surfaces. Mater. Sci. Eng. R Rep. **16**(3), 97–159 (1996). doi:10.1016/0927-796X(95)00185-9
30. J.M. Douillard, T. Zoungrana, S. Partyka, Surface Gibbs free energy of minerals: some values. J. Pet. Sci. Eng. **14**(1–2), 51–57 (1995). doi:10.1016/0920-4105(95)00018-6
31. L.A. Girifalco, R.J. Good, A theory for the estimation of surface and interfacial energies. I. Derivation and application to interfacial tension. J. Phys. Chem. **61**(7), 904–909 (1957). doi:10.1021/j150553a013
32. C.J. Van Oss, Acid-base interfacial interactions in aqueous media. Colloids Surf. A Physicochemical Eng. Aspects **78**, 1–49 (1993). doi:10.1016/0927-7757(93)80308-2
33. P.G. De Gennes, Wetting: statics and dynamics. Rev. Mod. Phys. **57**(3), 827 (1985)
34. A.W. Neumann, R.J. Good, Technique of measuring contact angle, in *Surface and Colloid Science*, vol. 11, ed. by R.J. Good, R.R. Stromberg (Plenum Press, New York, 1979), pp. 31–91
35. C.J. Van Oss, R.F. Giese, Z. Li, K. Murphy, J. Norris, M.K. Chaudhury, R.J. Good, Determination of contact angles and pore sizes of porous media by column and thin layer wicking. J. Adhes. Sci. Technol. **6**, 413–428 (1992). doi:10.1163/156856192X00755
36. H.G. Bruil, J.J. van Aartsen, The determination of contact angles of aqueous surfactant solutions on powders. Colloid Polym. Sci. **252**(1), 32–38 (1974). doi:10.1007/bf01381692
37. J.M. Douillard, V. Médout-Marère, A new interpretation of contact angle variations in view of a recent analysis of immersion calorimetry. J. Colloid Interface Sci. **223**(2), 255–260 (2000). doi:10.1006/jcis.1999.6679
38. V. Médout-Marère, S. Partyka, G. Chauveteau, J.M. Douillard, R. Dutartre, Surface heterogeneity of passively oxidized silicon carbide particles: vapor adsorption isotherms. J. Colloid Interface Sci. **262**(2), 309–320 (2003). doi:10.1016/S0021-9797(03)00198-X
39. C.J. Van Oss, The Apolar and Polar Properties of Liquid Water and Other Condensed-Phase Materials. in *Interface Science and Technology*, vol 16 (Elsevier, Amsterdam, 2008), pp. 13–30. doi:10.1016/S1573-4285(08)00202-0
40. V. Médout-Marère, A. El Ghzaoui, C. Charnay, J.M. Douillard, G. Chauveteau, S. Partyka, Surface Heterogeneity of Passively Oxidized Silicon Carbide particles: Hydrophobic-Hydrophilic partition. J. Colloid Interface Sci. **223**(2), 205–214 (2000). doi:10.1006/jcis.1999.6625
41. J.M. Douillard, Concerning the thermodynamic consistency of the "Surface Tension Components" equations. J. Colloid Interface Sci. **188**(2), 511–515 (1997). doi:10.1006/jcis.1997.4768
42. J.M. Douillard, J. Zajac, H. Malandrini, F. Clauss, Contact angle and film pressure: study of a talc surface. J. Colloid Interface Sci. **255**(2), 341–351 (2002). doi:10.1006/jcis.2002.8611
43. M.J. Meziani, J. Zajac, J.-M. Douillard, D.J. Jones, S. Partyka, J. Rozière, Evaluation of surface enthalpy of porous aluminosilicates of the MCM-41 type using immersional calorimetry: effect of the pore size and framework Si:Al ratio. J. Colloid Interface Sci. **233**(2), 219–226 (2001). doi:10.1006/jcis.2002.8611
44. V. Médout-Marère, H. Belarbi, P. Thomas, F. Morato, J.C. Giuntini, J.M. Douillard, Thermodynamic analysis of the immersion of a swelling clay. J. Colloid Interface Sci. **202**(1), 139–148 (1998). doi:10.1006/jcis.1998.5400
45. M.A. Wilson, A. Pohorille, L.R. Pratt, Molecular dynamics of the water liquid-vapor interface. J. Phys. Chem. **91**(19), 4873–4878 (1987). doi:10.1021/j100303a002
46. W. Drost-Hansen, Structure of water near solid interfaces. Ind. Eng. Chem. **61**(11), 10–47 (1969). doi:10.1021/ie50719a005
47. W.D. Harkins, *The Physical Chemistry of Surface Films* (Reinhold, New York, 1952)
48. Proceedings of BP Symposium on the Significance of the Heats of Adsorption at the Solid-Liquid Interface. in A.J. Groszek, Sunbury-on-Thames, BP Research Centre (1971)

49. S. Partyka, J.M. Douillard, Nature of interactions between organic pure liquids and model rocks: a calorimetric investigation. J. Pet. Sci. Eng. **13**(2), 95–102 (1995). doi:10.1016/0920-4105(94)00065-C
50. J.M. Douillard, What can really be deduced from enthalpy of immersional wetting experiments? J. Colloid Interface Sci. **182**(1), 308–311 (1996). doi:10.1006/jcis.1996.0468
51. T.W. Healy, D.W. Fuerstenau, The oxide-water interface-Interrelation of the zero point of charge and the heat of immersion. J. Colloid Sci. **20**(4), 376–386 (1965). doi:10.1016/0095-8522(65)90083-8
52. D.A. Griffiths, D.W. Fuerstenau, The effect of pH and temperature on the heat of immersion of alumina. J. Colloid Interface Sci. **80**(1), 271–283 (1981). doi:10.1016/0021-9797(81)90181-8
53. M. El Wafir, Approche thermodynamique des interactions entre les liquides et les solides modeles issus des roches reservoirs de petrole. Ph.D. Thesis, (University of Montpellier 2, Montpellier 1991)
54. S. Partyka, F. Rouquerol, J. Rouquerol, Calorimetric determination of surface areas: Possibilities of a modified Harkins and Jura procedure. J. Colloid Interface Sci. **68**(1), 21–31 (1979). doi:10.1016/0021-9797(79)90255-8
55. J. Fripiat, J. Cases, M. Francois, M. Letellier, Thermodynamic and microdynamic behavior of water in clay suspensions and gels. J. Colloid Interface Sci. **89**(2), 378–400 (1982). doi:10.1016/0021-9797(82)90191-6
56. X.-C. Zeng, Y. Chen, X.-N. Chen, J.-Q. Xie, F.-B. Jiang, Thermo-kinetic research method for faster reactions: modifier method of distorted thermoanalytical curve. Thermochim. Acta **332**(1), 97–102 (1999). doi:10.1016/S0040-6031(99)00092-1
57. W. Hemminger, G. Höhne, *Calorimetry—Fundamentals and Practice* (Verlag Chemie, Weinheim/Basel, 1984)
58. W. Zielenkiewicz, E. Margas, *Theory of Calorimetry* (Kluwer Academic Publishers, Dordrecht, 2002)
59. E. Calvet, H. Prat, *Microcalorimetrie, Applications Physico-Chimiques et Biologiques* (Masson, Paris, 1956)
60. H. Malandrini, Une etude thermodynamique de l'energie superficielle des solides divises : Determination de la tension superficielle de poudres talco-chloriteuses. Ph.D. Thesis, (University of Montpellier 2, Montpellier, 1995)
61. C. Tanford, *The Hydrophobic Effect. Formation of Micelles and Biological Membranes*, 2nd edn. (Wiley, New York, 1980)
62. M.J. Rosen, *Surfactants and Interfacial Phenomena*, 2nd edn. (Wiley, New York, 1989)
63. J. Lyklema, Adsorption at solid-liquid interfaces with special reference to emulsion systems. Colloids Surf. A Physicochemical Eng. Aspects **91**, 25–38 (1994). doi:10.1016/0927-7757(94)02718-8
64. R. Denoyel, F. Rouquerol, J. Rouquerol, Thermodynamics of adsorption from solution: Experimental and formal assessment of the enthalpies of displacement. Journal of Colloid and Interface Science **136**(2), 375–384 (1990). doi:10.1016/0021-9797(90)90384-Z
65. W. Rudzinski, J. Narkiewicz-Michalek, R. Charmas MD, Piasecki W, Zajac J, Thermodynamics of adsorption at heterogeneous solid—liquid interfaces, in *Interfacial Dynamics*, ed. by N. Kallay, Surfactant Science Series (Marcel Dekker, New York , 1999), pp. 83–162
66. F.D. Rossini, *Chemical Thermodynamics*, 3rd edn. (Wiley, New York, 1961)
67. I. Prigogine, A. Bellemans, V. Mathot, *The Molecular Theory of Solutions* (North-Holland Publishing Company, Amsterdam, 1957)
68. H.S. Harned, B.B. Owen, *The Physical Chemistry of Electrolytic Solutions* (Reinhold, New York, 1958)
69. R.M. Garrels, C.L. Christ, *Solutions, Minerals and Equilibria* (Freeman, Cooper & Co., San Francisco, 1965)
70. M.J. Sparnaay, *The Electrical Double Layer*, vol 4, 1st edn. Properties of Interfaces, (Pergamon Press, Glasgow, 1972)

71. L.K. Koopal, Adsorption of ions and surfactants, in *Coagulation and Flocculation: Theory and Applications*, ed. by B. Dobias, vol. 47, Surfactant Science Series, (Marcel Dekker, New York, 1993), pp. 101–208
72. H.-H. Kohler, Surface charge and surface potential, in *Coagulation and Flocculation: Theory and Applications*, ed. by B. Dobias, vol. 47, Surfactant Science Series, (Marcel Dekker, New York, 1993), pp. 37–56
73. J. Zajac, Adsorption microcalorimetry used to study interfacial aggregation of quaternary ammonium surfactants (zwitterionic and cationic) on powdered silica supports in dilute aqueous solutions. Colloids Surf. A Physicochemical Eng. Aspects **167**(1–2), 3–19 (2000). doi:10.1016/S0927-7757(99)00479-3
74. J. Zajac, C. Chorro, M. Lindheimer, S. Partyka, Thermodynamics of Micellization and Adsorption of Zwitterionic Surfactants in Aqueous Media. Langmuir **13**(6), 1486–1495 (1997). doi:10.1021/la960926d
75. J. Zajac, A.J. Groszek, Adsorption of C60 fullerene from its toluene solutions on active carbons: Application of flow microcalorimetry. Carbon **35**(8), 1053–1060 (1997). doi:10.1016/S0008-6223(97)00058-4
76. W. Rudzinski, J. Zajac, I. Dekany, F. Szanto, Heats of immersion in monolayer adsorption from binary liquid mixtures on heterogeneous solid surfaces: equations for excess isotherms and heats of immersion corresponding to condensation approximation and Rudzinski-Jagiello approach. J. Colloid Interface Sci. **112**(2), 473–483 (1986). doi:10.1016/0021-9797(86)90115-3
77. D.H. Everett, Enthalpy and entropy effects in adsorption from solution. J. Phys. Chem. **85**(22), 3263–3265 (1981). doi:10.1021/j150622a012
78. G.W. Woodbury Jr, L.A. Noll, Heat of adsorption of liquid mixtures on solid surfaces: comparison of theory and experiment. Colloids Surf. **8**(1), 1–15 (1983). doi:10.1016/0166-6622(83)80068-7
79. A.J. Groszek, Flow adsorption microcalorimetry. Thermochim. Acta **312**(1–2), 133–143 (1998). doi:10.1016/S0040-6031(97)00447-4
80. A.J. Groszek, M.J. Templer, Innovative flow-adsorption microcalorimetry. ChemTech **29**(11), 19–26 (1999)
81. R. Denoyel, F. Rouquerol, J. Rouquerol, Interest and requirements of liquid-flow microcalorimetry in the study of adsorption from solution in the scope of tertiary oil recovery, in *Adsorption from Solution*, ed. by C. Rochester (Academic Press, London, 1982), pp. 1–10
82. G.W. Woodbury Jr, L.A. Noll, Heats of adsorption from flow calorimetry: relationships between heats measured by different methods. Colloids Surf. **28**, 233–245 (1987). doi:10.1016/0166-6622(87)80187-7
83. R. Denoyel, F. Rouquerol, J. Rouquerol, Adsorption of anionic surfactants on alumina: complementarity of the information provided by batch and liquid flow microcalorimetry. Colloids Surf. **37**, 295–307 (1989). doi:10.1016/0166-6622(89)80126-X
84. J.M. Miller, *Chromatography: Concepts and Contrasts*, 2nd edn. (Wiley, New York, 2005)
85. Z. Kiraly, R.H.K. Borner, G.H. Findenegg, Adsorption and Aggregation of C8E4 and C8G1 Nonionic Surfactants on Hydrophilic Silica Studied by Calorimetry. Langmuir **13**(13), 3308–3315 (1997). doi:10.1021/la9620768
86. S. Partyka, E. Keh, M. Lindheimer, A. Groszek, A new microcalorimeter for the study of solutions, adsorption and suspensions. Colloids Surf. **37**, 309–318 (1989). doi:10.1016/0166-6622(89)80127-1
87. M. Chorro, C. Chorro, O. Dolladille, S. Partyka, R. Zana, Adsorption mechanism of conventional and dimeric cationic surfactants on silica surface: effect of the state of the surface. J. Colloid Interface Sci. **210**(1), 134–143 (1999). doi:10.1006/jcis.1998.5936
88. R. Chaghi, L.-C. de Ménorval, C. Charnay, G. Derrien, J. Zajac, Interactions of phenol with cationic micelles of hexadecyltrimethylammonium bromide studied by titration calorimetry, conductimetry, and 1H NMR in the range of low additive and surfactant concentrations. J. Colloid Interface Sci. **326**(1), 227–234 (2008). doi:10.1016/j.jcis.2008.07.035

89. J.L. Trompette, Contribution de la calorimetrie a l'etude de l'interaction tensioactif cationique - solide divise. Ph.D. Thesis (University of Montpellier 2, Montpellier, 1995)
90. A.J. Groszek, Graphitic and polar surface sites in carbonaceous solids. Carbon **25**(6), 717–722 (1987). doi:10.1016/0008-6223(87)90140-0
91. A.J. Groszek, S. Partyka, Measurements of hydrophobic and hydrophilic surface sites by flow microcalorimetry. Langmuir **9**(10), 2721–2725 (1993)
92. K. Szczodrowski, B. Prélot, S. Lantenois, J.-M. Douillard, J. Zajac, Effect of heteroatom doping on surface acidity and hydrophilicity of Al, Ti, Zr-doped mesoporous SBA-15. Microporous Mesoporous Mater. **124**(1–3), 84–93 (2009). doi:10.1016/j.micromeso.2009.04.035
93. J. Zajac, Mechanism of ionic and zwitterionic surfactant adsorption from dilute solutions onto charged non-porous and porous mineral oxides inferred from thermodynamic studies, in *Recent Research Developments in Surface and Colloids*, ed. by S.G. Pandalai (Research Signpost, Kerala, 2004), pp. 265–300
94. S. Lantenois, B. Prélot, J.-M. Douillard, K. Szczodrowski, M.-C. Charbonnel, Flow microcalorimetry: experimental development and application to adsorption of heavy metal cations on silica. Appl. Surface Sci. **253**(13), 5807–5813 (2007). doi:10.1016/j.apsusc.2006.12.064
95. B. Prelot, S. Lantenois, M.-C. Charbonnel, F. Marchandeau, J.M. Douillard, J. Zajac, What are the main contributions to the total enthalpy of displacement accompanying the adsorption of some multivalent metals at the silica–electrolyte interface? J. Colloid Interface Sci. **396**, 205–209 (2013) . doi:10.1016/j.jcis.2012.12.049
96. B. Prelot, S. Lantenois, C. Chorro, M.-C. Charbonnel, J. Zajac, J.M. Douillard, Effect of nanoscale pore space confinement on cadmium adsorption from aqueous solution onto ordered mesoporous silica: a combined adsorption and flow calorimetry study. J. Phys. Chem. C **115**(40), 19686–19695 (2011). doi:10.1021/jp2015885
97. J.L. Trompette, J. Zajac, E. Keh, S. Partyka, Scanning of the cationic surfactant adsorption on a hydrophilic silica surface at low surface coverages. Langmuir **10**(3), 812–818 (1994)
98. R. De Lisi, C. Ostiguy, G. Perron, J.E. Desnoyers, Complete thermodynamic properties of nonyl- and decyltrimethylammonium bromides in water. J. Colloid Interface Sci. **71**(1), 147–166 (1979). doi:10.1016/0021-9797(79)90229-7
99. R. Atkin, V.S.J. Craig, E.J. Wanless, S. Biggs, Mechanism of cationic surfactant adsorption at the solid-aqueous interface. Adv. Colloid Interface Sci. **103**(3), 219–304 (2003). doi:10.1016/S0001-8686(03)00002-2
100. J.H. Clint, *Surfactant Aggregation* (Blackie, Glasgow/London, 1992)
101. R.H. Aranow, L. Witten, The environmental influence on the behavior of long chain molecules. J. Phys. Chem. **64**(11), 1643–1648 (1960). doi:10.1021/j100840a010
102. H. Hoffmann, Fascinating phenomena in surfactant chemistry. Adv. Mater. **6**(2), 116–129 (1994). doi:10.1002/adma.19940060204
103. A. Bendjeriou, G. Derrien, P. Hartmann, C. Charnay, S. Partyka, Microcalorimetric studies of cationic gemini surfactant with a hydrophilic spacer group. Thermochim. Acta **434**(1–2), 165–170 (2005). doi:10.1016/j.tca.2005.01.034
104. L. Grosmaire, M. Chorro, C. Chorro, S. Partyka, R. Zana, Alkanediyl-alpha, omega-bis(dimethylalkylammonium bromide) surfactants - 9. Effect of the spacer carbon number and temperature on the enthalpy of micellization. J. Colloid Interface Sci. **246**(1), 175–181 (2002). doi:10.1006/jcis.2001.8001
105. M. Pisarcik, M.J. Rosen, M. Polakovicova, F. Devinsky, I. Lacko, Area per surfactant molecule values of gemini surfactants at the liquid-hydrophobic solid interface. J. Colloid Interface Sci. **289**(2), 560–565 (2005). doi:10.1016/j.jcis.2005.03.092
106. R. Zana, Dimeric (Gemini) surfactants: effect of the spacer group on the association behavior in aqueous solution. J. Colloid Interface Sci. **248**(2), 203–220 (2002). doi:10.1006/jcis.2001.8104
107. P. Somasundaran, J.T. Kunjappu, In-situ investigation of adsorbed surfactants and polymers on solids in solution. Colloids Surf. **37**, 245–268 (1989). doi:10.1016/0166-6622(89)80123-4

108. P. Somasundaran, D.W. Fuerstenau, Mechanisms of Alkyl Sulfonate Adsorption at the Alumina-Water Interface. J. Phys. Chem. **70**(1), 90–96 (1966). doi:10.1021/j100873a014
109. M.A. Yeskie, J.H. Harwell, On the structure of aggregates of adsorbed surfactants: the surface charge density at the hemimicelle/admicelle transition. J. Phys. Chem. **92**(8), 2346–2352 (1988). doi:10.1021/j100319a048
110. H. Rupprecht, T. Gu, Structure of adsorption layers of ionic surfactants at the solid/liquid interface. Colloid Polym. Sci. **269**(5), 506–522 (1991). doi:10.1007/bf00655889
111. B. Li, E. Ruckenstein, Adsorption of Ionic Surfactants on charged solid surfaces from Aqueous solutions. Langmuir **12**(21), 5052–5063 (1996). doi:10.1021/la951559t
112. S.D. Christian, J.F. Scamehorn (eds.), *Solubilisation in Surfactant Aggregates, Surfactant Science Series*, vol. 55 (Marcel Dekker, New York, 1995)
113. R. Zana, Aqueous surfactant-alcohol systems: a review. Adv. Colloid Interface Sci. **57**, 1–64 (1995). doi:10.1016/0001-8686(95)00235-I
114. M.J. Meziani, H. Benalla, J. Zajac, S. Partyka, D.J. Jones, Adsorption of a cationic gemini surfactant from aqueous solution onto aluminosilicate powders of the MCM-41 type: effect of pore size and co-adsorption of phenol. J. Colloid Interface Sci. **262**(2), 362–371 (2003). doi:10.1016/S0021-9797(03)00204-2
115. H. Benalla, J. Zajac, S. Partyka, J. Rozière, Calorimetric study of phenol adsolubilisation by cationic surfactants adsorbed on a flat silica surface or confined within small mesopores of powdered MCM-41 aluminosilicates. Colloids Surf. A Physicochem. Eng. Aspects **203**(1–3), 259–271 (2002). doi:10.1016/S0927-7757(01)01109-8
116. M.N. Khan, *Micellar Catalysis. Surfactant Science Series*, vol. 133 (Taylor and Francis Group, Boca Raton, 2006)
117. C.-C. Yu, L. Lobban Lance, Admicellar catalysis. in *Surfactant Adsorption and Surface Solubilization*, vol. 615, ACS Symposium Series. American Chemical Society, (1996), pp 67–76. doi:doi:10.1021/bk-1995-0615.ch005.
118. A.D.W. Carswell, E.A. O'Rea, B.P. Grady, Adsorbed surfactants as templates for the synthesis of morphologically controlled polyaniline and polypyrrole nanostructures on flat surfaces: from spheres to wires to flat films. J. Am. Chem. Soc. **125**(48), 14793–14800 (2003). doi:10.1021/ja0365983